

**International
Progress Report**

IPR-09-10

Äspö Hard Rock Laboratory

Prototype Repository

Acoustic emission and ultrasonic monitoring results from deposition hole DA3545G01 in the Prototype Repository between October 2007 and March 2008

D. Duckworth
J. Haycox
W.S. Pettitt
Applied Seismology Consultants

December 2008

Svensk Kärnbränslehantering AB
Swedish Nuclear Fuel
and Waste Management Co

Box 250, SE-101 24 Stockholm
Phone +46 8 459 84 00



**Äspö Hard Rock
Laboratory**

Report no.	No.
IPR-09-10	F63K
Author	Date
D. Duckworth	December 2008
J. Haycox	
W.S. Pettitt	
Checked by	Date
Lars-Erik Johannesson	2009-08-18
R.P. Young	
Approved	Date
Anders Sjöland	2009-08-20

Äspö Hard Rock Laboratory

Prototype Repository

Acoustic emission and ultrasonic monitoring results from deposition hole DA3545G01 in the Prototype Repository between October 2007 and March 2008

D. Duckworth
J. Haycox
W.S. Pettitt
Applied Seismology Consultants

December 2008

Keywords: Field test, Prototype Repository, Acoustic emission, Ultrasonic monitoring, P-wave velocity, S-wave velocity, Rock fractures, Rock properties

This report concerns a study which was conducted for SKB. The conclusions and viewpoints presented in the report are those of the author(s) and do not necessarily coincide with those of the client.

Executive summary

This report describes results from acoustic emission (AE) and ultrasonic monitoring around a canister deposition hole (DA3545G01) in the Prototype Repository Experiment at SKB's Hard Rock Laboratory (HRL), Sweden. The experiment has been designed to simulate a disposal tunnel in a real deep repository environment for storage of high-level radioactive waste. The test consists of a 90m long, 5m diameter sub-horizontal tunnel excavated in dioritic granite. The monitoring aims to examine changes in the rock mass caused by an experimental repository environment, in particular due to thermal stresses induced from canister heating and pore pressures induced from tunnel sealing.

Two techniques are utilised here to investigate the processes occurring within the rock mass around the deposition hole: ultrasonic survey and acoustic emission (AE). Ultrasonic surveys are used to 'actively' examine the rock. Velocity changes are measured between transmitter-receiver pairs using a cross-correlation technique that allows a velocity resolution of $\pm 2 \text{ m.s}^{-1}$. Amplitude and velocity changes on the ray-paths can then be interpreted in terms of changes in the material properties of the rock. Calculations using the velocities can determine the changes in dynamic moduli, Young's modulus and Poisson's ratio, to give direct indications of the properties of the rock through which the ray-paths travel. Crack density and saturation can also be calculated to determine changes in crack properties in the damaged and disturbed zones. AE monitoring is a 'passive' technique similar to earthquake monitoring but on a much smaller distance scale (source dimensions of millimetres). AEs occur on fractures in the rock when they are created or when they propagate.

Ultrasonic monitoring has been conducted at the Prototype Repository since September 1999. During excavation, monitoring of both deposition holes in section 2 of the Prototype Tunnel was undertaken to delineate zones of stress related fracturing and quantitatively measure fracturing in the damaged zone. A permanent ultrasonic array was installed in the rock mass in June 2002 around deposition hole DA3545G01. The period covered by this report is between 1st October 2007 and 31st March 2008, and is the sixth instalment of a six-monthly processing and interpretation of the continuous data stream for the heating and pressurisation phase of the experiment. The pulsing system malfunctioned on the 17th December, 2007 therefore there is no survey data after this time through to July 2008, when a maintenance visit to HRL was performed by an ASC Geophysicist. The passive AE data is not reliant on the pulsing system therefore the data coverage remained continuous throughout the entire monitoring period.

Results from the velocity analysis reveal a drop in the average velocity between 21st October and 25th October 2007, and is of similar order ($\sim 0.7 \text{ ms}^{-1}$) for both P- and S-waves (Figure I). P- and S- wave velocities increase steadily after this time, and overall exhibit greater variations ($\pm 1 \text{ ms}^{-1}$) than during previous report periods. The magnitude of the average changes are less than the velocity resolution of 2 ms^{-1} estimated for ultrasonic measurements, however, changes on individual ray-paths can be greater and appear more pronounced. Similar changes are also observed for amplitudes with a decrease of $\sim 0.3 \text{ dB}$ for both P- and S-waves between 21st and 25th October, remaining low until the 6th November, followed by a steady increase for the remainder of the period. P-wave amplitude variations are small, approximately -0.3 to $+0.1 \text{ dB}$, with an

overall increase in P-wave amplitude of ~ 0.12 dB at the end of the monitoring period. S-wave amplitudes exhibit the same behaviour as P-wave amplitudes but with an overall increase of ~ 0.3 dB by the end of the monitoring period. These changes can be attributed to the rapid changes in pressure and temperature in the backfill and/or adjacent to the deposition hole DA3545G01.

Ray-paths have been categorised following the spatial criteria presented in previous report periods (S3, S1, C1, C2 and Far). The greatest change, in both amplitudes and velocity, is observed along category C2 ray-paths. Changes in Young's Modulus very closely mimic the changes in temperature and pressure, Crack Density undergoes the same changes at the same times but the changes in magnitude are opposite in sign, i.e. when Young's Modulus increases Crack Density decreases. Poisson's ratio shows very little variation throughout the data record. Saturation exhibits similar behaviour to Young's Modulus but with much greater variation than the other parameters. Overall, the ray-path categories follow the same general trend with the largest response evident in: categories 'S3' and 'C2' for Young's Modulus and Crack density; category 'Far' for Poisson's ratio; and categories 'Far' and 'C1' for Saturation. These changes are again attributed to the rapid changes in pressure and temperature in the tunnel backfill and in the rockmass surrounding the deposition hole. It remains unclear whether changes in temperature, pressure or both combined are influencing the changes in velocity and amplitude, as these occur simultaneously.

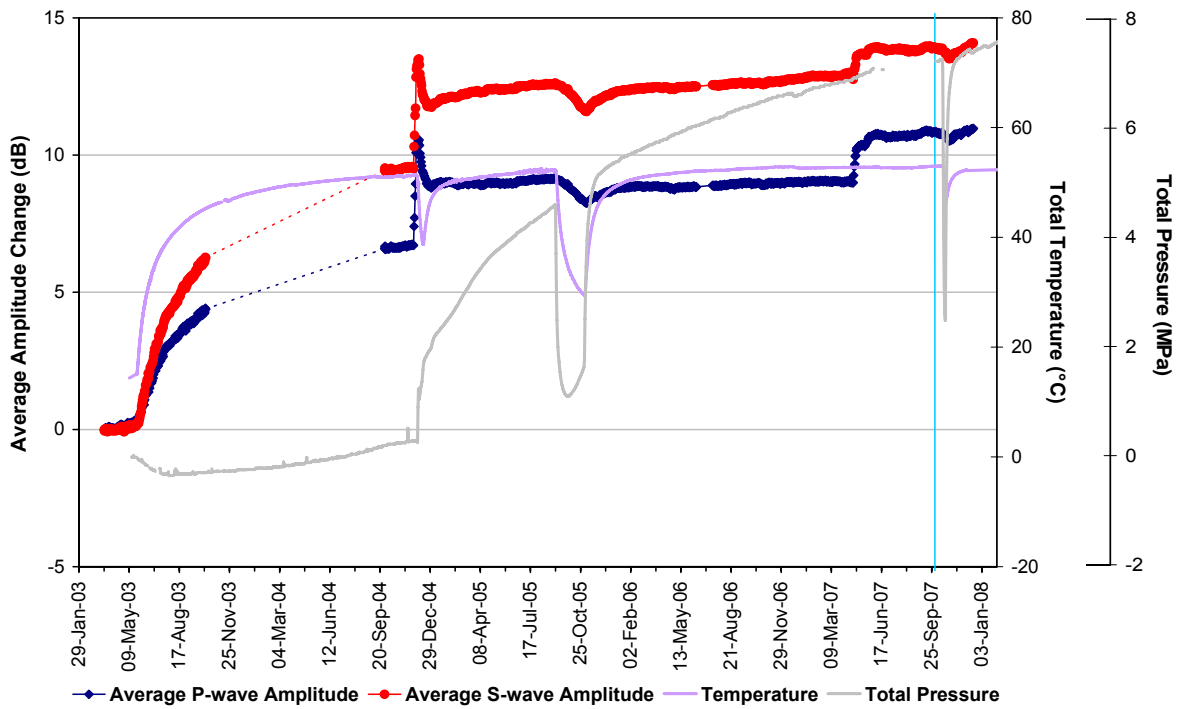
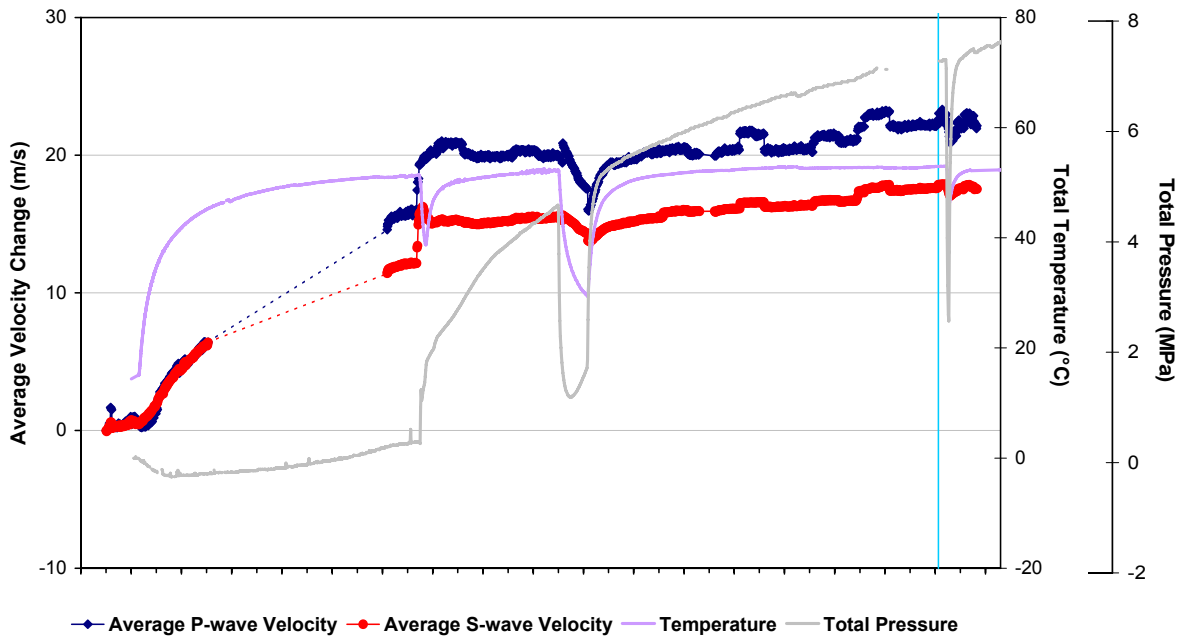


Figure I: Average velocity and amplitude changes since the start of heating and pressurisation at the Prototype repository. The vertical blue line indicates the start of the period analysed in this report (October 2007 – March 2008).

There are over five years of monitoring ultrasonic survey measurements at the Prototype experiment with velocity and amplitude measurements conducted through a number of variations in pressure and temperature conditions. It would now be beneficial to perform an additional integrated interpretation of changes in these measurements with available data on the thermal and hydro-mechanical conditions in the repository, in order to better understand the rock response in the immediate vicinity of the deposition hole. This could help resolve whether pressure or temperature, or an optimal combination of the two, has a leading role in reducing crack density (and hence permeability) and thus provide a best practise for working conditions of a future repository.

In total there were 171 located AE events (Figure II) for the entire six month period. All AE events have good waveforms with clear P- and S-wave arrivals. The rate of AE triggering increased considerably from the previous monitoring period, with an average of 0.9 triggers recorded each day. There were two notable periods of increased AE activity; on 16th January when 7 events were triggered, and on the 22nd January when 21 events were triggered. This second period of increased AE activity occurs in a cluster some distance from the deposition hole and is labelled 'Cluster T'. The cluster consists of 24 AE's, 21 of which all occurred within a 12 hour period. Blasting records will be included in the next 6-monthly report to establish whether there is a correlation between excavation of a nearby tunnel and the AE activity.

A further study of the spatial distribution of AEs shows that there are four distinct clusters, labelled A, B, C and D. Events in the individual clusters are located close enough together to be considered to occur along the same feature. Cluster A is made up of 55 events located on the SE side, Cluster B (24 events) is located on the SW side, Cluster C (9 events) is located to the West, and Cluster D (12 events) is located NE of deposition hole DA3545G01.

Clusters A, B and C have been observed in the previous two reports [Zolezzi *et al.* 2007 and 2008]. Cluster D has not been identified recently but is located in a region of activity which occurred during excavation [Pettitt *et al.* 2000]. Cluster A locates in a region of low-compressive or tensile stresses, while Clusters B and C are located in a region of high compressive stresses induced around the excavation [Pettitt *et al.*, 1999]. AEs are thought to be occurring at these positions due to the presence of pre-existing micro-cracks generated during excavation. The AEs are characterized by relatively low magnitudes with respect to previous periods indicating that the clusters do not represent significant activity.

Although changes in measured velocities, signal amplitudes and AE activity have been observed, the rock mass has remained relatively stable, representing a continuation of conditions in the tunnel and around the canister deposition hole.

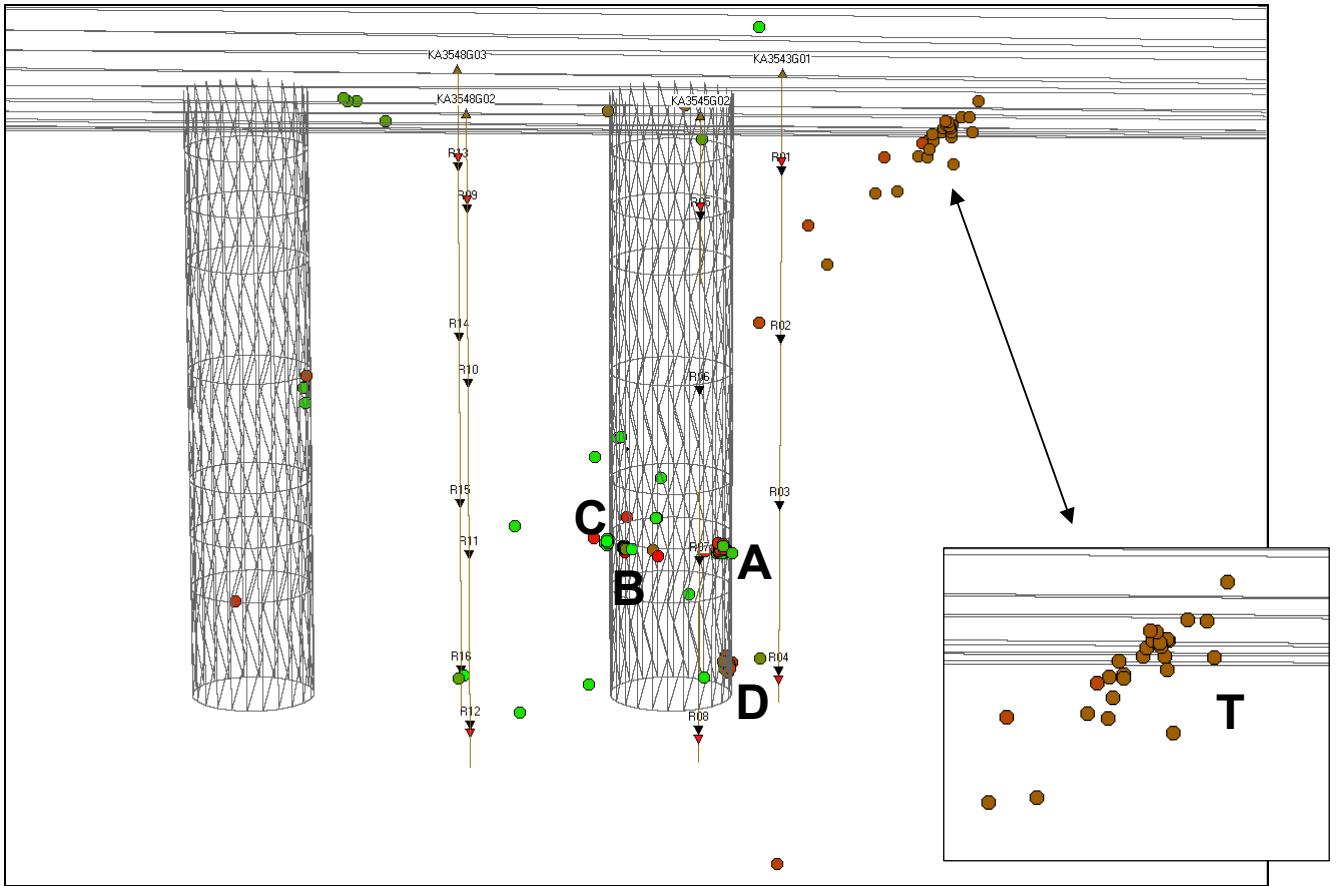


Figure II: Located AE events observed around the deposition hole for this monitoring period, and the 24 events labelled cluster T (inset) occurring some distance away from the deposition hole.

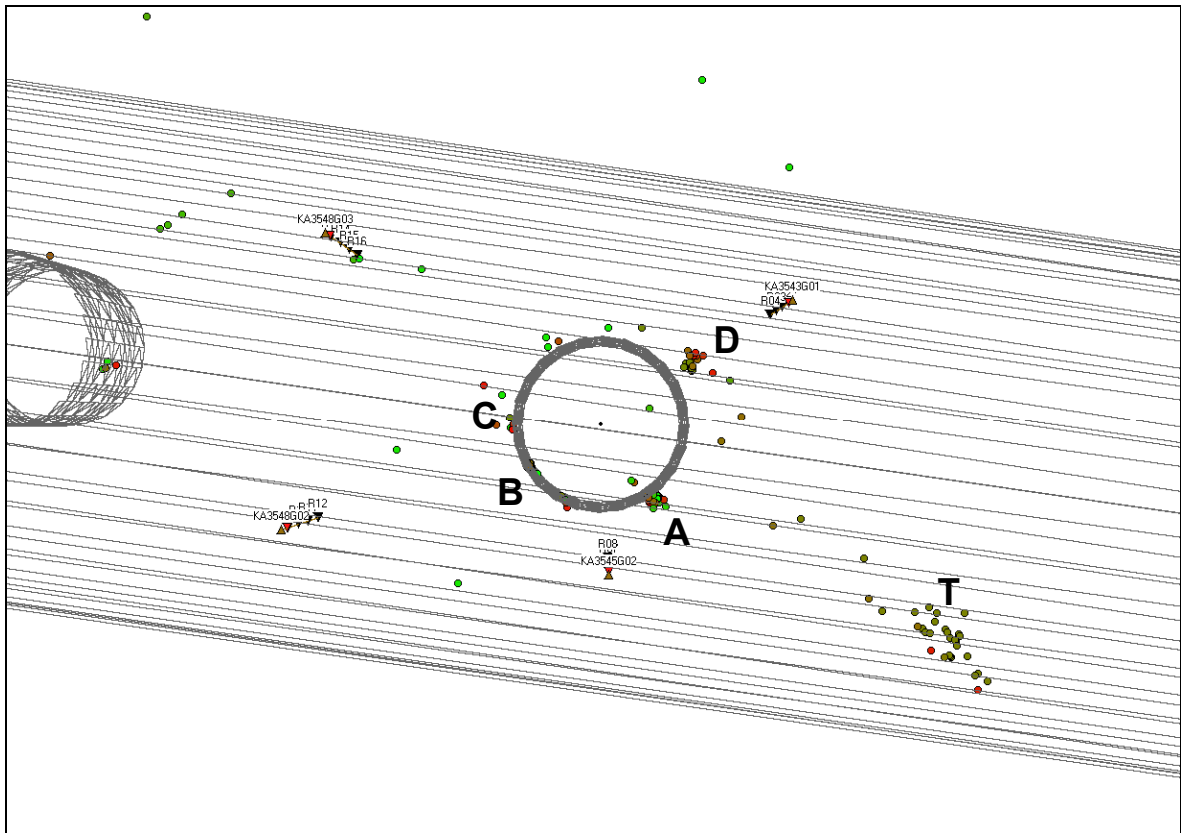
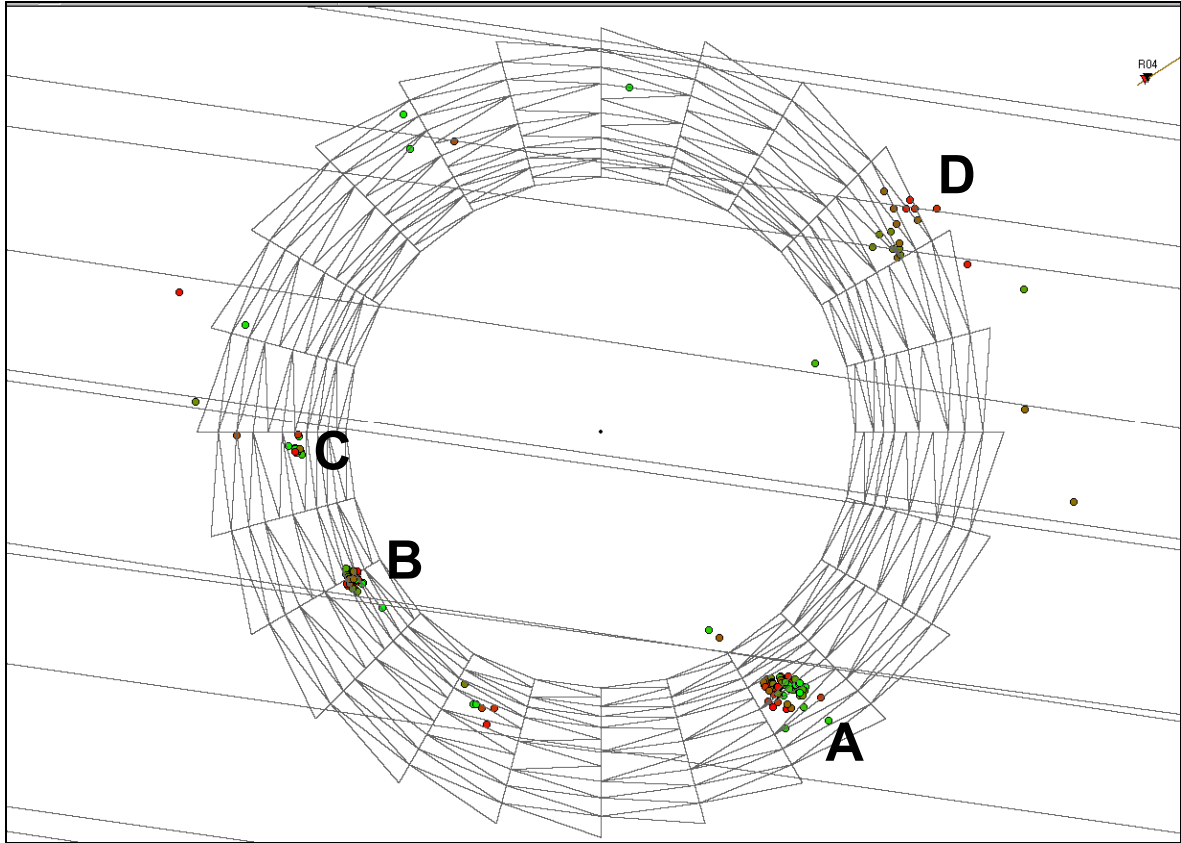


Figure III: Clusters (defined A, B, C, D and T) of AE activity observed around deposition hole DA3545G01.

Sammanfattning

Denna rapport beskriver resultaten från AE-mätningar (Acoustic Emission) och ultraljudsmätningar runt deponeringshål DA3545G01 i prototypförvaret vid SKB:s Hard Rock Laboratory. Experimentet har designats för att simulera en deponeringstunnel i ett verkligt djupförvar för högaktivt radioaktivt avfall. Det består av en 90 m lång horisontell tunnel med en diameter på 5 m, uttagen ur en dioritisk granit. Syftet med mätningen är att undersöka förändringar i bergmassan som orsakats av en experimentell förvarsmiljö, speciellt med avseende på värmespanning från uppvärmning av kapseln och porttryck orsakade av förseglingen av tunneln.

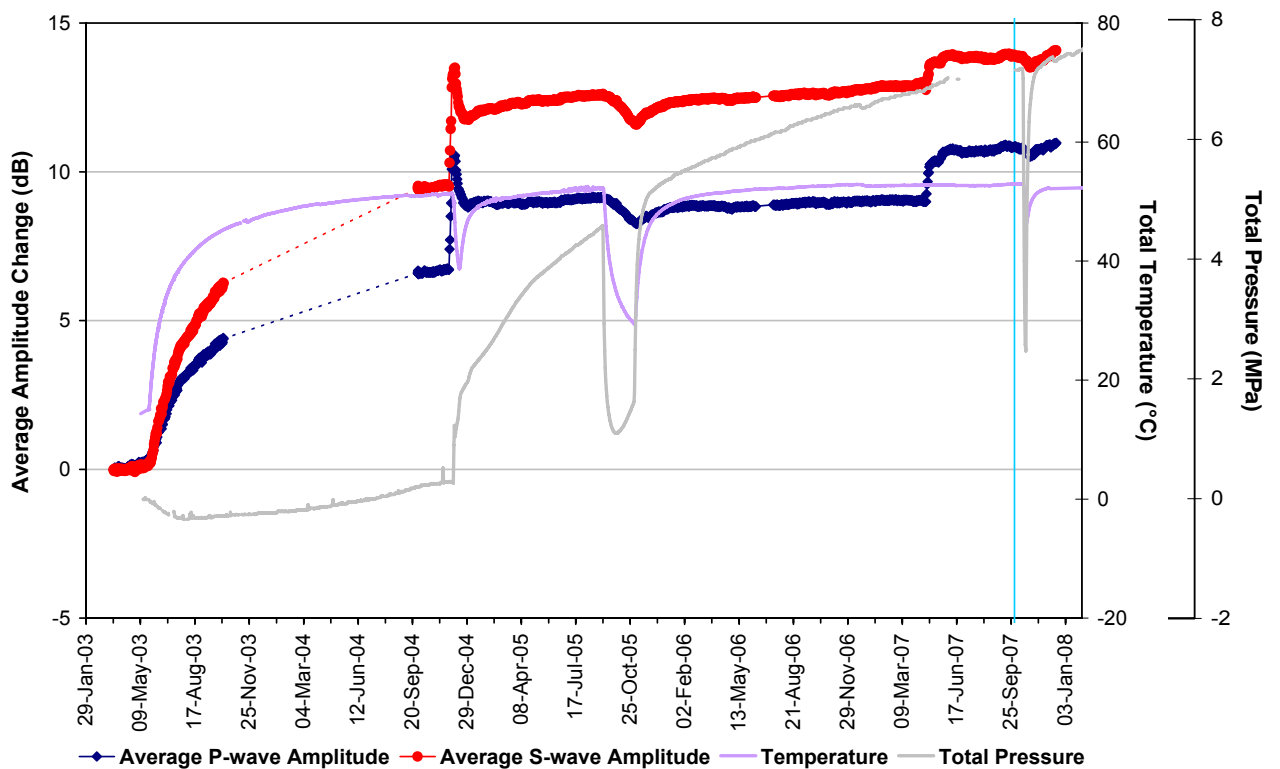
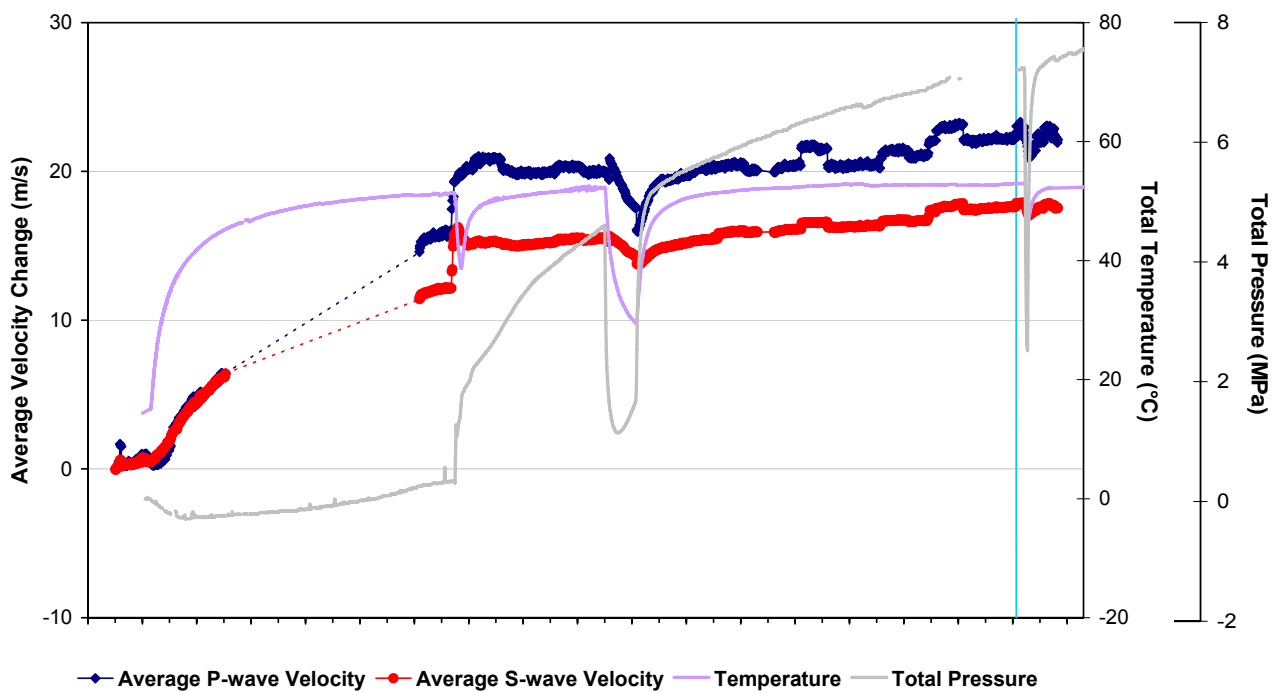
Två tekniker används för att undersöka de processer som förekommer i bergmassan runt deponeringshålet; ultraljudsmätning och AE-mätningar. Ultraljudsmätning används för att ”aktivt” undersöka berget. Hastighetsförändringar mäts mellan sändare - givare genom att utnyttja en kors-korrelationsteknik som möjliggör en mätnoggrannhet på $\pm 2 \text{ ms}^{-1}$. Förändringar i amplitud och hastighet hos signalen när den passerat genom bergmassan längs olika signalvägar relativt deponeringshålen, (”ray path”) har sedan använts för att undersöka förändringar i bergegenskaperna. Hastigheterna användas för att bestämma förändringar i dynamisk modul, elasticitetsmodul och tvärkontraktionstal som ger direkta indikationer på egenskaperna på berget genom vilket vågen passerar. Sprickdensitet och vattenmättnadsgrad kan också beräknas för att fastställa förändringar i sprickornas egenskaper i de skadade och störda zonerna. AE-mätning är en ”passiv” teknik som liknar jordbävningsovervakning men på en mycket mindre avståndsskala (dimensioner på källan i millimetrar). AE uppkommer hos bergssprickor när de bildas eller när de rör sig.

Ultraljudsmätningar har utförts i projektet Prototype Repository sedan september 1999. Mätningar gjordes runt de båda deponeringshålen i sektion 2 under borringen av dessa. Syftet med mätningarna var att beskriva zoner med spänningsrelaterade sprickor och kvantitativt mäta sprickutbildningen i den störda zonen runt deponeringshålen. Ett permanent ultraljudssystem installerades i berget runt deponeringshål DA3545G01 i juni 2002. Denna rapport behandlar mätningar under perioden 1:a oktober 2007 till 31:e mars 2008 och är den sjätte sexmånadersrapporten med processning och tolkning av data från försökets uppvärmnings- och trycksättningsperiod. Systemet som genererar pulser slutade fungera den 17:e december 2007 och därför finns inga mätdata från ultraljudsmätningarna efter den tidpunkten fram till juli 2008 då service gjordes på systemet av en geofysiker från ASC. AE-mätningarna är inte beroende av systemet som genererar pulser varför dessa mätningar gjordes kontinuerligt under hela mätperioden.

Resultaten från analyserna av våghastigheterna uppvisar en minskning i medelhastigheten mellan den 21:e och den 25:e oktober 2007. Minskningen är i samma storleksordning ($\sim 0.7 \text{ ms}^{-1}$) för både P- och S-vågorna (se Figur 1). Hastigheterna för P- och S-vågorna ökade stadigt efter den perioden och uppvisade generellt större variation ($\pm 1 \text{ ms}^{-1}$) än under tidigare perioder. Magnituden på förändringen i medeltal är mindre än mätnoggrannheten på 2 ms^{-1} (uppskattade för ultraljudsmätningar), men ändringarna för individuella signalvägar kan vara större och framträda mer uttalat. Liknande förändringar observeras också för amplituderna med en minskning på $\sim 0.3 \text{ dB}$ för både P och S-vågorna under perioden 21:e till den 25:e oktober, förblir låg fram till den 6:e november, följd av en stabil ökning under återstoden av mätperioden.

Variationerna i P-vågens amplitud är små; approximativt -0.3 till +0.1 dB, med en generell ökning av P-vågsamplitud av ~0.12 dB vid slutet av mätperioden. Amplituderna för S-vågen uppträder på samma sätt som amplituderna för P-vågen men med en generell ökning på ~0.3 dB vid slutet av mätperioden. Dessa förändringar kan hänföras till den snabba förändringen i tryck och temperatur i återfyllningen och i närheten av deponeringshål DA3545G01.

De olika signalvägarna relativt deponeringshålen ("ray path") har kategoriserats enligt rumsliga kriterier som presenterats i tidigare rapporteringar (S3, S1, C1, C2 och "Far"). De största förändringarna i amplitud och hastighet observeras för kategorin C2. Förändringar i E-modul följer förändringar i temperatur och tryck, sprickdensiteten uppvisar liknande förändringar vid samma tidpunkter men förändringarna i magnitud har omvänt tecken, d.v.s. när E-modulerna ökar minskar sprickdensiteten. Tvärkontraktionstalet visar mycket små variationer i hela dataserien. Parametern vattenmättnadsgrad uppvisar liknande beteende som E-modulen men med mycket större variation. På det hela taget följer de olika signalvägarna samma generella trend med den största responsen för kategorierna "S3" och "C2" vad gäller E-modulen och sprickdensitet; kategorin "Far" för tvärkontraktionstalet; och kategorierna "Far" och "C1" för vattenmättnadsgrad. Dessa förändringar är som tidigare nämnts kopplade till de snabba förändringarna av tryck och temperatur i tunneln och i bergmassan runt deponeringshålet. Det är fortfarande oklart om temperatur- och tryckförändringarna eller kombinationen av båda parametrarna påverkar förändringarna i hastighet och amplitud, eftersom temperatur- och tryckförändringarna uppträder samtidigt.



Figur I: Förändringar i medelhastighet och medelamplitud sedan starten av uppvärmningen och trycksättningen av Prototyp Repository. Den vertikala blå linjen indikerar början på perioden som analyserats i denna rapport (oktober 2007 - mars 2008).

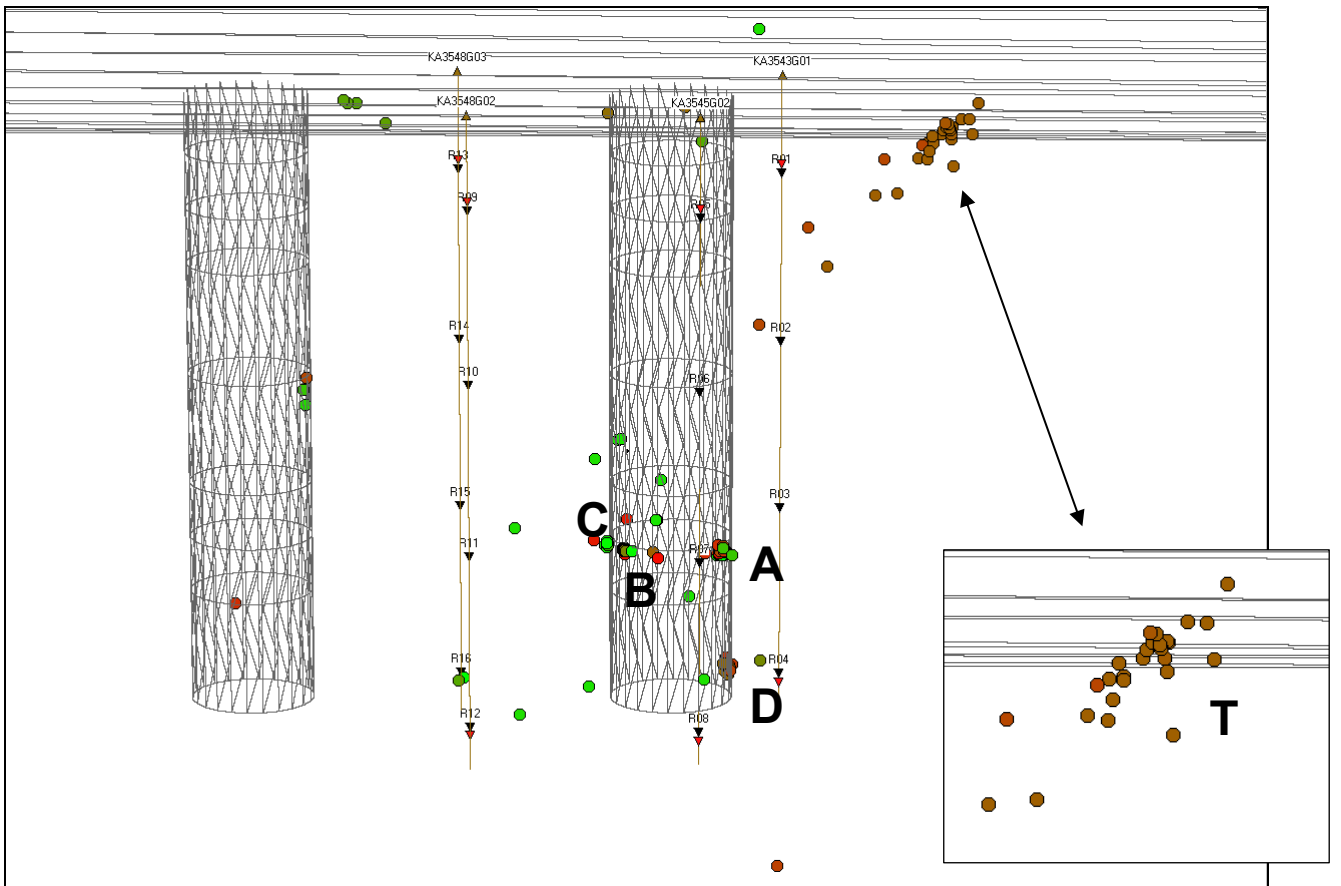
Över fem års ultrasonicmätningar vid Prototypförvaret har genomförts innefattande hastighets- och amplitudmätningar. Mätningarna har gjorts vid varierande tryck- och temperaturförhållanden. Det vore fördelaktigt om man nu kunde genomföra en ytterligare integrerade tolkning av förändringarna i dessa mätningar med tillgänglig data gällande termiska och hydromekaniska förhållanden i förvaret i syfte att bättre kunna förstå bergets beteende i närheten av deponeringshålet. En sådan analys kan hjälpa till lösa frågeställningen huruvida tryck eller temperatur eller en optimal kombination av de två parametrarna har en betydande roll i reduktionen av sprickdensitet (och medföljande permeabilitet) och därför sörja för en bästa uppskattning gällande funktionen av ett framtida förvar.

Totalt lokaliserades 171 AE (Figur II) under hela sexmånadersperioden. Alla AE har en bra vågform med tydlig ankomst av P- och S-vågorna. Takten på AE ökade markant jämfört med tidigare mätperioder. Antalet AE i medeltal per dag var 0.9. Det fanns två noterbara perioder med ökande AE, en den 16:e januari när 7 händelser observerades, och en den 22:e januari när 21 händelser observerades. Den andra perioden med ökad antal AE uppträder i ett kluster ett litet avstånd från deponeringshålet och benämns "Cluster T". Klustret består av 24 AE, varav 21 uppträdde inom en period av 12 timmar. Data från sprängning kommer att inkluderas i nästa 6-månadersrapport för att reda ut om det finns en korrelation mellan uttaget av en ny närbelägen tunnel och AE-aktivitet.

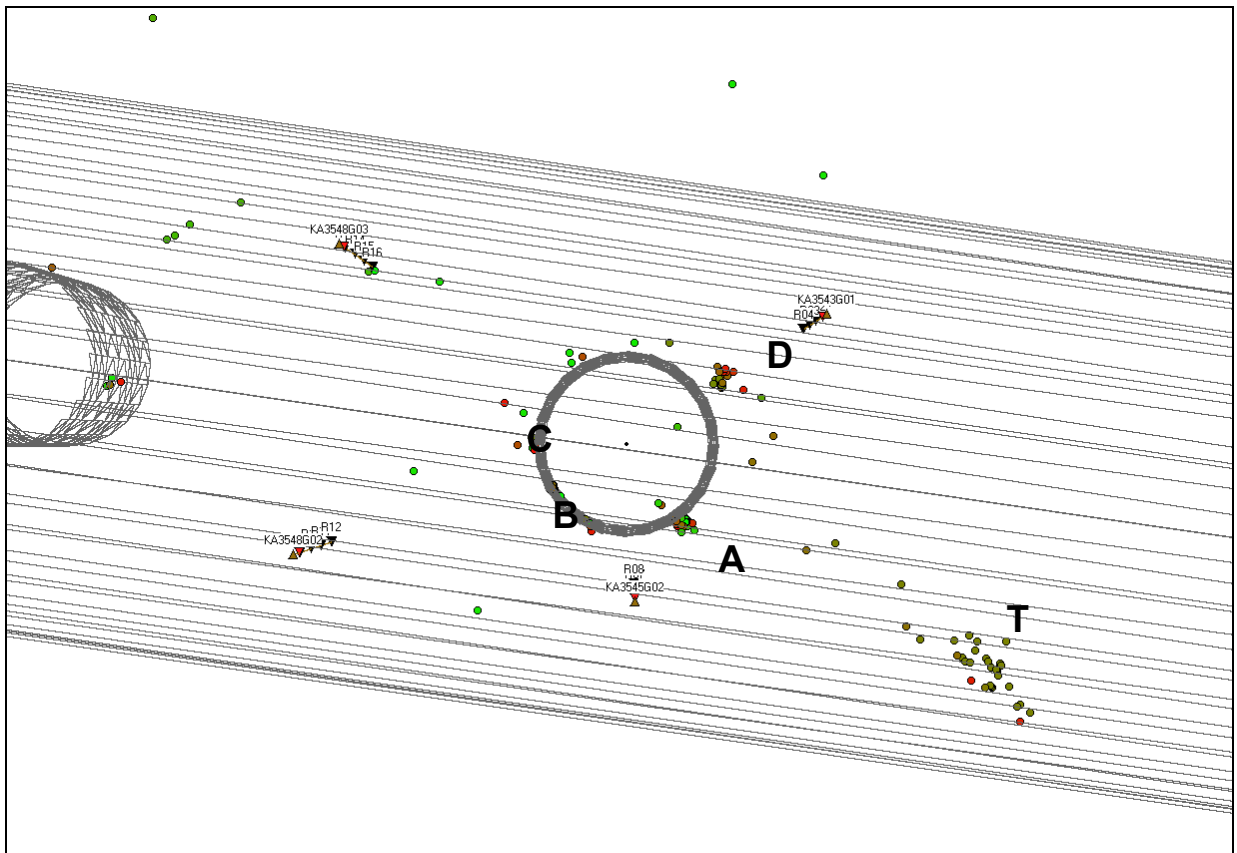
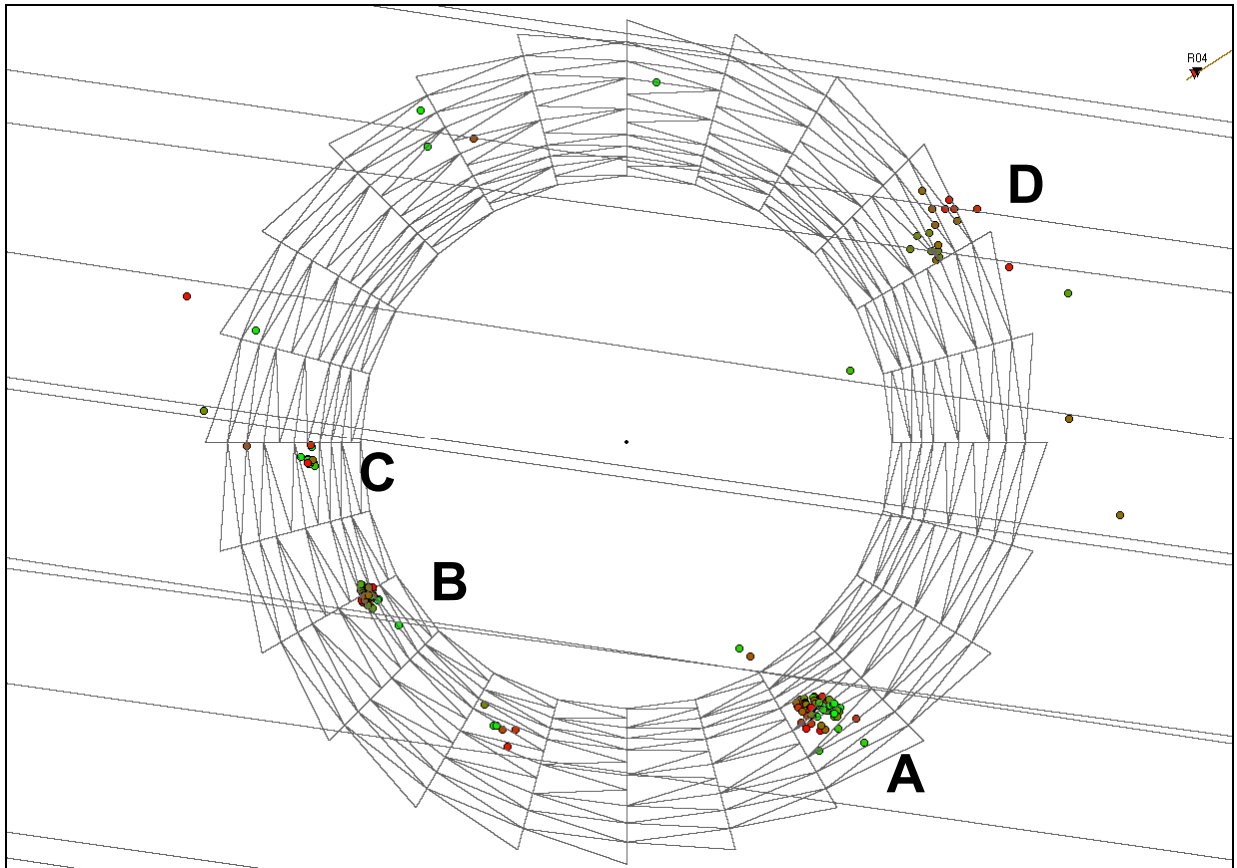
En närmare studie av den rumsliga fördelningen av AE visar att det finns fyra distinkta kluster, med beteckningarna A, B, C och D. Händelser i det enskilda klustret är lokaliserade så nära varandra att de kan anses uppträda på samma anomali. Kluster A består av 55 händelser lokaliserade till SE sidan, Kluster B (24 händelser) är lokaliserat till SW sidan, Kluster C (9 händelser) är lokaliserat till V sidan, och Kluster D (12 händelser) är lokaliserat till NE sidan av deponeringshål DA3545G01.

Kluster A, B och C har observerats i de två senaste avrapporteringarna (Zolezzi et al. 2007 och 2008). Kluster D har inte blivit identifierad tidigare men den är lokaliserad till regionen med aktiviteter som uppstod under uttaget för deponeringshålet (Pettitt et al. 2000). Kluster A ligger i regioner med låga tryckspänningar eller med dragspänningar. De andra klustren (B och C) ligger i regioner med höga kompressionsspänningar inducerade runt deponeringshålet (Pettitt et al. 1999). AE kan uppstå i dessa positioner på grund av närvaro av mikrosprickor som uppstod under uttaget av deponeringshålet. De registrerade AE karakteriseras av relativt låga magnituder i förhållande till tidigare perioder vilket betyder att klustren inte representerar betydande aktivitet.

Fastän förändringar i uppmätta hastigheter, signalamplitud och AE observerats har bergmassan förblivit relativt stabil vilket betyder att förhållandena i tunneln och runt deponeringshålet upprätthålls.



Figur II: Lokaliserade AE observerade runt deponeringshålet under denna mätperiod, och de 24 händelser belägna i kluster T (infällt) uppkomna ett litet avstånd från deponeringshålet.



Figur III: Kluster (betecknade A, B, C, D and T) of AE aktiviteter observerade runt deponeringshål DA3545G01.

Contents

Executive summary	3
Sammanfattning	9
Contents	15
1 Introduction	23
2 Specific Objectives	25
3 Results	27
3.1 Ultrasonic surveys	27
3.2 Acoustic Emissions	42
4 Conclusions	53
4.1 Monitoring Between October 2007 and March 2008	53
4.2 Summary of Monitoring from the Heating and Pressurisation Phase	54
4.3 Recommendations	55
References	71
Appendix I Previous Monitoring at the Prototype Repository	73
Appendix II Methodology	75
Appendix III Processing Parameters	85

Table of Figures

Figure 1-1: Plan view of the experimental tunnels at the Äspö HRL and the location of the Prototype Repository. A schematic illustration of the final experimental set up is shown with canisters and bentonite clay buffer installed in the 1.75m diameter deposition holes. Note the entrance of the tunnel is towards the left. Graphics are modified from SKB [1999]...... 24

Figure 3-1: Temperature of the rockmass around deposition hole DA3545G01. The sensors are positioned mid-way up the deposition hole at different depths through the rockmass (see right-hand inset) [Goudarzi, 2007]. 27

Figure 3-2: Total pressure in (a) the backfill over deposition hole DA3545G01 and (b) the rock adjacent to deposition hole DA3545G01 for the period between 1st September 2007 and 31st March 2008 [Goudarzi, 2008]. The dashed vertical lines indicate the period when simultaneous pressure changes occur in both the backfill above the deposition hole, and in the rockmass surrounding the deposition hole. 30

Figure 3-3: Average P- and S-wave (a) velocity change (ms^{-1}) and (b) amplitude change (dB), for this reporting period. Temperature of the surrounding rockmass (TR6045) and total pressure in the backfill (UFA15) are displayed on the secondary axes. Note that the graph covers the period up until 17th December when survey data stopped due to equipment malfunction..... 31

Figure 3-4: Summary diagram showing the correlation between P- and S-wave velocity and amplitude changes with the short-term temperature and pressure changes observed in the rockmass surrounding the deposition hole. It is unclear whether the average velocity and amplitudes are more strongly reacting to changes in temperature, pressure, or both as these changes occur over the same time period..... 32

Figure 3-5: Example plots of (a) raw waveform data (dashed red line are the first arrivals of P (first) and S (secondary)); and cross correlation (CCR) windows for the ray-path between transmitter seven and receiver six for (b) P- waves and (c) S-waves. Example surveys from before the recorded drop in amplitudes on 10th October (orange line), during the drop 26th October (green line). 33

Figure 3-6: Interpretation of the ultrasonic results during excavation in terms of disturbed and damaged regions around the deposition hole. Zones of induced stress are inferred from elastic modelling and the σ_1 orientation, after Pettitt et al. [1999]. 34

Figure 3-7: Velocity changes measured on ray-path category 'S3' (Figure 3-6) for deposition hole DA3545G01. Ray-paths shown are from transmitter (t_n) to receiver (r_n) for (a) $t_n=1, r_n=5$; (b) $t_n=1, r_n=6$; (c) $t_n=1, r_n=7$ and (d) $t_n=4, r_n=1$. Schematic diagrams on the right indicate the relative positions of transmitter (red) and receiver (gold). Temperature (TR6045, blue line) is displayed on the secondary axes..... 37

Figure 3-8: Velocity changes measured on ray-path category 'S1' (Figure 3-6) for deposition hole DA3545G01. Ray-paths shown are from transmitter (t_n) to receiver (r_n) for (a) $t_n=7, r_n=5$; (b) $t_n=7, r_n=6$; (c) $t_n=7, r_n=7$ and (d) $t_n=7, r_n=8$. Schematic diagrams on the right indicate the relative positions of transmitter (red) and receiver (gold). Temperature (TR6045, blue line) is displayed on the secondary axes..... 38

Figure 3-9: Average velocity change for the five category ray-paths (S1, S3, C1, C2, Far) around deposition hole DA3545G01 for (a) P-waves shown with temperature (instrument TR6045) on the secondary axis; and (b) S-waves shown with pressure (instrument UFA15) on the secondary axes..... 39

Figure 3-10: Average amplitude change for the five category ray-paths (S1, S3, C1, C2, Far) around deposition hole DA3545G01 for (a) P-waves shown with temperature (instrument TR6045) on the secondary axis; and (b) S-waves shown with pressure (instrument UFA15) on the secondary axes.....	40
Figure 3-11: Changes in rock parameters, calculated using average P- and S-wave velocities and amplitudes, for the five ray-path categories for (a) Young's Modulus, (b) Poisson's Ratio, (c) Crack Density and (d) Saturation. Temperature (TR6045) and pressure (UFA15) are displayed on the secondary axes.	41
Figure 3-12: Temporal distribution of (a) located AEs and (b) AE triggers; number of events per day on left axis (shown by the blue line) and cumulative AE events on the right-hand axis (shown by the purple line) also shown in (a) is the pressure (UFA15) in the tunnel backfill over the deposition hole.	45
Figure 3-13: Three views showing the clustered AE activity located around deposition hole DA3545G01. (Top: Oblique view looking north; Bottom left: Plan view with the five category ray-paths used in the ultrasonic survey shown relative to the deposition hole; Bottom right: Close-up view of the deposition hole).....	46
Figure 3-14: Waveforms for a selected event from each of the four clusters shown in relation to a transverse view of AE activity.	47
Figure 3-15: Close up views of Cluster A (top) containing 55 events, Cluster B (top-middle) containing 24 events, Cluster D (bottom-middle) containing 12 events and Cluster T (bottom) containing 24 events. Cluster T is located some distance away from the deposition hole and the majority of the events occurred during a twelve hour period on the 22 nd January, 2008. Note the apparent strike of the events.	48
Figure 3-16: Temporal distribution of located AEs in clusters a) Cluster A and b)Cluster B. Plots show the number of events (blue line) per day on left axes and cumulative number (purple line) of events for the entire monitoring period on right axes.	49
Figure 3-17: Temporal response plot of located AEs in the identified clusters for a) Cluster D and b) Cluster T. Plots show the number of events per day (blue line) on left axes and cumulative number of events (purple line) for the entire monitoring period on right axes.	50
Figure 3-18: Plan view of total AEs located around deposition hole DA3545G01 during (a) the excavation phase, (b) monitoring during heating through to 01/04/2007, (c) previous monitoring phase during heating, from 01/04/2007 until 31/09/2007, and (d) this monitoring phase (01/10/2007 – 31/03/2008). The red arrows mark the orientation of principle stresses.....	51
Figure 3-19: Chart displaying AE magnitudes recorded from the beginning of heating and pressurisation. Events are coloured by response period as defined in Table 4-1. During this latest period there has been a slight increase in event magnitudes (both in peak magnitude and distribution) compared to the previous one, but remain below the highest magnitudes observed in the initial phase of heating (response periods 1 and 2).....	52
Figure 4-1: P- and S-wave velocity change (a) and amplitude change (b) from the start of monitoring, plotted alongside temperature (TR6045) and pressure (PB616) measurements in deposition hole DA3545G01. The vertical blue lines differentiate between periods of similar environmental conditions (see Table 4-1).	59
Figure 4-2: Average P- and S-wave velocity change for ray-paths on category 'S1' together with temperature (TR6045) and total pressure (PB616) (top), Young's Modulus and Poison's Ratio change (middle), and Crack Density and Saturation change (bottom).	60

Figure 4-3: Average P- and S-wave velocity change for ray-paths on category ‘S3’ together with temperature (TR6045) and total pressure (PB616) (top), Young’s Modulus and Poison’s Ratio change (middle), and Crack Density and Saturation change (bottom).	61
Figure 4-4: Average P- and S-wave velocity change for ray-paths on category ‘C1’ together with temperature (TR6045) and total pressure (PB616) (top), Young’s Modulus and Poison’s Ratio change (middle), and Crack Density and Saturation change (bottom).	62
Figure 4-5: Average P- and S-wave velocity change for ray-paths on category ‘C2’ together with temperature (TR6045) and total pressure (PB616) (top), Young’s Modulus and Poison’s Ratio change (middle), and Crack Density and Saturation change (bottom).	63
Figure 4-6: Average P- and S-wave velocity change for ray-paths on category ‘Far’ together with temperature (TR6045) and total pressure (PB616) (top), Young’s Modulus and Poison’s Ratio change (middle), and Crack Density and Saturation change (bottom).	64
Figure 4-7: Projections of all AEs located during the heating phase (20 th March 2003 to 31 st March 2008). Events are scaled to time.	65
Figure 4-8: (a) Number and cumulative number of located events from the start of monitoring in March 2003, (b) 17 day moving average of located AE’s, and (c) temperature (TR6045) and pressure (PB616) measurements in deposition hole DA3545G01.	66
Figure 4-9: Schematic diagram of the deposition hole and explanation of changes experienced during Period 1.....	67
Figure 4-10: Schematic diagram of the deposition hole and explanation of changes experienced during Period 2.....	67
Figure 4-11: Schematic diagram of the deposition hole and explanation of changes experienced during Period 3.....	68
Figure 4-12: Schematic diagram of the deposition hole and explanation of changes experienced during Period 4.....	68
Figure 4-13: Top: Schematic diagram of the locations of all transducers on a single frame. Left: Photo of a section of the transducer assembly. Right: The transducer assembly during installation.	75
Figure 4-14: Plan view of the array geometry for Deposition Hole DA3545G01 during heating in the Prototype Tunnel. The blue solid lines represent direct ray-paths between sondes illustrating their ‘skimming’ nature. The blue dashed line represents a ray-path that travels through the deposition hole.	77
Figure 4-15: Schematic diagram of the hardware used for the heating stage in the Prototype Repository. The ultrasonic pulse generator sends a signal to each transmitter and the resulting signal is recorded on each receiver. The receivers are also used to listen for AE activity. The archive PC is required to make a copy of the data for backup purposes.....	78
Figure 4-16: Waveforms recorded from one transmitter on the array of sixteen receivers. The gold markers indicate the transmission time. The blue and green markers indicate picked P- and S-wave arrivals respectively.	80
Figure 4-17: Locations of calibration shots obtained from a series of tests at 1 metre intervals down the wall of deposition hole DA3545G01. The two views show that these line up and are located close to the surface of the hole.....	83
Figure 4-18: Example waveforms from each of the 16 receiving channels for a ‘pencil-lead break’ test undertaken against the Deposition Hole (DA3545G01) wall 6 metres below the tunnel floor.	83

Table of Tables

Table 3-1: Average daily number of located AEs events for the six monthly report periods starting 1 st October 2004 and finishing with the end of this report period on 31 st March 2008.....	42
Table 3-2: Mean Position for the 55 events located in Cluster A.....	43
Table 3-3: Mean Position for the 24 events located in Cluster B.....	43
Table 3-4: Mean Position for the 12 events located in Cluster D.....	44
Table 3-5: Mean Position for the 24 events located in Cluster T.....	44
Table 4-1: Summary of velocity, amplitude and AE variation measured during five response periods of temperature and/or pressure change.....	56
Table 4-2: Summary of key interpretation of rock response from the ultrasonic measurements.....	57
Table 4-3: Summary of ultrasonic monitoring at the Prototype Repository to-date. ..	73
Table 4-4: Boreholes used for AE monitoring of deposition hole DA3545G01.....	77

1 Introduction

This report describes results from acoustic emission (AE) and ultrasonic monitoring around a canister deposition hole (DA3545G01) in the Prototype Repository Experiment at SKB's Hard Rock Laboratory (HRL), Sweden. The monitoring aims to examine changes in the rock mass caused by an experimental repository environment, in particular due to thermal stresses induced from canister heating and pore pressures induced from tunnel sealing. Monitoring of this volume has previously been performed during excavation [Pettitt *et al.* 1999], and during stages of canister heating and tunnel pressurisation [Haycox *et al.* 2005a and 2005b; Haycox *et al.* 2006a and 2006b, Zolezzi *et al.* 2007]. Further information on this monitoring can be found in Appendix I. This report relates to the period between 1st October 2007 and 31st March 2008, and is the sixth instalment of a 6-monthly processing and interpretation of the results for the experiment.

The Prototype Repository Experiment (Figure 1-1) has been designed to simulate a disposal tunnel in a real deep repository for disposal of high-level radioactive waste. Its objective is 'to test and demonstrate the integrated function of the repository components under realistic conditions on a full scale and to compare results with models and assumptions'. The experiment consists of a 90m long, 5m diameter sub-horizontal tunnel excavated in dioritic granite using a Tunnel Boring Machine (TBM). The rock mass has two main discontinuous sets of sparse, en-echelon fractures [Patel *et al.* 1997]. The Prototype Repository design incorporates six full-scale canister deposition holes which have been excavated vertically into the floor of the tunnel using a TBM converted to vertical boring. Each deposition hole measures 1.75m in diameter and approximately 8.8m in length. Simulated waste canisters, encased in a bentonite buffer, have been placed into each deposition hole and heated from within by specially designed electric heaters to simulate disposed radioactive material at elevated temperatures. The tunnel was then backfilled using a mixture of bentonite and crushed rock, and sealed using concrete plugs. A range of measurements are made in and around the tunnel and deposition holes.

AE and ultrasonic monitoring is a tool for remotely examining the extent and severity of damage and disturbance around an excavation. This can be induced by the excavation method itself; by the redistribution of stresses (loading or unloading) resulting from the void or by environmental affects such as heating, saturation or pressurisation. Acoustic techniques are particularly adept at assessing the Excavation Damaged or Disturbed Zone (EDZ) as they allow it to be mapped spatially and temporally with high resolution, and they allow the effect on the rock mass to be quantifiably measured. Furthermore, acoustic techniques allow investigations to be conducted remotely, without the need for potentially damaging coring. Young and Pettitt [2000] give a review of AE and ultrasonic results from a number of experiments conducted in different underground environments.

- AE monitoring is a 'passive' technique similar to earthquake monitoring but on a much smaller distance scale (source dimensions of millimetres). AEs occur on fractures in the rock sample when they are created or when they move. The data acquisition system triggers on AEs when they occur and records full-waveform information that can then be used to delineate the amount, time, location and fracture mechanism.

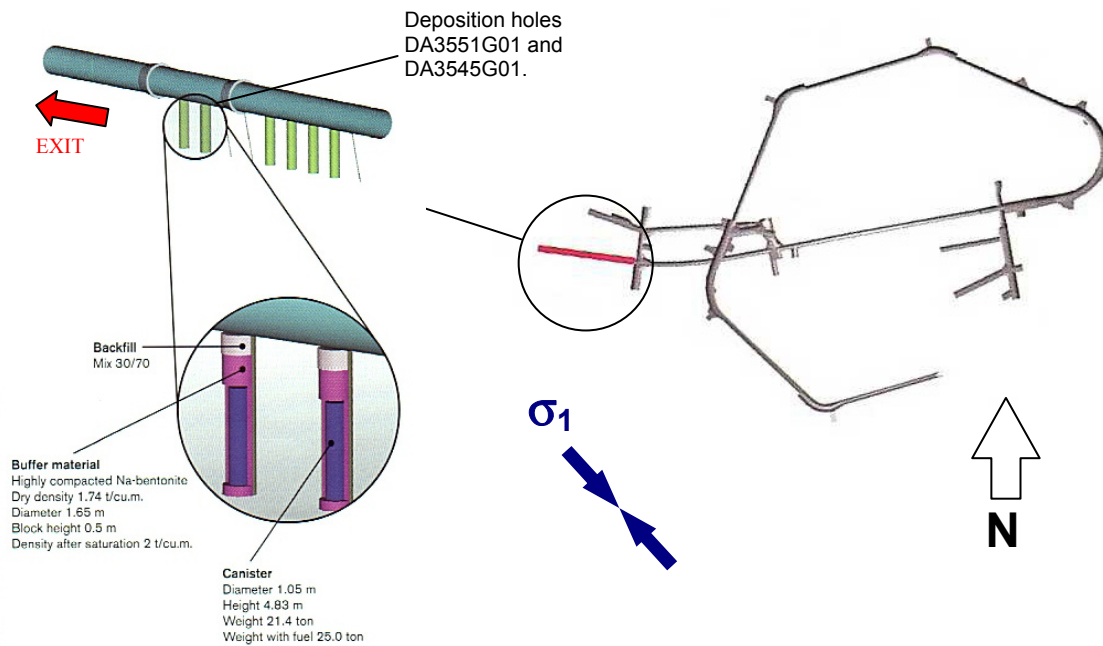


Figure 1-1: Plan view of the experimental tunnels at the Äspö HRL and the location of the Prototype Repository. A schematic illustration of the final experimental set up is shown with canisters and bentonite clay buffer installed in the 1.75m diameter deposition holes. Note the entrance of the tunnel is towards the left. Graphics are modified from SKB [1999].

- Ultrasonic surveys are used to ‘actively’ examine the rock. In this case an array of transmitters sends signals to an array of receivers. Amplitude and velocity changes on the ray-paths can be interpreted in terms of changes in the material properties of the rock. Calculations using the velocities can determine changes in dynamic moduli, Young’s modulus and Poisson’s ratio, to give direct indications of the properties of the rock through which the ray-paths travel. Crack density and saturation can also be calculated to determine changes in crack properties in the damaged and disturbed zones.

Appendix II provides detailed descriptions of the data acquisition and processing used during this and past monitoring periods. The ultrasonic array consists of twenty-four ultrasonic transducers configured as eight transmitters and sixteen receivers installed into four instrumentation boreholes using specially designed installation frames sealed within slightly expansive grout. The array is designed to provide good coverage for AE locations and provide ‘skimming’ ray-paths so as to sample the rock immediately adjacent to the wall of the deposition hole. ASC’s InSite Seismic Processor [Pettitt *et al.* 2007], has been used to automatically process both the AE and ultrasonic survey data. Appendix III A and Appendix III B give the processing parameters used. Data from daily ultrasonic surveys have been automatically picked and arrivals cross-correlated to a reference survey for high-precision measurements of P- and S-wave velocity changes through the experiment. Arrivals of AEs have been manually picked and three dimensional source locations have been calculated.

2 Specific Objectives

This six-month period of ultrasonic monitoring in the Prototype Repository Experiment, has been undertaken with the following objectives;

- Produce accurate source locations for AEs so as to delineate the spatial and temporal extent of any brittle micro-cracking within the rock mass around the deposition hole and locate any movements on pre-existing macroscopic fractures;
- Conduct regular ultrasonic surveys to assess the effect of heating and other environmental changes on the velocity and amplitude of transmitted ultrasonic waves;
- Investigate changes in dynamic moduli and crack density to show how the properties of the rock volume around the deposition hole changes throughout the experiment;
- Relate the AE and ultrasonic measurements to the measured *in situ* stress regime and other operating parameters such as temperature and fluid pressure;
- Outline how the results from this reporting period relate to previous monitoring periods, and into the overall experimental aims and objectives.

3 Results

3.1 Ultrasonic surveys

An indication of any major environmental changes occurring in the tunnel and deposition holes can be ascertained from the temperature and pressure measurements supplied by SKB [Goudarzi, 2008]. The temperature of the rock around the deposition hole is shown in Figure 3-1. The temperature on these instruments describes a significant drop starting 17th October 2007 (reaching a low on 23rd October), where a temperature drop of 6°C is recorded on some instruments, and steadily returns to stable, but lower temperatures, than the preceding report period (~0.4°C less at the end of the monitoring period).

The total pressure in the backfill above deposition hole DA3545G01 is shown in Figure 3-2a. In general, the pressure increases by approximately 0.5MPa (to an average period maximum of ~1.1MPa) between 9th November and 23rd December 2007, remains at this level until 9th January 2008 when it undergoes a sudden drop (to an average 0.7MPa) over the next six days, and an equally sudden return (to an average 1.0MPa) for the remainder of the period.

The total pressure in the rock adjacent to deposition hole DA3545G01 is displayed in Figure 3-2b. In this case the pressure remains fairly consistent on all instruments throughout the entire period apart from a sudden decrease of ~5MPa that occurs on the 16th October (reaching a period low on the 22nd October). The pressure then returns to values similar to those preceding the sudden drop (across the following 17 days), and proceeds to increase gently (by ~0.5MPa) until the end of the recording period. A minor drop of ~0.2MPa also occurs mid-January (indicated by the dashed vertical lines on Figure 3-2), most notably on instruments PB601 and PB610, which coincides with the pressure drop observed in the backfill above the deposition hole (whereas the pressure drop observed in the rockmass next to deposition hole on the 22nd October 2007 is not observed in the tunnel backfill above).

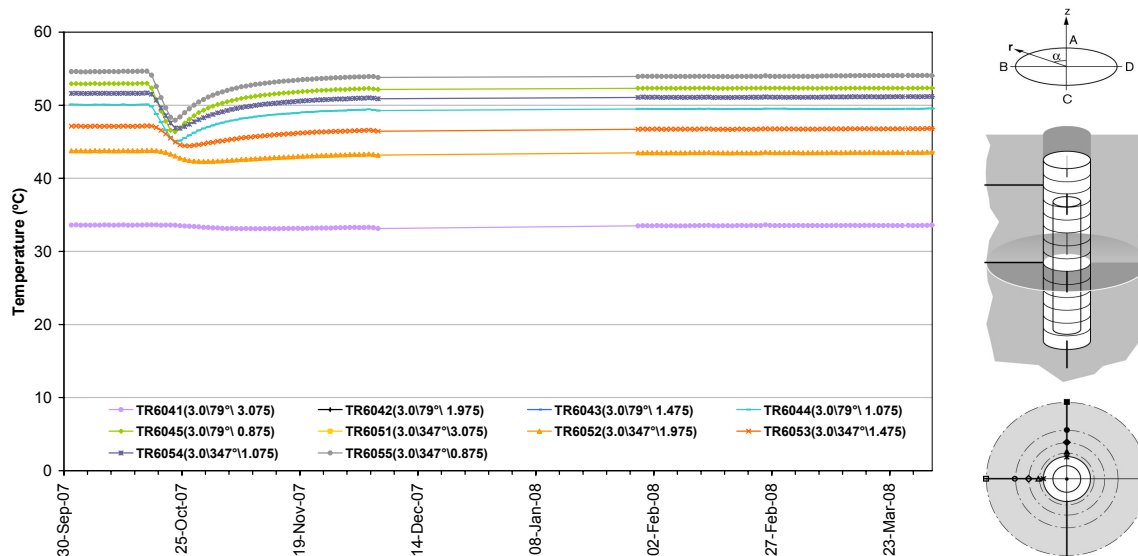


Figure 3-1: Temperature of the rockmass around deposition hole DA3545G01. The sensors are positioned mid-way up the deposition hole at different depths through the rockmass (see right-hand inset) [Goudarzi, 2007].

Velocity changes are measured between transmitter-receiver pairs by cross-correlating (CCR) data from the daily ultrasonic surveys. A reference survey, taken from previous monitoring periods, is used to process the ultrasonic results. The reference survey was recorded on 8th December 2004 and has had first P- and S-wave arrivals manually picked from the waveforms [Haycox *et al.* 2006a]. Data recorded during this monitoring period will use the same reference survey so that results from previous periods can be accurately compared. Since transmitter and receiver locations are known, the ultrasonic velocity for each ray-path can be calculated with an estimated uncertainty of $\pm 30 \text{ ms}^{-1}$ (± 3 data points). Cross-correlation is then used to automatically process subsequent surveys. This technique cross-correlates P- and S-wave arrivals from a transmitter-receiver pair with arrivals recorded on the same transmitter-receiver pair from the reference survey. Manual picking of arrivals by the examiner can often be erroneous due to random noise superimposed on the first few data points of the first break. By using the cross-correlation procedure it reduces this uncertainty and allows a high-resolution analysis to be performed, with an estimated uncertainty of $\pm 2 \text{ ms}^{-1}$ between surveys on individual ray-paths, and hence small changes in velocity to be observed. This is extremely important when changes in rock properties occur over only a small section ($\sim 5\%$) of the ray-path.

Average P- and S-wave velocity change is shown in Figure 3-3a. We observe a decrease in velocity between 17th and 24th October 2007 that coincides with the temperature and pressure drops observed in the rockmass surrounding the canister. The decrease in peak velocity is of a similar order for both P- and S-waves ($\sim 0.7 \text{ ms}^{-1}$). Both P- and S-wave velocities gradually increase and remain of similar order until 21st November when P-wave velocity increases by $\sim 0.35 \text{ ms}^{-1}$ in a single day. Velocities then gradually decrease (S-waves by $\sim 0.2 \text{ ms}^{-1}$ and P-waves by $\sim 0.6 \text{ ms}^{-1}$) for the remainder of the period. Similar changes in velocity over one day have been noted in previous monitoring periods [Haycox *et al.* 2005b; Haycox *et al.* 2006a, 2006b]. The magnitude of the average velocity changes are significantly less than the velocity resolution of 2 ms^{-1} estimated for ultrasonic measurements, however, changes on individual ray-paths are more pronounced. For example, the greatest magnitude change in velocity is observed on the ray-path between transmitter one and receiver six (between 17th and 24th October 2007), when P-wave velocity decreases by $\sim 8 \text{ ms}^{-1}$ and S-wave velocity by $\sim 2 \text{ ms}^{-1}$.

Amplitude change for this monitoring period is shown in Figure 3-3b. P- and S-wave amplitudes decrease between the 16th and 24th October 2007. The decrease in amplitude is of similar order for both P- and S-waves ($\sim 0.3 \text{ dB}$) and again relates to the change in pressure and/or temperature adjacent to the deposition hole. Amplitudes remain low until the 6th November 2007 after which they gradually increase until the end of the data record; P-wave amplitudes increase by $\sim 0.3 \text{ dB}$ whilst S-wave amplitudes by $\sim 0.53 \text{ dB}$. Therefore, the temperature and pressure changes experienced around the deposition hole appear to influence S-wave amplitudes more than P-wave amplitudes. We cannot determine whether the velocity and amplitude changes observed here are due to either temperature, pressure, or both as the environmental changes occur almost synchronously (Figure 3-4).

The changes in amplitude and velocity between the 17th and 24th October 2007 have been further investigated by studying waveform data. We examined waveform data from along the ray-path between transmitter seven and receiver six since this path exhibited large variations in both velocity and amplitude. Figure 3-5 shows raw waveform data and CCRs for two periods of interest: preceding the amplitude and velocity low (10th October) and during the low (26th October). Waveforms recorded on 10th October (Figure 3-5a) are more energetic than waveforms recorded at the 26th October low. The short-term changes in pressure and temperature in the rockmass surrounding the deposition hole thus result in a decrease in signal amplitude. Changes in the attenuation of ultrasonic waves may occur due to changes in saturation (less/more fluid contained in micro-fractures and pore spaces) or a result of changes in crack density caused by opening or closing of pre-existing micro-cracks, or most probably a combination of the two. Similar, but opposing, behaviour has been noted in previous reporting periods [e.g. *Zolezzi at al. 2008*] although changes reported then were much larger (amplitude increased by ~3 times).

Figure 3-5b-c shows the cross correlation results for the waveforms shown in Figure 3-5a. Before the decrease in amplitude the waveforms are displaced to the left, for both P- and S-waves, indicating that the waveforms were faster before the amplitude drop. These differences can be interpreted as localised changes in the general rock properties rather than a systematic effect caused by the equipment since different transmitter-receiver ray-path pairs are affected to different extents.

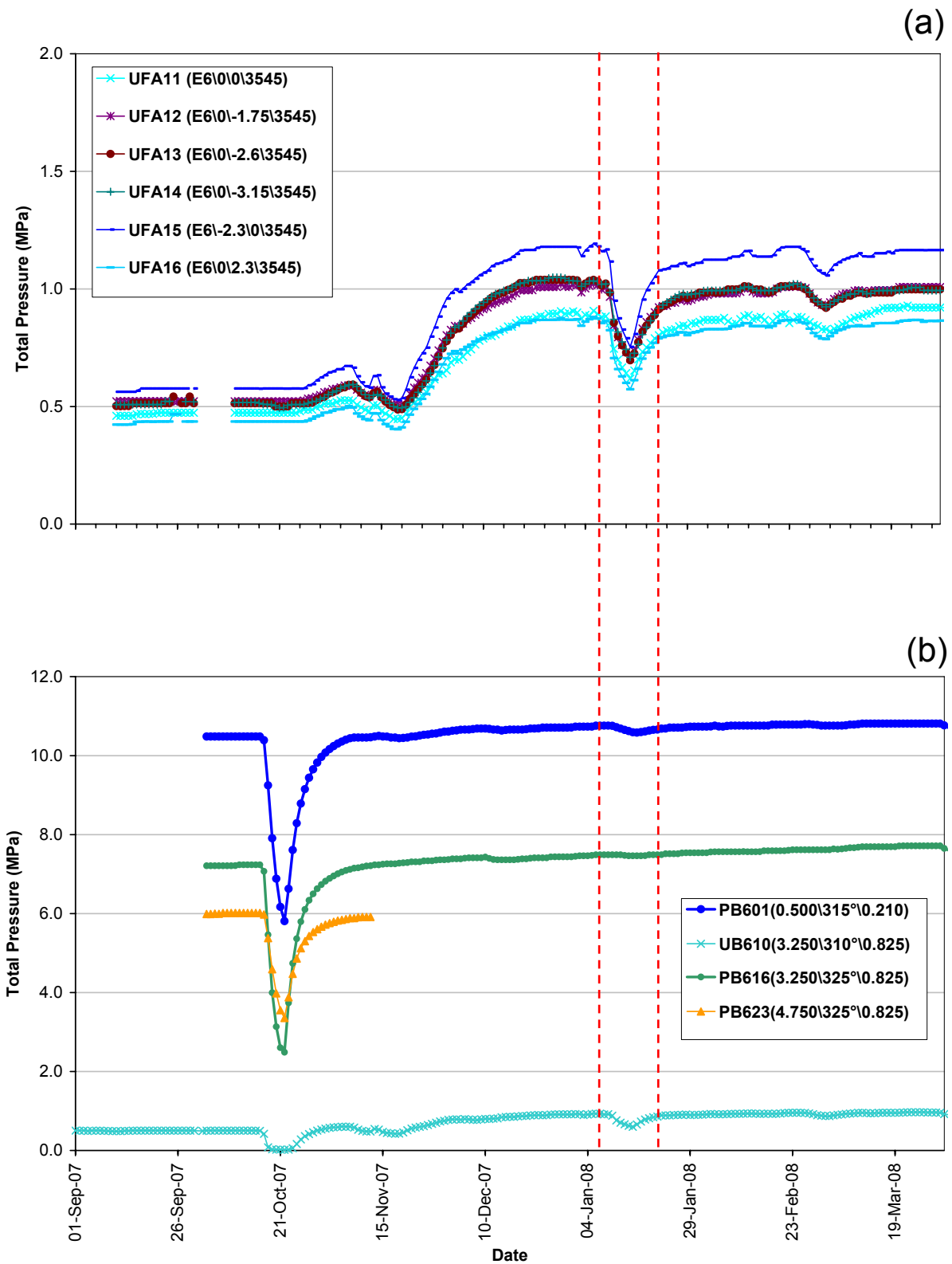


Figure 3-2: Total pressure in (a) the backfill over deposition hole DA3545G01 and (b) the rock adjacent to deposition hole DA3545G01 for the period between 1st September 2007 and 31st March 2008 [Goudarzi, 2008]. The dashed vertical lines indicate the period when simultaneous pressure changes occur in both the backfill above the deposition hole, and in the rockmass surrounding the deposition hole.

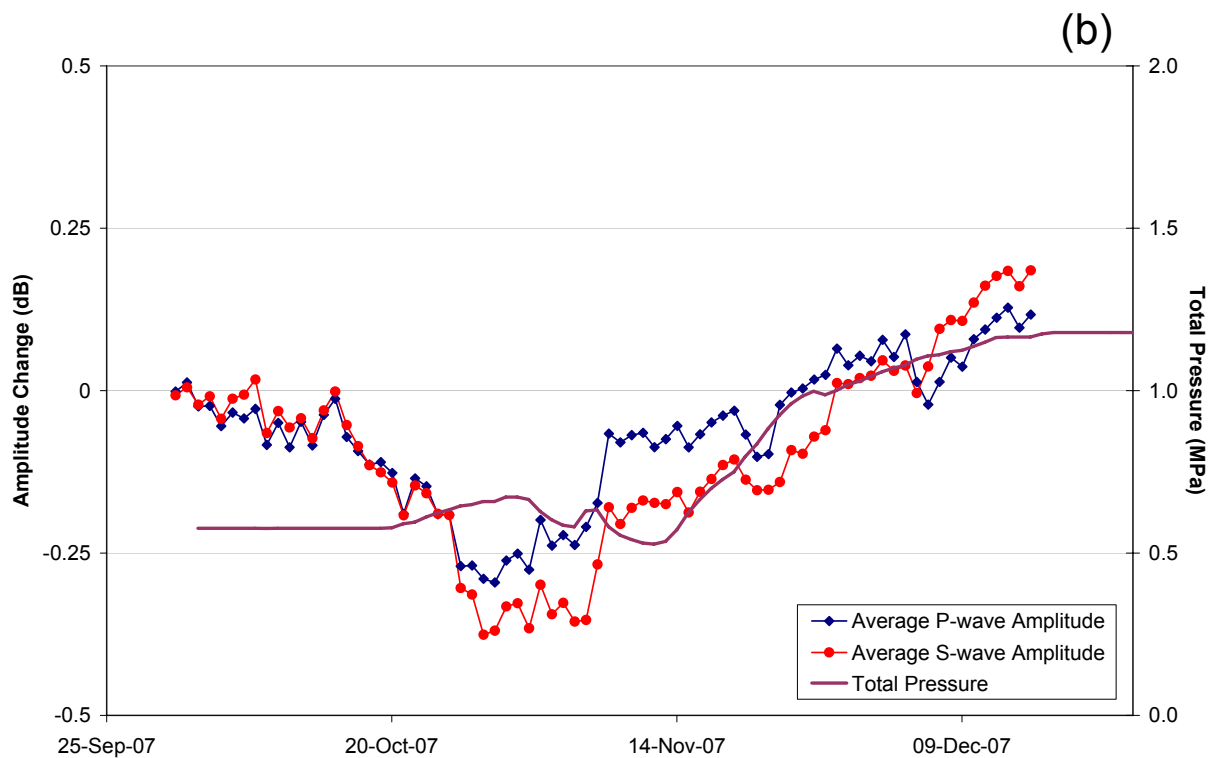
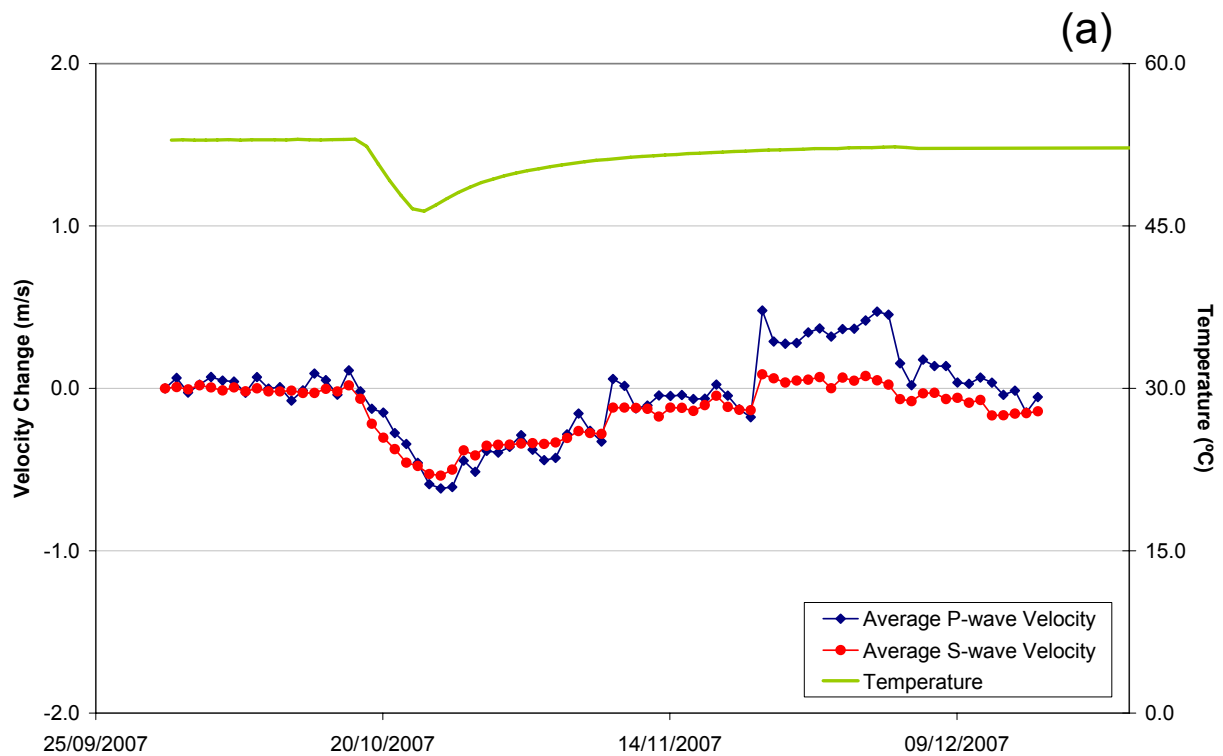


Figure 3-3: Average P- and S-wave (a) velocity change (ms^{-1}) and (b) amplitude change (dB), for this reporting period. Temperature of the surrounding rockmass (TR6045) and total pressure in the backfill (UFA15) are displayed on the secondary axes. Note that the graph covers the period up until 17th December when survey data stopped due to equipment malfunction.

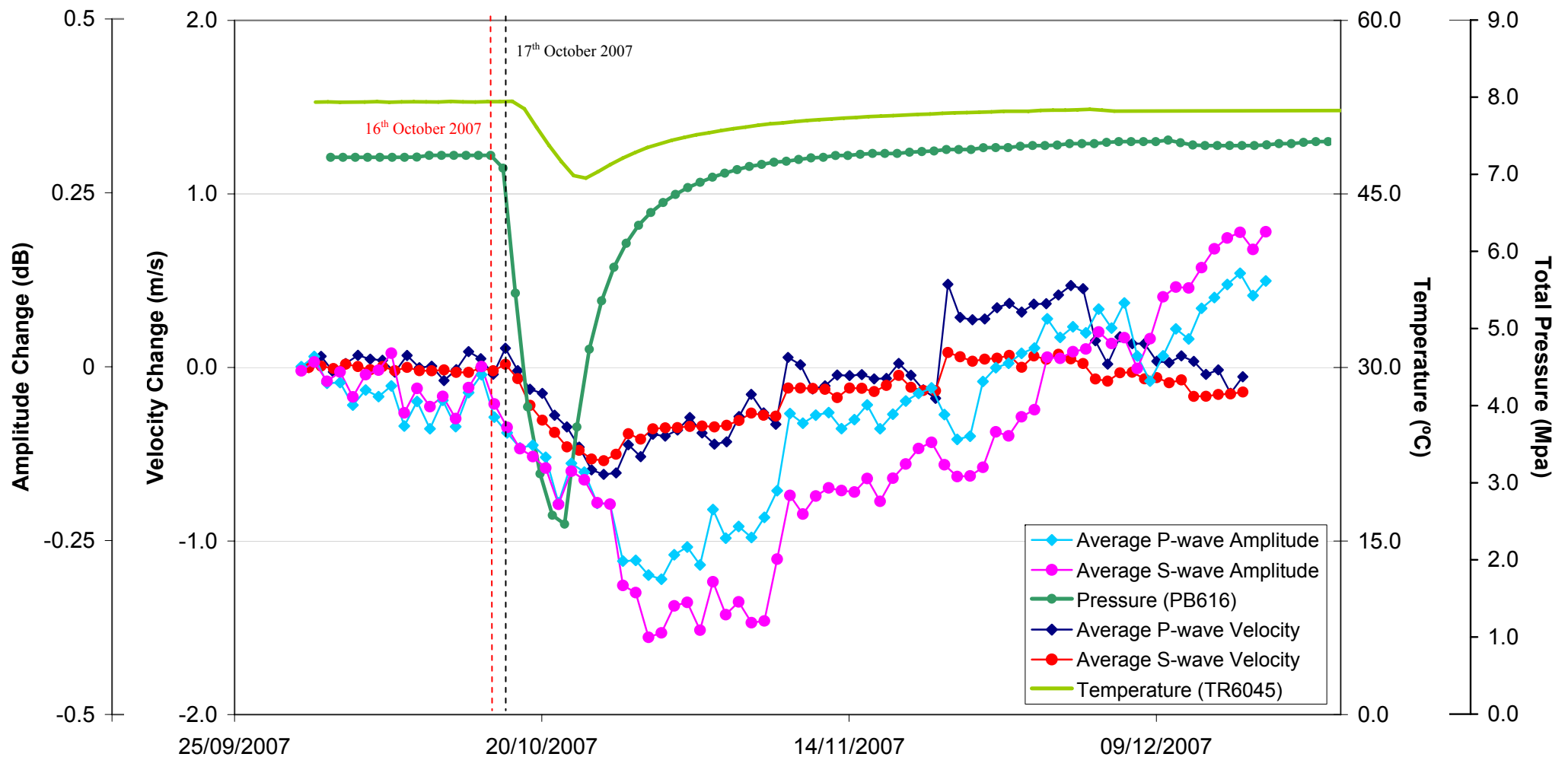


Figure 3-4: Summary diagram showing the correlation between P- and S-wave velocity and amplitude changes with the short-term temperature and pressure changes observed in the rockmass surrounding the deposition hole. It is unclear whether the average velocity and amplitudes are more strongly reacting to changes in temperature, pressure, or both as these changes occur over the same time period.

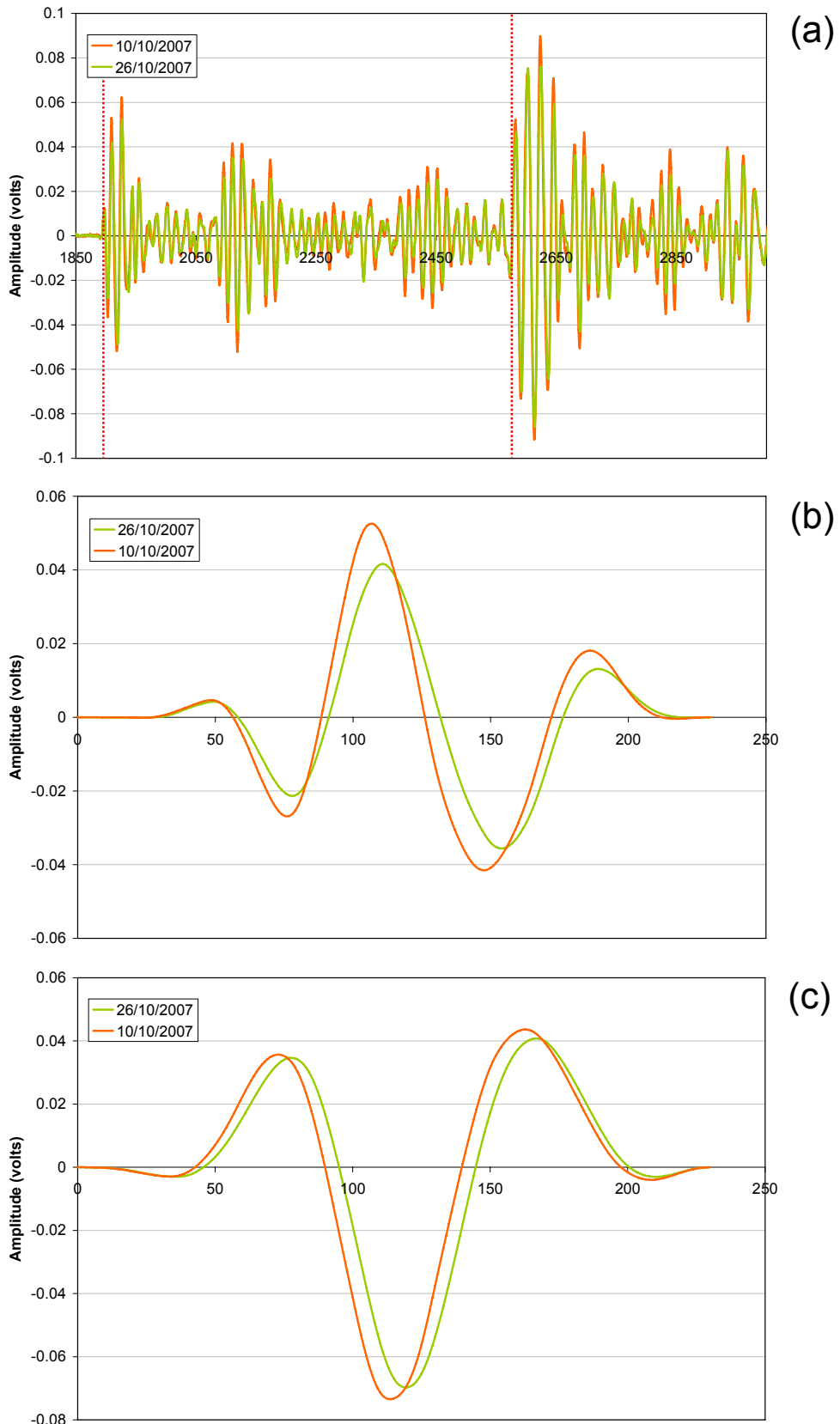


Figure 3-5: Example plots of (a) raw waveform data (dashed red line are the first arrivals of P (first) and S (secondary)); and cross correlation (CCR) windows for the ray-path between transmitter seven and receiver six for (b) P- waves and (c) S-waves. Example surveys from before the recorded drop in amplitudes on 10th October (orange line), during the drop 26th October (green line).

Pettitt et al. [1999] categorised ray-paths from ultrasonic surveys into six types depending on their orientation with respect to the deposition hole and the in-situ stress field (Figure 3-6). Ultrasonic results are interpreted in terms of the disturbed and damaged regions around the void during the excavation phase of the experiment. *Pettitt et al.* [2000] undertook three-dimensional elastic stress modelling to describe these zones of stress.

Figure 3-7a-d shows the velocity changes recorded along the ‘S3’ category of ray-paths. Category ‘S3’ ray-paths pass within centimetres of the deposition hole through the excavation damaged zone, in a region of low compressive or tensile stress. These particular ray-paths have been chosen because they provide a comparison of velocity changes along the length of the deposition hole. Each plot is accompanied by a schematic diagram showing a perspective of the region through which the ray-path passes and also the transmitter-receiver configuration. Two of the four ‘S3’ category ray-paths selected show changes in velocity for both P- and S-waves. Ray-path 1-6 (Figure 3-7b) registers velocity changes of -8ms^{-1} (P-wave) and -2ms^{-1} (S-wave). Further ray-paths associated with velocity changes will be presented later in this section.

Figure 3-8 shows velocity changes recorded along the ‘S1’ category of ray-paths. These ray-paths pass through a region of compressive stress and permanent damage close to the wall of the deposition hole and are imaged by relatively high AE activity during periods of excavation. In general there is very little change in velocity with the only exception being ray-path 7-6 (Figure 3-8b) where similar velocity changes as those along the ‘S3’ category are recorded.

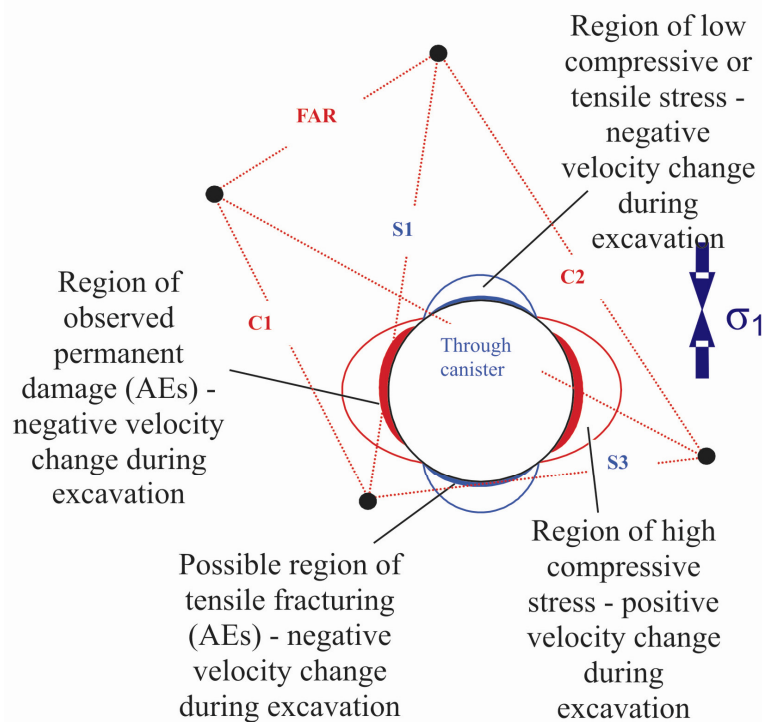


Figure 3-6: Interpretation of the ultrasonic results during excavation in terms of disturbed and damaged regions around the deposition hole. Zones of induced stress are inferred from elastic modelling and the σ_1 orientation, after *Pettitt et al.* [1999].

In order to accurately analyse small and consistent changes in the recorded measurements we compare the average velocity changes across each of the ray-path categories described in Figure 3-6. All of the ray-path categories show the same general trend (Figure 3-9a-b). Both P- and S-wave velocities are fairly consistent until 20th October 2007 when the average value decreases; this is followed by a much more gradual increase until the end of the data record. Ray-path 'C2' exhibits the greatest change with average changes in the region of 3ms⁻¹ (for P-waves) and 2ms⁻¹ (for S-waves). For P-waves, category 'Far' exhibits a greater reduction in velocity than S-waves, and overall P-wave velocities display more variation. For S-waves, category 'S1' and 'Far' remain almost constant throughout and exhibit virtually no response to the changes occurring around mid-October. For each of the ray-path categories (for both P- and S-waves) the lowest velocity measured is on the 24th October 2007 which coincides with the temperature and pressure drop recorded in the rockmass surrounding the canister (Figure 3-3).

The amplitude change across the five category ray-paths is shown in Figure 3-10. The trend is very similar for each of the ray-paths and very similar to the changes noted in velocity. P-wave amplitudes show a reduction in magnitude on the 20th October, reaching a low on the 25th October and increasing steadily after this time. S-wave amplitudes exhibit more variation with the same change recorded on the 20th October and also a rapid increase occurring on the 28th November. The largest change occurs along category 'S3' and 'C2' ray-paths with an average drop in amplitude of ~0.5dB (on the 25th October) for both P- and S-waves, and an average increase of ~0.3dB (on the 28th November) for S-waves. The smallest change occurs along category 'Far' with a maximum change of ~0.2dB (for S-waves) and ~0.1dB (for P-waves) recorded on the 25th October. There is also a decrease (~0.3dB) in S-wave amplitudes for categories 'C1' and 'S1' that starts on the 19th November that is not registered in any of the other records.

Figure 3-11 shows the changes in rock properties calculated using average velocities and amplitudes for the five category ray-paths. Young's Modulus (Figure 3-11a) describes the stiffness of the rockmass and Poisson's Ratio (Figure 3-11b) is the ratio of latitudinal to longitudinal strain. Crack Density (Figure 3-11c) is a measure of the extent of fracturing per unit volume, and Saturation (Figure 3-11d) relates to the number of cracks per unit volume containing fluids. Crack Density and Saturation of the rock mass are determined using the method of *Zimmerman and King* [1985], as described in Appendix II.

Young's Modulus starts decreasing on the 20th October, reaching a low on the 25th October, showing the same trend as P- and S-wave velocity and mimicking the temperature and pressure changes in the rock around the deposition hole (green line is the temperature change, Figure 3-11a). Poisson's ratio exhibits very little change throughout the entire data record. Crack density shows opposing behaviour to that of Young's Modulus, showing an increase on the 20th October, reaching a period high on 25th October. Saturation exhibits the same overall trend as P-wave velocity change (Figure 3-9a) but with much greater variation than any of the other parameters. The largest response is evident in categories 'S3' and 'C2' for Young's Modulus and Crack density, 'Far' for Poisson's ratio, and 'Far' and 'C1' for Saturation. These changes can be attributed to the rapid changes in pressure and/or temperature in the rockmass surrounding the deposition hole.

During the period for which data were actively recorded (1st October to 17th December) the velocity and amplitude results have shown a decrease that starts on 20th October, reaching a peak excursion on the 24th – 25th October. Following this excursion the velocity and amplitude results tend to return to values similar to those before the onset of the change. The variations are particularly relevant for rays that belong to ray-path categories ‘C2’ and ‘S3’. Response to environmental change is more evident in P-wave velocity than S-wave velocity (compare Figure 3-9a and Figure 3-9b). Likewise, S-wave amplitudes are more sensitive to environmental changes than P-wave amplitudes (compare Figure 3-10a and Figure 3-10b). Amplitude and velocity changes are lower than the previous report period and apart from the short-term changes in temperature and pressure this report period is comparably stable. It is unclear whether the velocity and amplitude changes are responding more strongly to the drop in temperature, pressure or both as these changes occur over the same time period.

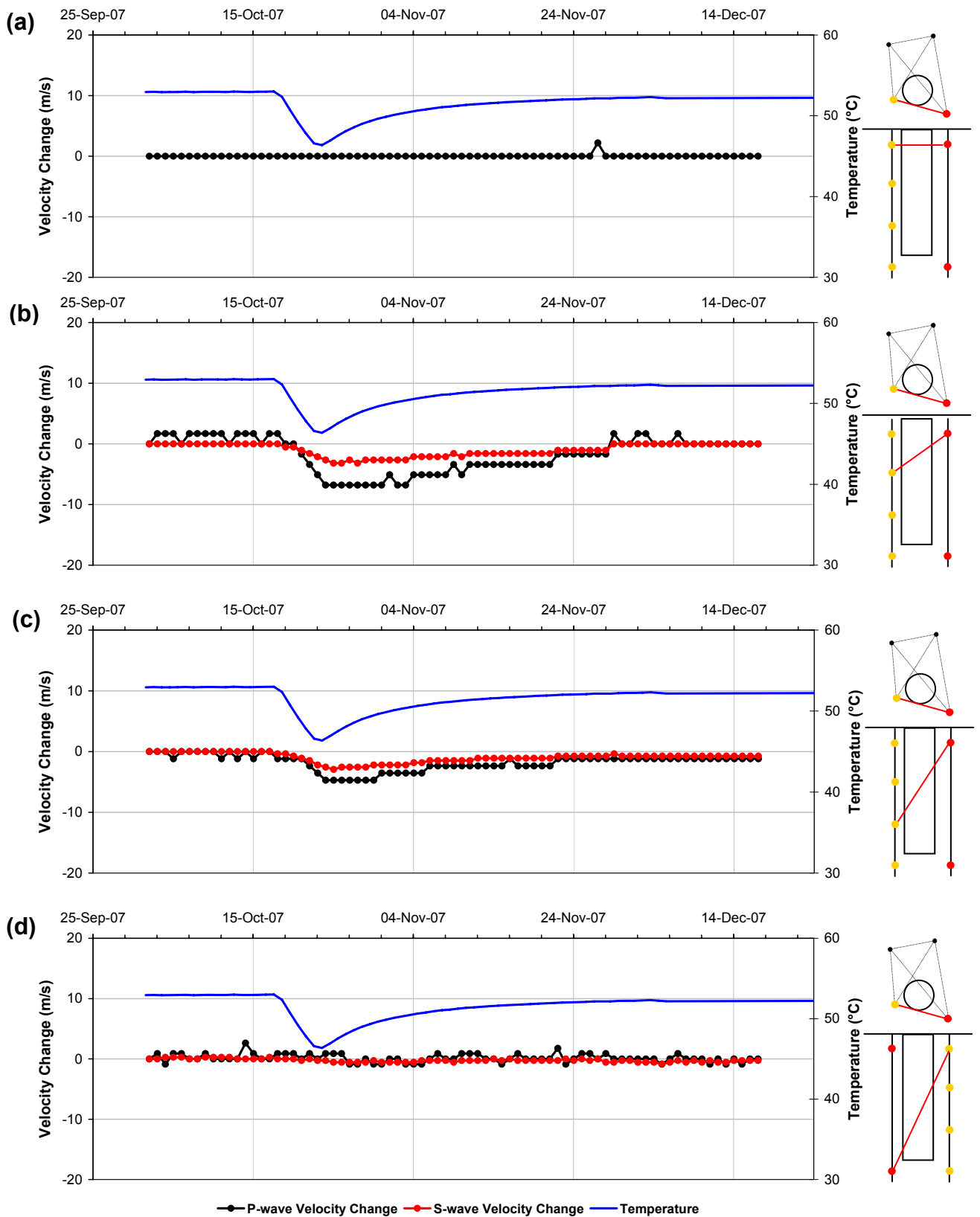


Figure 3-7: Velocity changes measured on ray-path category 'S3' (Figure 3-6) for deposition hole DA3545G01. Ray-paths shown are from transmitter (t_n) to receiver (r_n) for (a) $t_n=1, r_n=5$; (b) $t_n=1, r_n=6$; (c) $t_n=1, r_n=7$ and (d) $t_n=4, r_n=1$. Schematic diagrams on the right indicate the relative positions of transmitter (red) and receiver (gold). Temperature (TR6045, blue line) is displayed on the secondary axes.

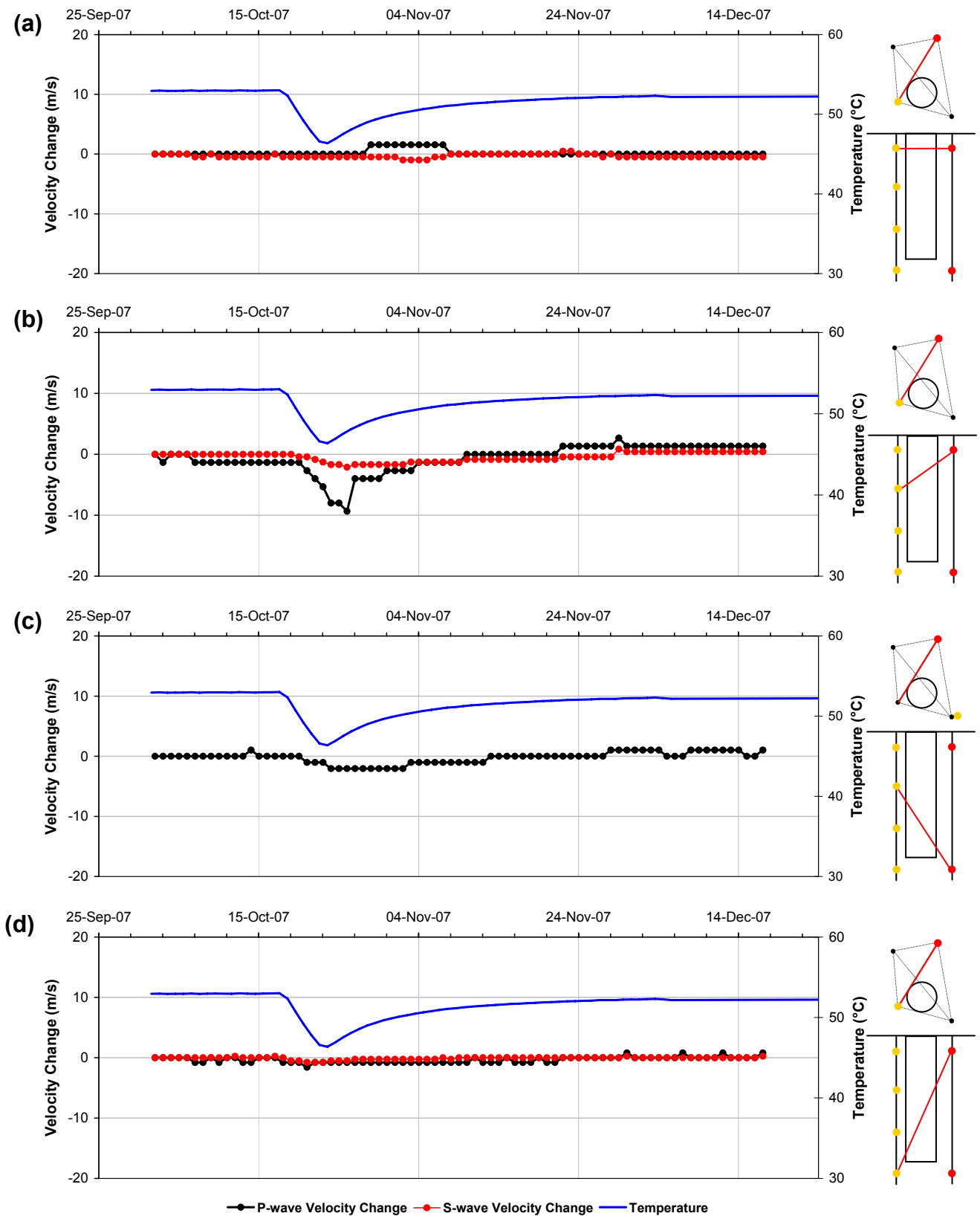


Figure 3-8: Velocity changes measured on ray-path category 'SI' (Figure 3-6) for deposition hole DA3545G01. Ray-paths shown are from transmitter (t_n) to receiver (r_n) for (a) $t_n=7, r_n=5$; (b) $t_n=7, r_n=6$; (c) $t_n=7, r_n=7$ and (d) $t_n=7, r_n=8$. Schematic diagrams on the right indicate the relative positions of transmitter (red) and receiver (gold). Temperature (TR6045, blue line) is displayed on the secondary axes.

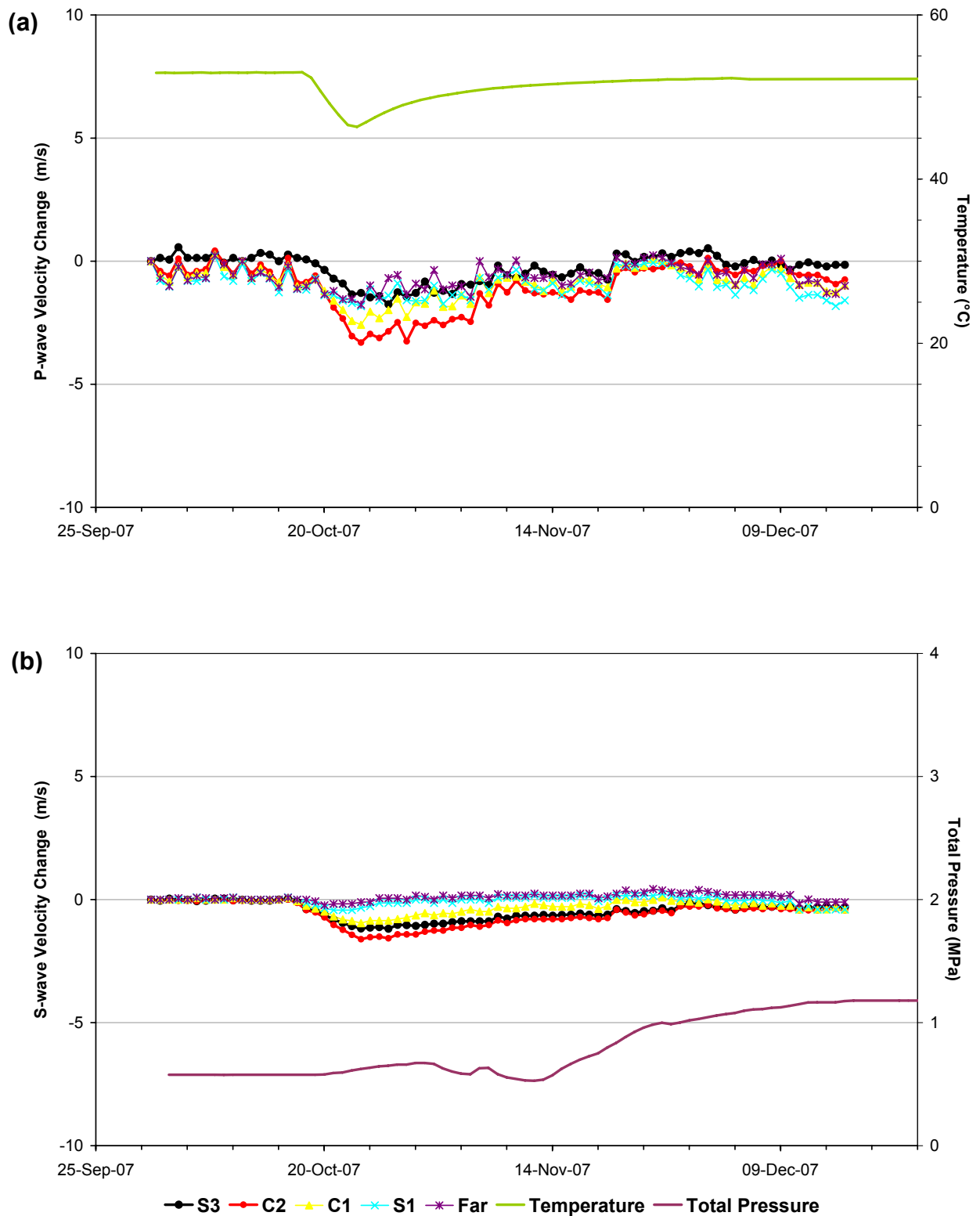


Figure 3-9: Average velocity change for the five category ray-paths (S1, S3, C1, C2, Far) around deposition hole DA3545G01 for (a) P-waves shown with temperature (instrument TR6045) on the secondary axis; and (b) S-waves shown with pressure (instrument UFA15) on the secondary axes.

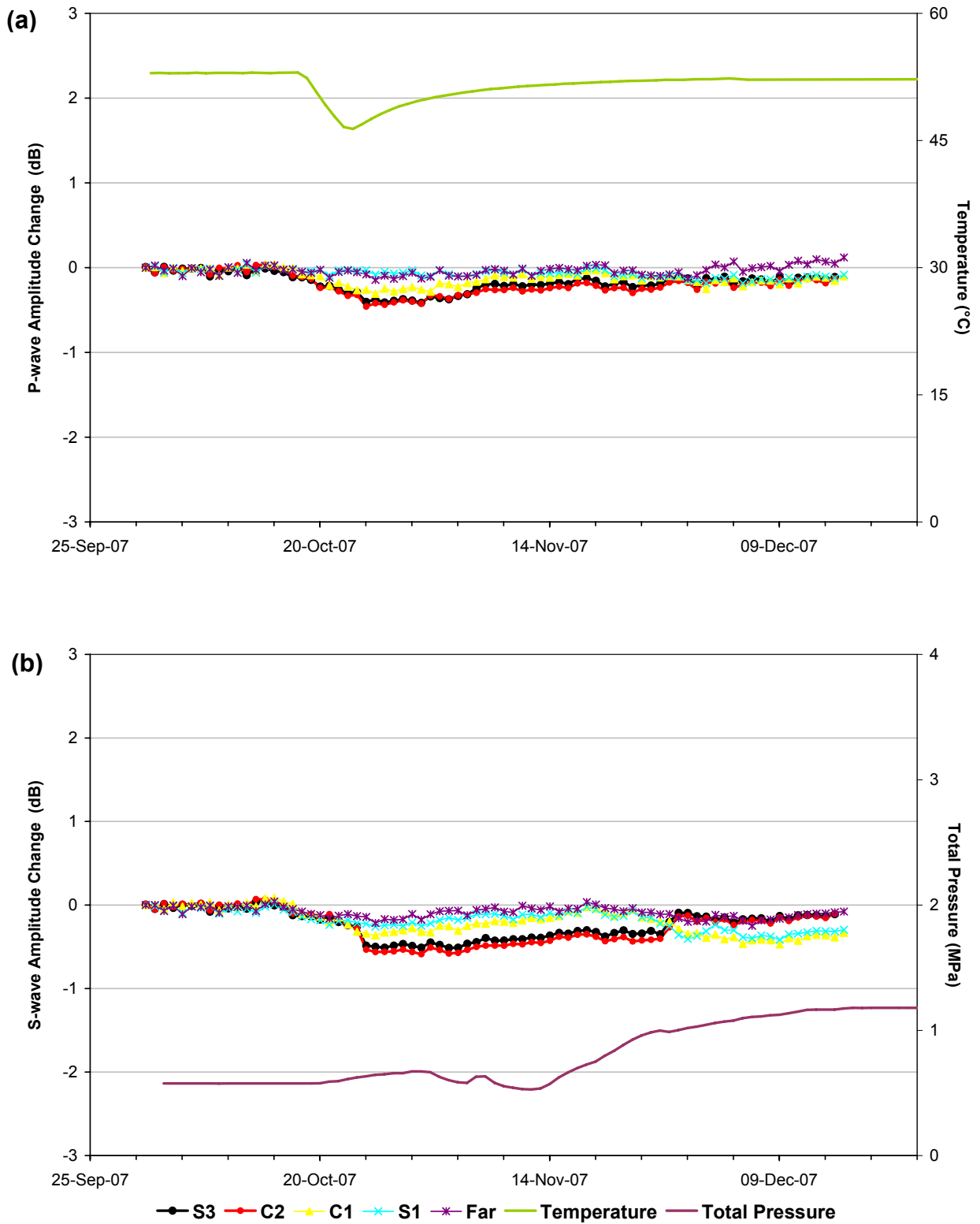


Figure 3-10: Average amplitude change for the five category ray-paths (S1, S3, C1, C2, Far) around deposition hole DA3545G01 for (a) P-waves shown with temperature (instrument TR6045) on the secondary axis; and (b) S-waves shown with pressure (instrument UFA15) on the secondary axes.

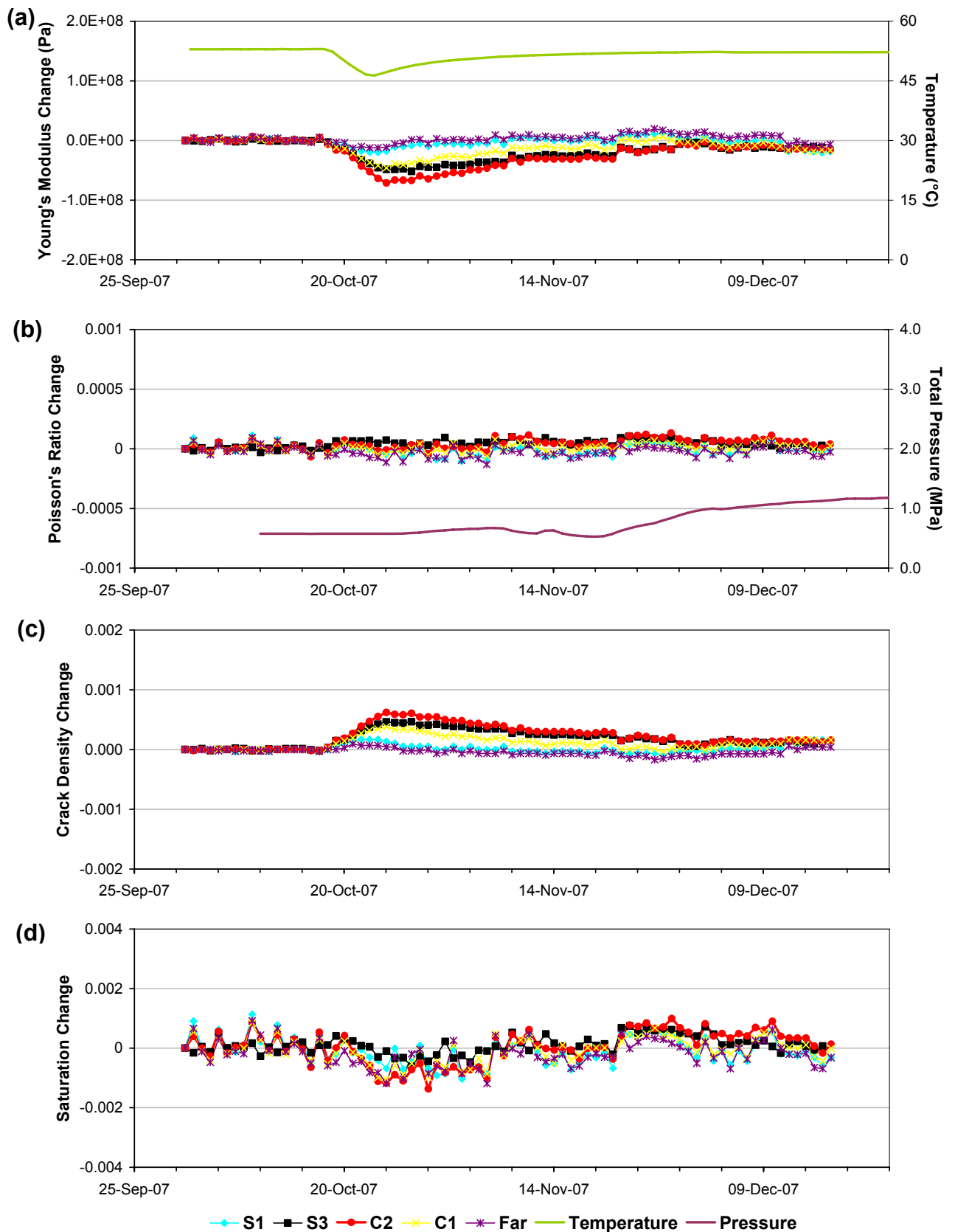


Figure 3-11: Changes in rock parameters, calculated using average P- and S-wave velocities and amplitudes, for the five ray-path categories for (a) Young's Modulus, (b) Poisson's Ratio, (c) Crack Density and (d) Saturation. Temperature (TR6045) and pressure (UFA15) are displayed on the secondary axes.

3.2 Acoustic Emissions

The parameters used to process AEs are displayed for reference in Appendix III. In total there are 171 located events from 180 triggered events. All of the events have good waveforms with clear P- and S-wave arrivals and are therefore located with a high degree of accuracy and confidence. The estimated uncertainty for these events around the deposition hole is less than 5cm, determined using calibration ‘hits’ performed within the deposition holes after excavation (see Appendix II for further details).

A trigger is described as an event that has been acquired by the monitoring system, but may not be of sufficient energy or ‘quality’ to be located during the processing procedure. Noisy events, those that appear masked by electrical, environmental, or man-made noise, have been removed from the dataset allowing a more accurate representation of the fracturing occurring within the rock. The temporal distributions of the 180 AE triggers is shown in Figure 3-12b, and the 171 successfully located AE events in Figure 3-12a. The average number of located AE’s per day throughout this monitoring period is 0.90 so there is a constant (although low-level) increase in activity over the past three six-month reporting periods (Table 3-1). The maximum number of AEs recorded in a single day was on the 22nd January, 2008 when 21 events were triggered during a twelve hour period.

Table 3-1: Average daily number of located AEs events for the six monthly report periods starting 1st October 2004 and finishing with the end of this report period on 31st March 2008.

Time Period	Average Number of Events per Day
1 st October 2004 to 31 st March 2005	0.32
1 st April 2005 to 30 th September 2005	0.21
1 st October 2005 to 31 st March 2006	0.27
1 st April 2006 to 30 th September 2006	0.80
1 st October 2006 to 31 st March 2007	0.40
1 st April 2007 to 30 th September 2007	0.63
1 st October 2007 to 31 st March 2008	0.90

Figure 3-13 shows the locations of AEs relative to the physical features of the Prototype Repository. Instrumentation boreholes are represented by the brown vertical lines, and the tunnel and deposition hole are represented by the grey wireframe structures. Most of the events (115) are tightly clustered around the deposition hole. Several events do locate away from the deposition hole, most notably a cluster of events that occur close to the tunnel floor (Cluster T in Figure 3-13). Example waveforms, recorded on different channels, from each of the clusters are shown Figure 3-14 and demonstrate the high quality data that is recorded using the array.

Cluster A consists of 55 AE events and is located on the SE side of deposition hole DA3545G01. This cluster was observed in previous monitoring periods [*Haycox et al.* 2006a and 2006b; *Zolezzi et al.* 2007 and 2008]. The centre of this cluster is N, E, D = (268.7, 921.1, 455.1) (Table 3-2). The events in this cluster occur along the S3 ray-path category (Figure 3-13), which passes through a region of low-compressive or tensile

stresses (Figure 3-6), and are close enough together to be considered as occurring on the same feature (Figure 3-15). The temporal distribution of these events is presented in Figure 3-16a, and shows that they occur throughout the monitoring period.

Cluster B consists of 24 AE events located on the SW side of deposition hole DA3545G01 (Figure 3-15) and are very tightly grouped together with an average location of N, E, D = (269.1, 919.7, 455.1) (Table 3-3). The same cluster was observed in the previous report by Zolezzi et al. [2008]. The events in clusters B and C are distributed evenly throughout the monitoring period (Figure 3-16b) and along the S1 ray-path category which passes through a region characterised by compressive stress (Figure 3-6).

Cluster C occurs in a previously active volume and contains 9 events, it is included in this report for continuity between this and the previous report by Zolezzi et al., [2007].

Cluster D (Figure 3-15) occurs in the high compressive stress region diametrically opposite to clusters B and C during excavation, and occurs early in 2008 (Figure 3-17a). No evidence of this cluster was present in the previous two reporting periods. Activity has been seen in this volume (*Pettit et al. 1999*) although not at the precise depths observed here. The average event location in this cluster (consisting of 12 events) is N, E, D = (270.2, 921.5, 457.2) (Table 3-4).

Cluster T consists of 24 events and occurs some distance from the deposition hole, close to the tunnel floor (Figure 3-14), and is associated with the peak in AE activity observed in this monitoring period. Activity in this area has not been observed during previous monitoring periods, or during the excavation and heating phases of the project. The events are located around the base of the tunnel (Table 3-5) and appear to strike in a NE-SW direction toward deposition hole DA3545G01 (Figure 3-15). This cluster has an orientation along the axis of principle stress (red arrows, Figure 3-18), but could also be associated with increased uncertainties as the events are located outside the array volume. The majority of the events (21) in this cluster are concentrated into a single 12 hour period on the 22nd January, 2008 (Figure 3-17b) so represent a considerable increase in AE activity, the largest reported since November 2004.

Table 3-2: Mean Position for the 55 events located in Cluster A.

	Northing (m)	Easting (m)	Depth (m)
Minimum	268.60	921.00	455.00
Maximum	268.80	921.25	455.20
Mean	268.74	921.07	455.11
Standard Deviation	0.022	0.039	0.022

Table 3-3: Mean Position for the 24 events located in Cluster B.

	Northing (m)	Easting (m)	Depth (m)
Minimum	269.12	919.69	454.90
Maximum	269.00	919.81	455.15
Mean	269.07	919.73	455.08
Standard Deviation	0.017	0.014	0.021

Table 3-4: Mean Position for the 12 events located in Cluster D.

	Northing (m)	Easting (m)	Depth (m)
Minimum	269.90	921.30	457.00
Maximum	270.40	921.80	457.40
Mean	270.22	921.53	457.21
Standard Deviation	0.076	0.074	0.064

Table 3-5: Mean Position for the 24 events located in Cluster T.

	Northing (m)	Easting (m)	Depth (m)
Minimum	266.90	924.30	448.03
Maximum	268.20	923.10	449.90
Mean	267.39	923.91	448.89
Standard Deviation	0.202	0.211	0.274

Figure 3-18 shows plan views of events recorded during excavation, the initial phase of heating, the previous monitoring period and this reporting period. The majority of the events are located in the NE and SW quadrants. These regions are subject to increased compressive stresses, as identified from the in-situ stress field by *Pettitt et al.* [1999]. Smaller clusters are observed in the orthogonal regions of low-compressive or tensile stress. This pattern is consistent throughout the excavation and heating phases.

Clusters A, B and C are located in the same area as clusters observed in previous monitoring periods and are thus occurring along the same structures. The events could be a continuation of activity in the damage zone, created either by movement on pre-existing micro-cracks, or as a result of extension or formation of new micro-cracks in the existing damaged region. It is important to note that some events have positioned in regions where no activity has been observed in the past. Cluster D occurs in the high compressive stress region, events have been seen to occur in this location but not at the precise depths reported here. Cluster T is apparently occurring in a new volume in the floor of the tunnel not previously highlighted as an existing damaged region, so the link between these events and pre-existing macrofractures should be investigated further. In the previous six-month report *Zolezzi et al.* [2008] investigated the possibility that the clustering of events was related to movement of the instrumentation but no evidences of this was found. Figure 3-19 shows AE magnitudes for the five response periods discussed in Table 4-1 from the beginning of heating and pressurisation. During the latest six-month period there has been a slight increase in both the peak magnitude and overall distribution of magnitudes compared to the previous report period, but they remain below the highest magnitudes observed in the initial phases of heating and pressurisation (response periods 1 and 2).

Most of the event locations are consistent with previous results and low magnitudes characterise the entire acoustic emission data set therefore we can assume that the rock mass around the deposition holes has remained relatively stable throughout this six-month period.

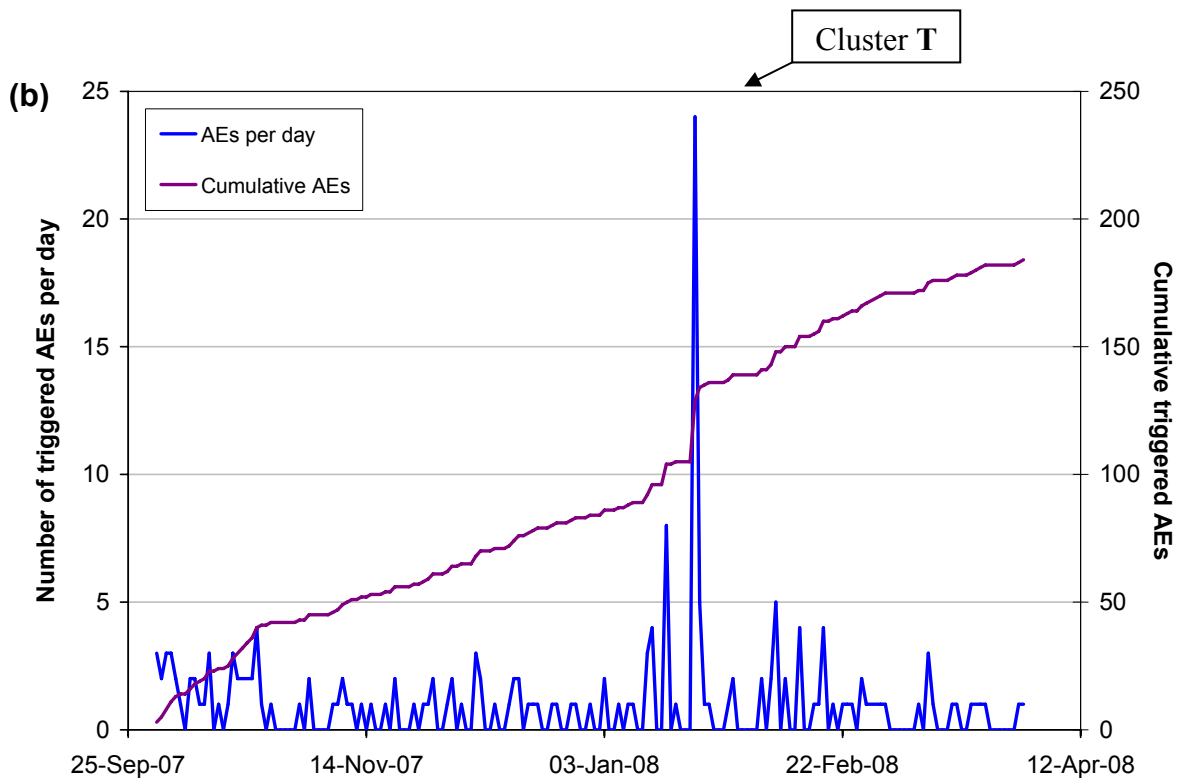
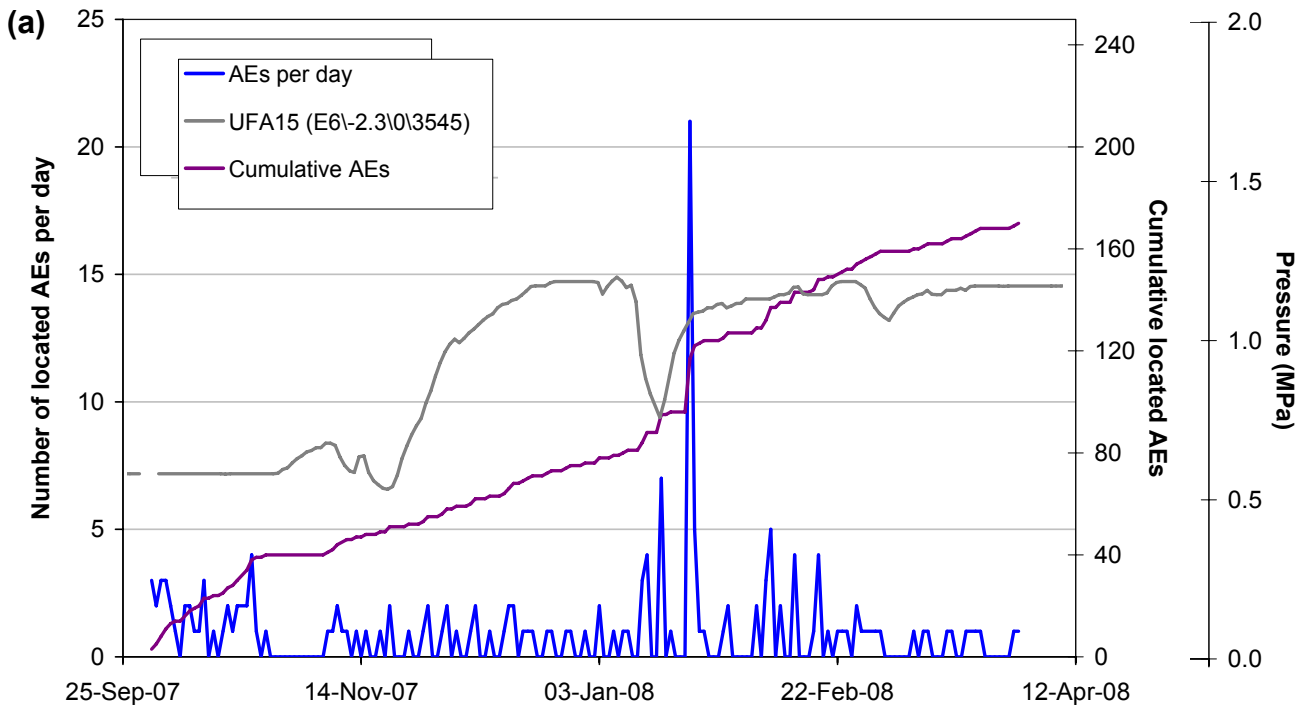


Figure 3-12: Temporal distribution of (a) located AEs and (b) AE triggers; number of events per day on left axis (shown by the blue line) and cumulative AE events on the right-hand axis (shown by the purple line) also shown in (a) is the pressure (UFA15) in the tunnel backfill over the deposition hole.

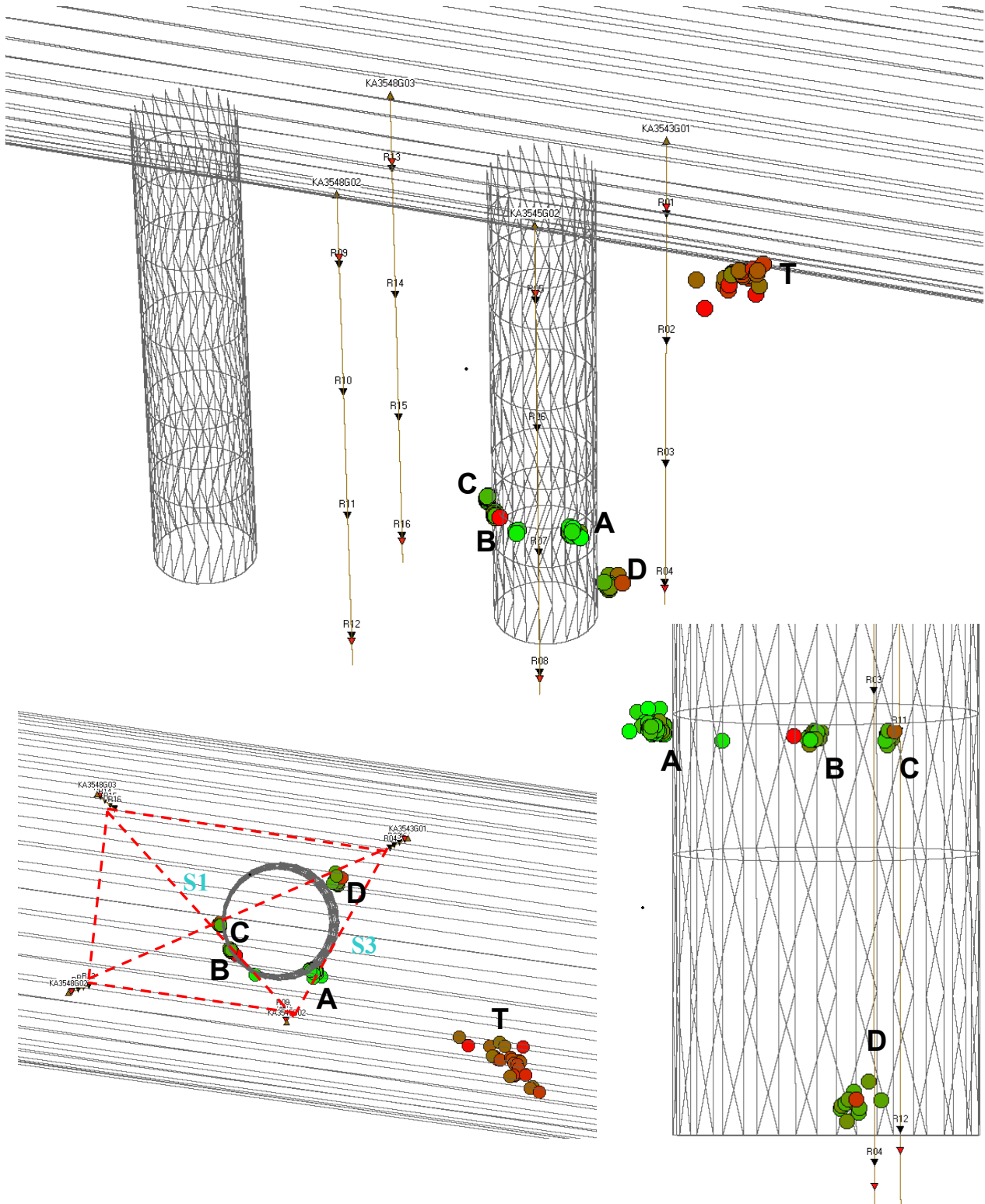


Figure 3-13: Three views showing the clustered AE activity located around deposition hole DA3545G01. (Top: Oblique view looking north; Bottom left: Plan view with the five category ray-paths used in the ultrasonic survey shown relative to the deposition hole; Bottom right: Close-up view of the deposition hole).

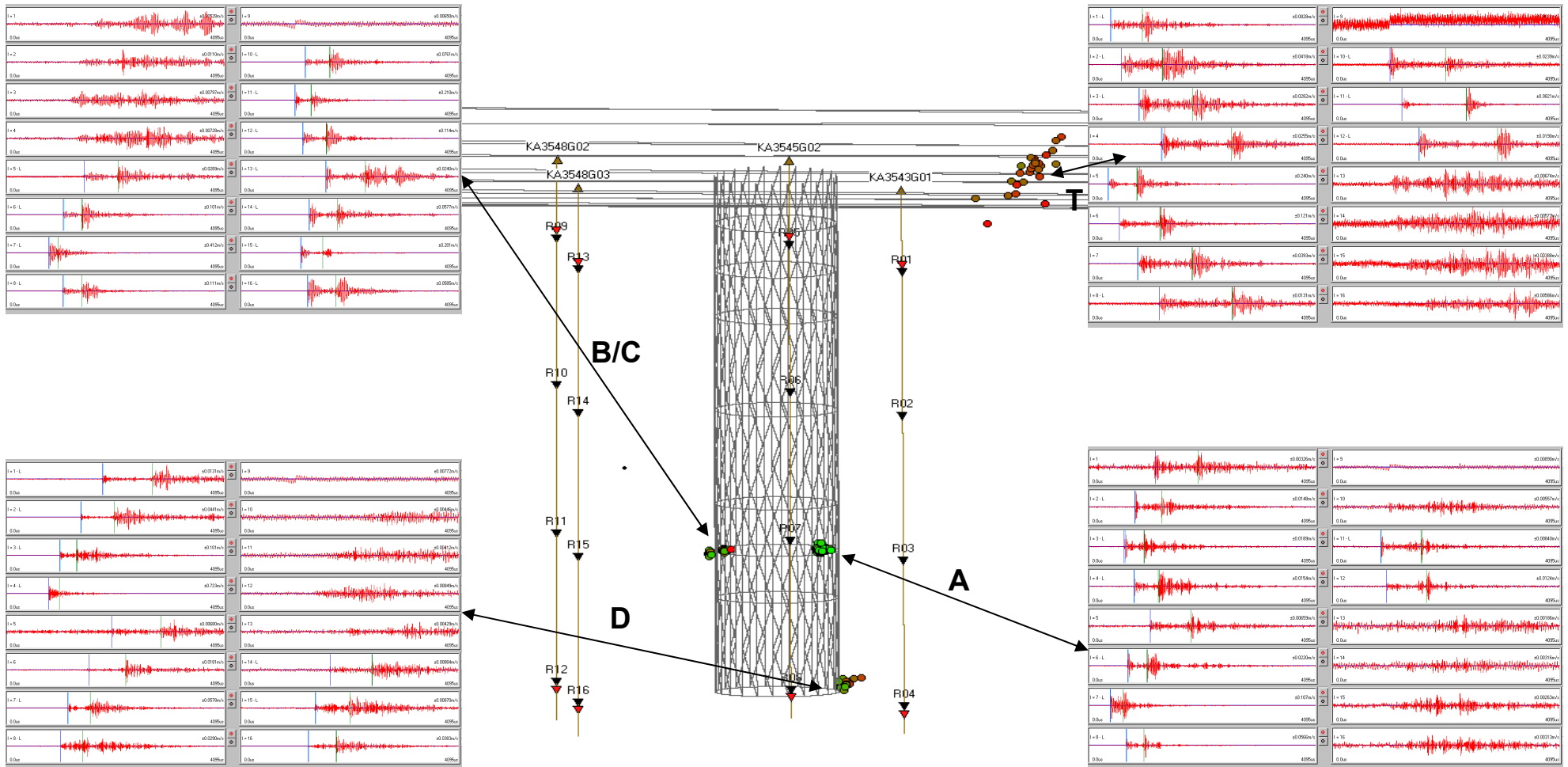


Figure 3-14: Waveforms for a selected event from each of the four clusters shown in relation to a transverse view of AE activity.

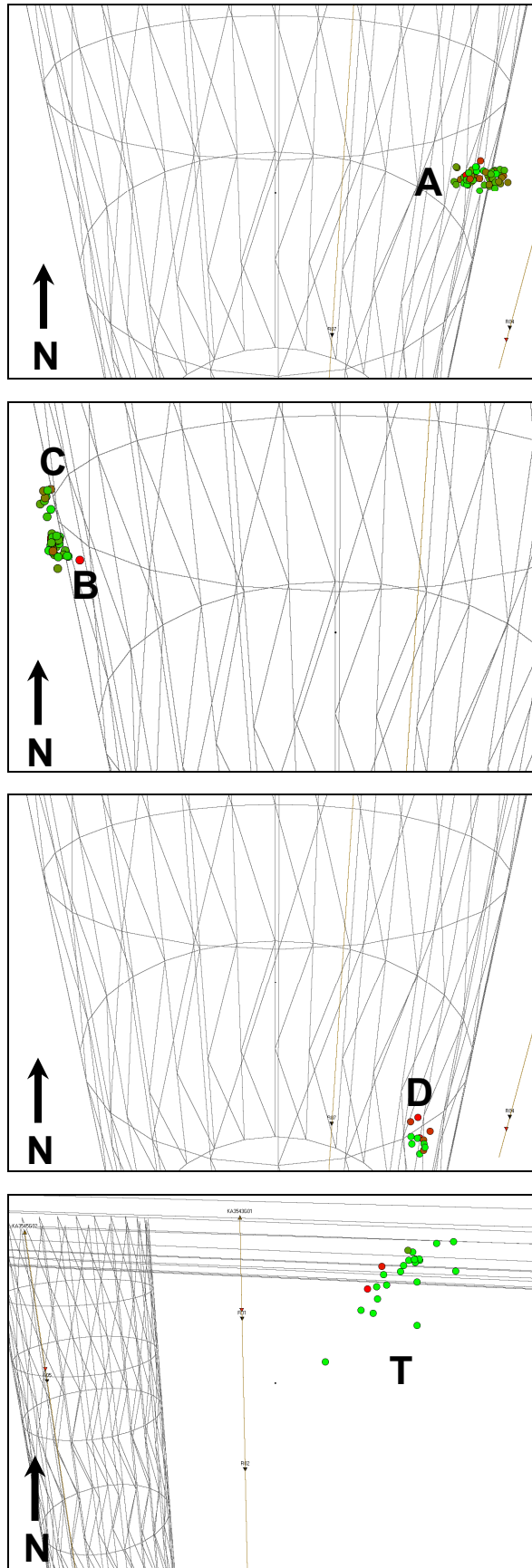


Figure 3-15: Close up views of Cluster A (top) containing 55 events, Cluster B (top-middle) containing 24 events, Cluster D (bottom-middle) containing 12 events and Cluster T (bottom) containing 24 events. Cluster T is located some distance away from the deposition hole and the majority of the events occurred during a twelve hour period on the 22nd January, 2008. Note the apparent strike of the events.

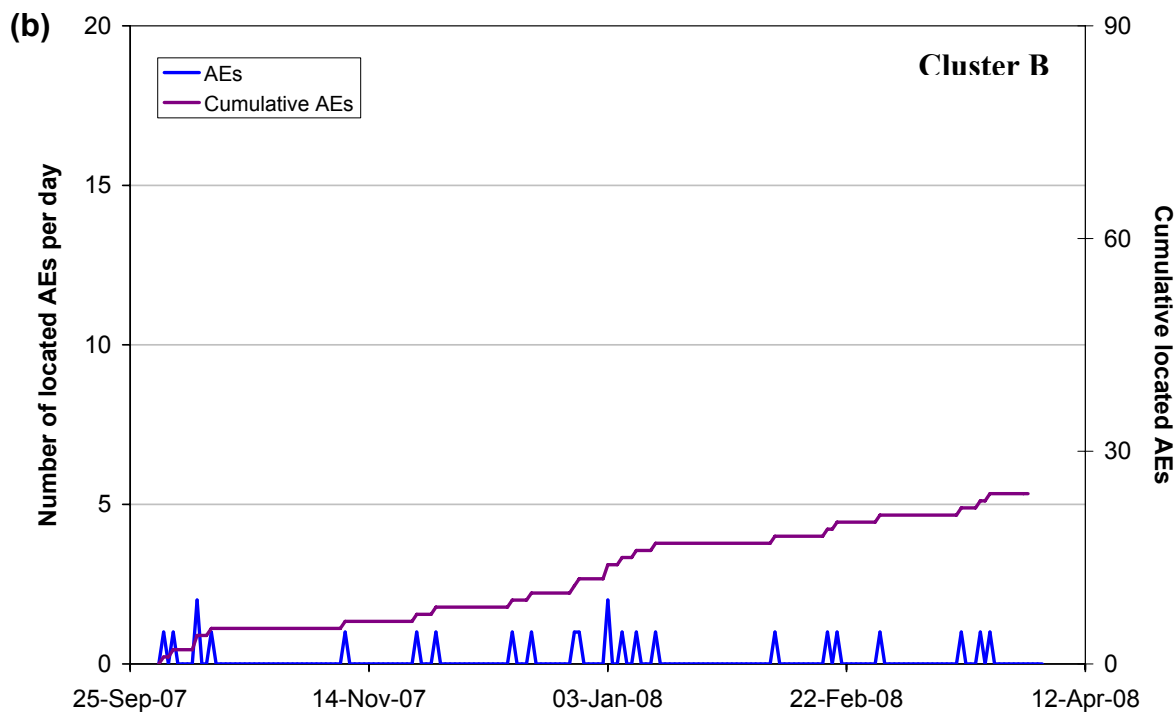
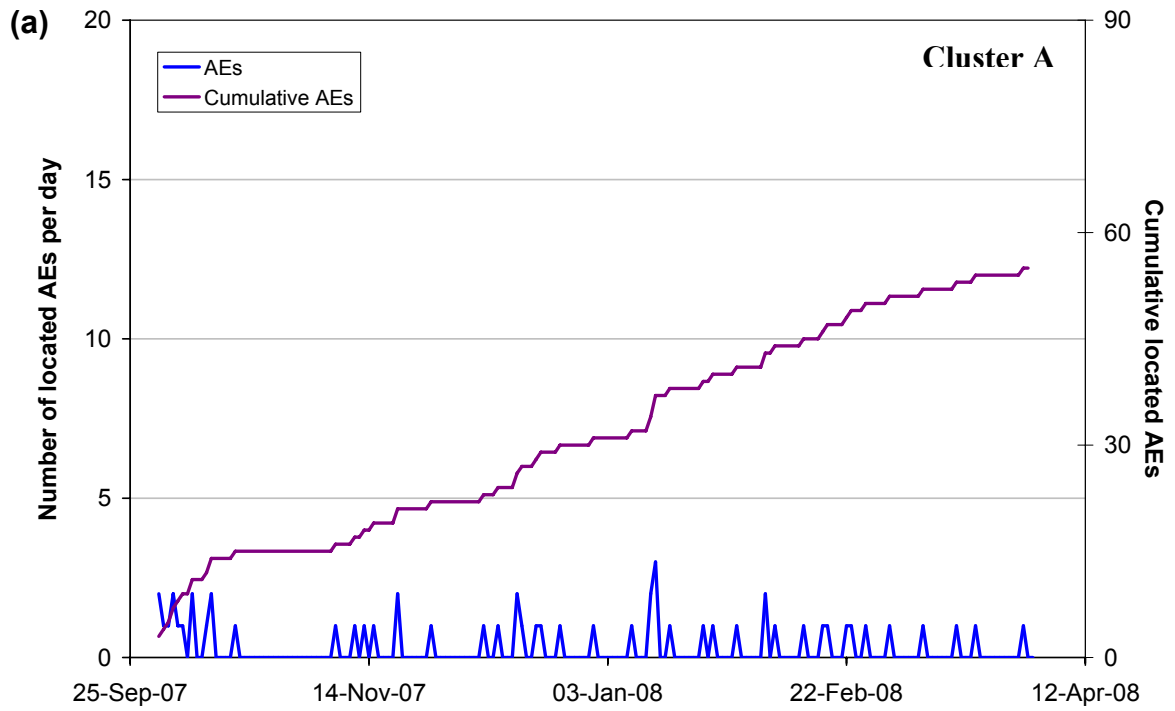


Figure 3-16: Temporal distribution of located AEs in clusters a) Cluster A and b) Cluster B. Plots show the number of events (blue line) per day on left axes and cumulative number (purple line) of events for the entire monitoring period on right axes.

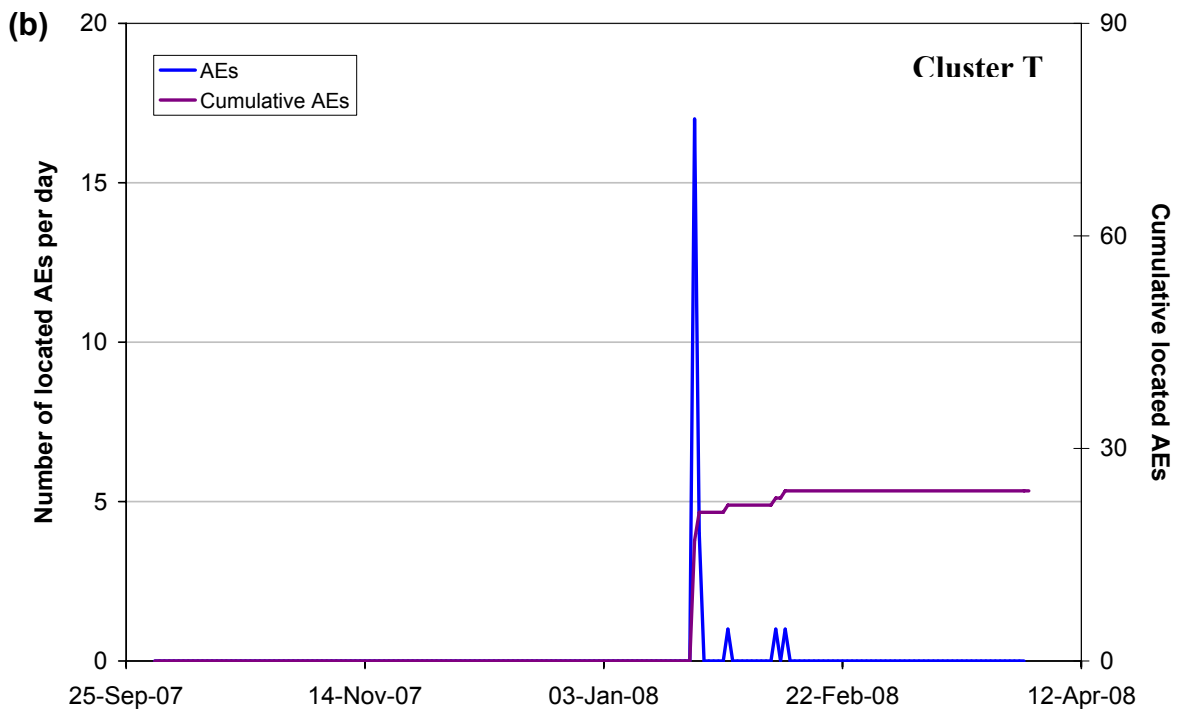
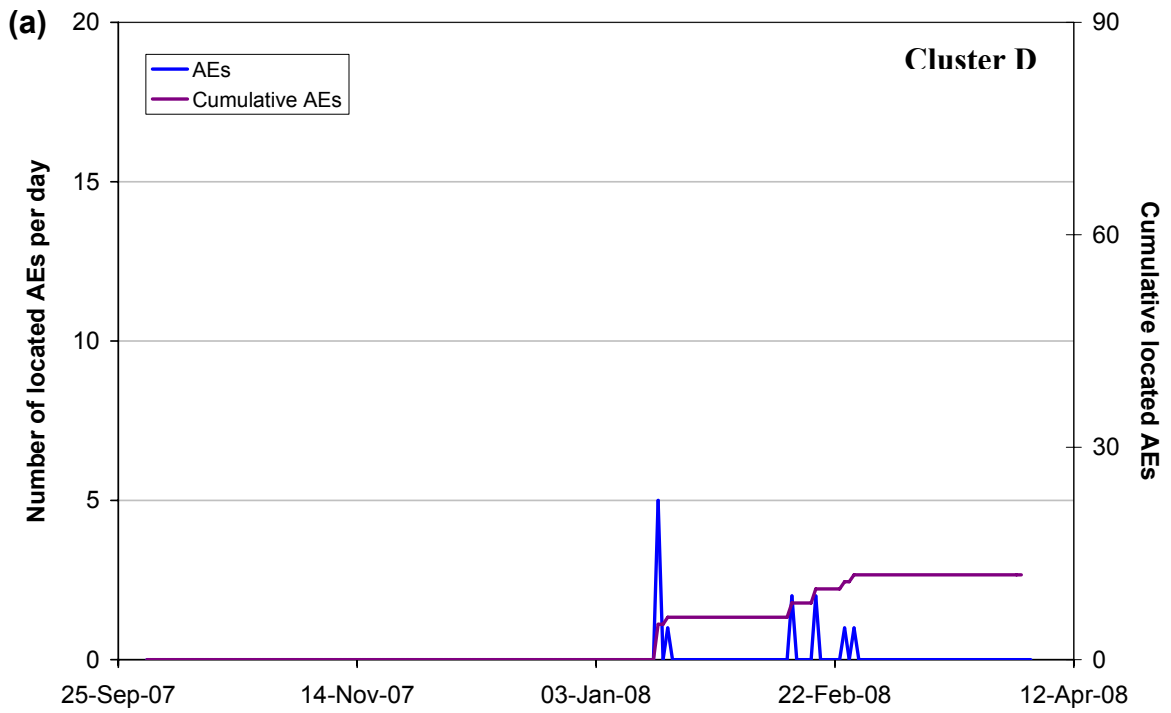


Figure 3-17: Temporal response plot of located AEs in the identified clusters for a) Cluster D and b) Cluster T. Plots show the number of events per day (blue line) on left axes and cumulative number of events (purple line) for the entire monitoring period on right axes.

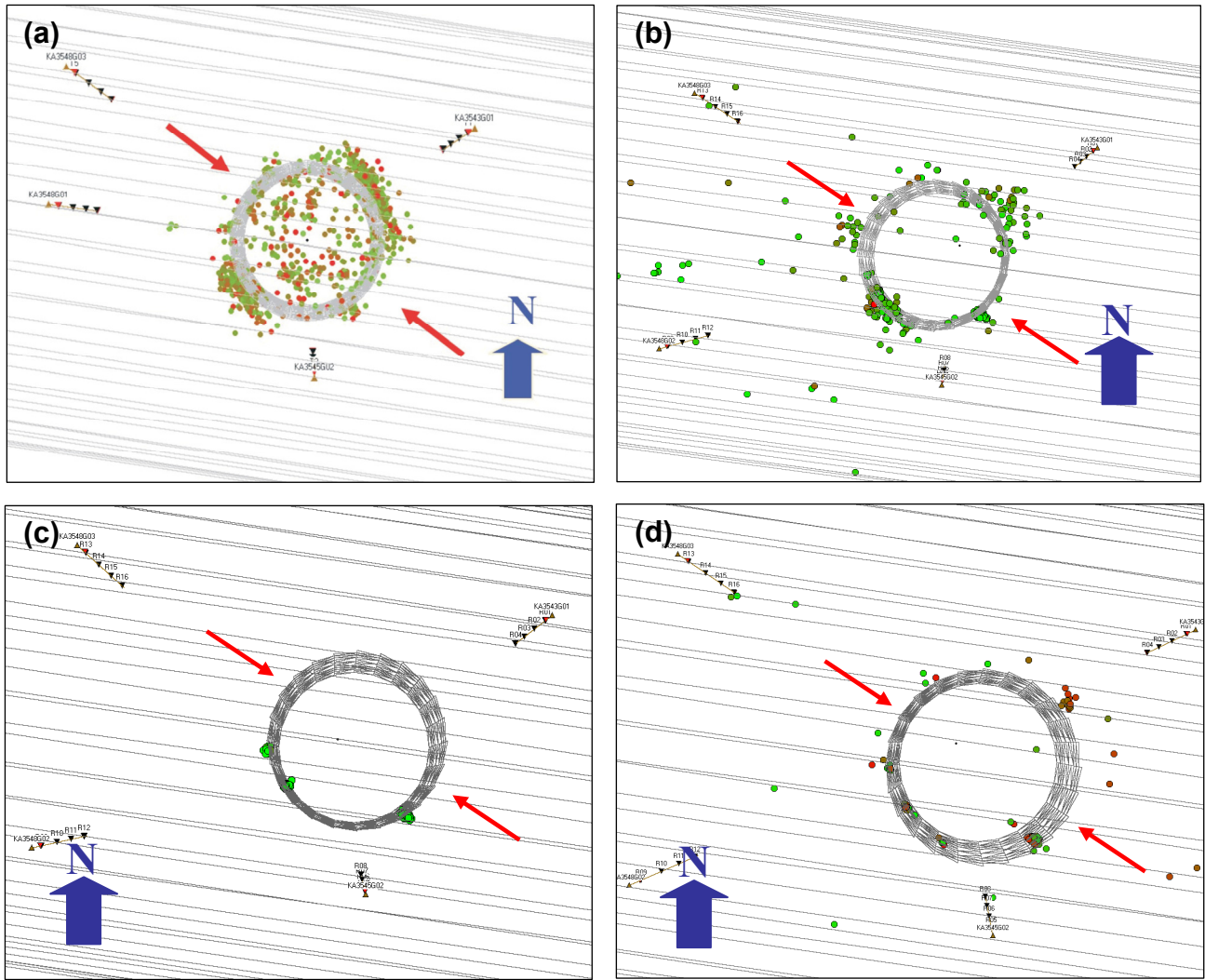


Figure 3-18: Plan view of total AEs located around deposition hole DA3545G01 during (a) the excavation phase, (b) monitoring during heating through to 01/04/2007, (c) previous monitoring phase during heating, from 01/04/2007 until 31/09/2007, and (d) this monitoring phase (01/10/2007 – 31/03/2008). The red arrows mark the orientation of principle stresses.

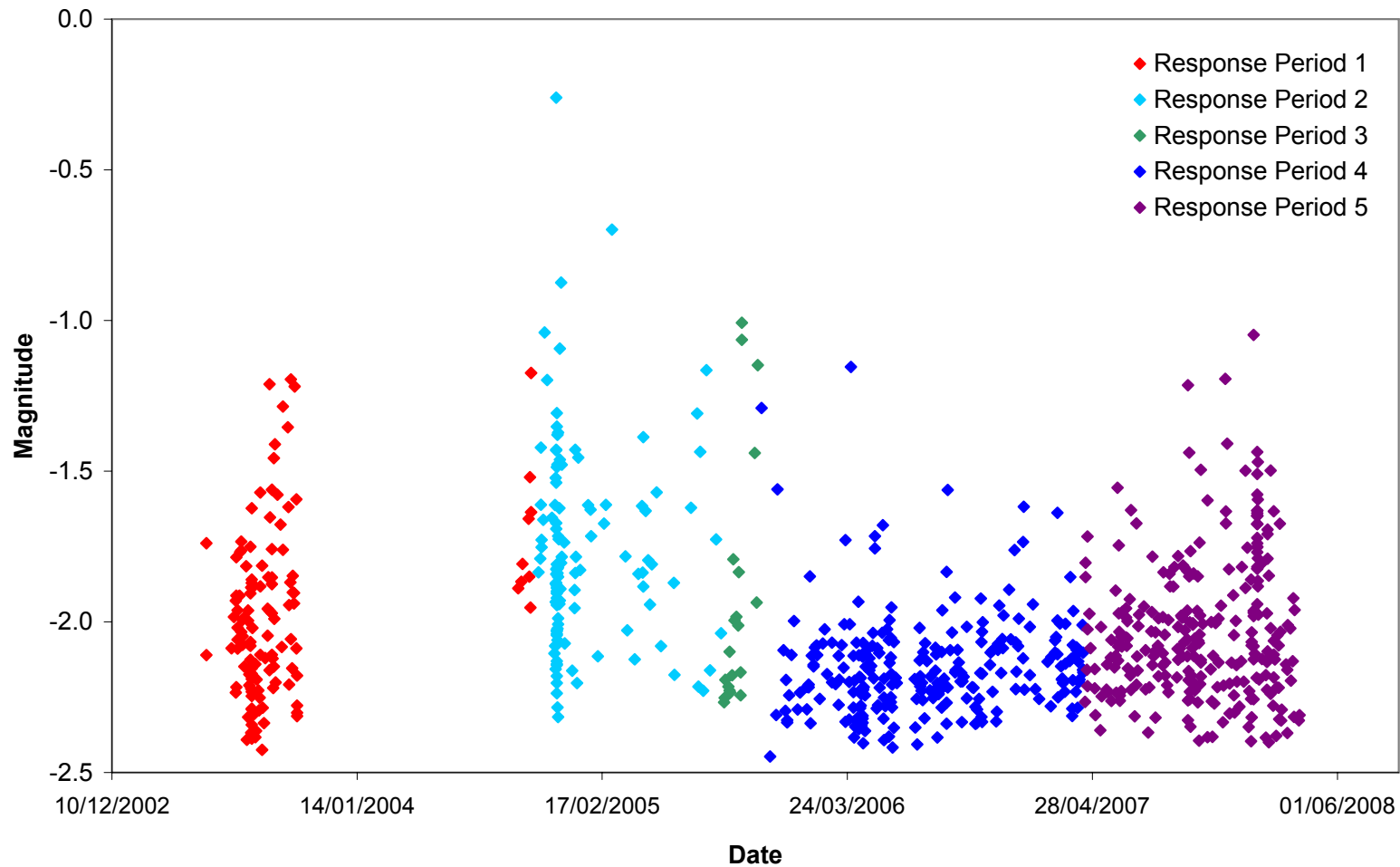


Figure 3-19: Chart displaying AE magnitudes recorded from the beginning of heating and pressurisation. Events are coloured by response period as defined in Table 4-1. During this latest period there has been a slight increase in event magnitudes (both in peak magnitude and distribution) compared to the previous one, but remain below the highest magnitudes observed in the initial phase of heating (response periods 1 and 2).

4 Conclusions

4.1 Monitoring Between October 2007 and March 2008

- This report describes the results from acoustic emissions (AE) and ultrasonic monitoring around a canister deposition hole (DA3545G01) in the Prototype Repository Experiment at SKB's Hard Rock Laboratory (HRL), Sweden. The monitoring aims to examine changes in the rock mass caused by an experimental repository environment, in particular due to thermal stresses induced from canister heating and pore pressures induced from tunnel sealing. Monitoring of this volume has been performed during excavation [*Pettitt et al.* 1999], and during stages of canister heating and tunnel pressurisation [*Haycox et al.* 2005a and 2005b; *Haycox et al.* 2006a and 2006b; *Zolezzi et al.* 2007 and 2008]. The period covered by this report is between 1st October 2007 and 31st March 2008, and is the sixth instalment of a six-monthly processing and interpretation of the observations and results.
- Results from the velocity analysis reveal a drop in the average velocity between 21st October and 25th October, 2007, and is of similar order for both P- and S-waves ($\sim 0.7\text{ms}^{-1}$). The largest change in velocity is observed on the ray-path between transmitter seven and receiver six when P-wave velocity decreases by $\sim 8.0\text{ms}^{-1}$ and S-wave velocity by $\sim 2.0\text{ms}^{-1}$ between 21st and 25th October. After this, both P- and S-wave velocities gradually increase for the next month ($\sim 0.6\text{ms}^{-1}$). Another velocity jump ($\sim 0.35\text{ms}^{-1}$ for P-waves) is observed on the 21st November, 2007 and following this the velocities increase steadily for the remainder of the period (S-waves by $\sim 0.2\text{ms}^{-1}$ and P-waves by $\sim 0.6\text{ms}^{-1}$) (Figure 3-3).
- The decrease in velocity at the end of October, 2007 can be attributed to the drop in pressure and/or temperature in the rock adjacent to the deposition hole. The magnitude of the average velocity change is less than the resolution of 2ms^{-1} estimated for ultrasonic measurements, but changes on individual ray-paths are more significant.
- Similar changes are also observed for amplitudes: a decrease of $\sim 0.3\text{dB}$ for both P- and S-waves between 21st and 25th October, remaining low until the 6th November, followed by a steady increase for the remainder of the period: P-waves by $\sim 0.3\text{dB}$ and S-waves $\sim 0.53\text{dB}$. This would indicate that environmental changes (pressure, temperature) appear to influence S-wave amplitudes more than P-wave amplitudes.
- Changes in Young's Modulus very closely mimic the changes in temperature, Crack Density undergoes the same changes at the same times but the changes in magnitude are opposite in sign, i.e. when Young's Modulus increases Crack Density decreases. Poisson's ratio shows very little variation throughout the data record. Saturation exhibits similar behaviour to Young's Modulus but with much greater variation than the other parameters. Overall, the ray-path categories follow the same general trend with the largest response evident in: categories 'S3' and 'C2' for Young's Modulus and Crack density; category 'Far'

for Poisson's ratio; and categories 'Far' and 'C1' for Saturation. These changes can be attributed to the rapid changes in pressure and temperature in the backfill and/or adjacent to the deposition hole DA3545G01.

- In total there were 180 acoustic emissions, of which 171 have been located with a high degree of confidence. The frequency of triggering increased by ~50% since the last monitoring period with a maximum of 21 triggers recorded in a single 12 hour period on the 22nd January, 2008.
- The majority of located AEs are positioned in four tight clusters around deposition hole DA3545G01; labelled A, B, C and D. Cluster A is made up of 55 events and located on the south-east side, Cluster B (24 events) and Cluster C are on the south-west side, and Cluster D (17 events) is on the NE side of the deposition hole. Clusters A, B and C were observed in the last two report periods [Zolezzi *et al.* 2007 and 2008]. Cluster D has not been identified previously but is located in a region of activity which occurred during excavation [Pettitt *et al.* 2000]. The events in each cluster are close enough together to be considered as occurring along the same geological feature, and may be occurring at specific positions due to the presence of pre-existing structures, either generated during excavation or at an intersection with a pre-existing micro-fracture. Zolezzi *et al.* [2008] investigated the possibility that any of the instruments had moved in order to explain the presence of these clusters, but found no evidence to support this hypothesis.
- A number of AE's (24) have located some distance from the deposition hole (Cluster T). This has not been observed in previous reports, either during the excavation or the pressurisation phases. The events position SE of the deposition hole around the base of the tunnel and appear to strike towards the deposition hole along the axis of principle stresses (Figure 3-18d). The rapid occurrence of the events in this cluster indicates that there may be a newly formed structure in a region not previously highlighted as an existing damaged region. It would be interesting to examine the relationship between these locations and pre-existing macroscopic fractures in the floor and the tunnel.
- Apart from the events in Cluster T, the AEs located during this reporting period are consistent with previous results, i.e. no events are positioned in regions where activity has not been observed in the past. The events can therefore be interpreted as a continuation of activity in the damaged zone. We observed an increase in the number of AEs with respect to the previous monitoring period; however, the numbers of events are relatively low and indicate that the rock mass around the deposition holes has remained fairly stable during this period.

4.2 Summary of Monitoring from the Heating and Pressurisation Phase

- Monitoring of the heating and pressurisation phase at the Prototype Repository Experiment has been conducted since March 2003. Analysis of the AEs and ultrasonic measurements is split into five response periods (following previous reports). Table 4-1 presents a summary of the observations from ultrasonic monitoring thus far, and Table 4-2 provides interpretations of the rock response.

- Figure 4-1 shows average P- and S-wave velocity and amplitude recorded during the monitoring period. Figure 4-2 to Figure 4-6 provides average velocity and modulus changes for the six ray-path categories selected in terms of disturbed and damaged regions. Figure 4-7 and Figure 4-8 show all locations and the temporal distribution of located AEs recorded since March 2003. Figure 4-9 to Figure 4-12 summarise changes that take place at different regions around the deposition hole in schematic diagrams for each period, identifying the primary changes in the properties of the rock as described in Table 4-2.

4.3 Recommendations

The rock mass around the deposition holes has remained relatively stable during this monitoring period. There is however, a sudden drop in both temperature and pressure in the buffer surrounding the canister that occurs on 21st October 2007 that directly influences P- and S-wave velocities and amplitudes.

- There are over five years of monitoring ultrasonic survey measurements at the Prototype experiment with velocity and amplitude measurements conducted through a number of variations in pressure and temperature conditions. It would now be beneficial to perform an additional integrated interpretation of changes in these measurements with available data on the thermal and hydro-mechanical conditions in the repository, in order to better understand the rock response in the immediate vicinity of the deposition hole. This could help resolve whether pressure or temperature, or an optimal combination of the two, has a leading role in reducing crack density (and hence permeability) and thus provide a best practise for working conditions of a future repository.
- AE clustering is thought to occur in regions of pre-existing micro-cracks following the excavation phase [Pettitt et al. 2000] and might suggest a re-activation of pre-existing fractures. Clustering of AE events is observed around the walls of the deposition hole. It would be interesting to carry out further study on these events to investigate the fracture mechanism, and their temporal evolution with respect to changing environmental variables. The objective would be to resolve the primary factors responsible for causing AEs to locate in specific locations around the deposition hole.
- A further study may be warranted on the events that have located near the tunnel floor, away from the deposition hole (Cluster T), if their occurrence cannot be linked to a specific event. There is a new tunnel being excavated nearby that may have caused increased activity and possibly opened up a network of new fractures. Blasting records will be included in the next report to establish the correlation between blasting and AE activity.

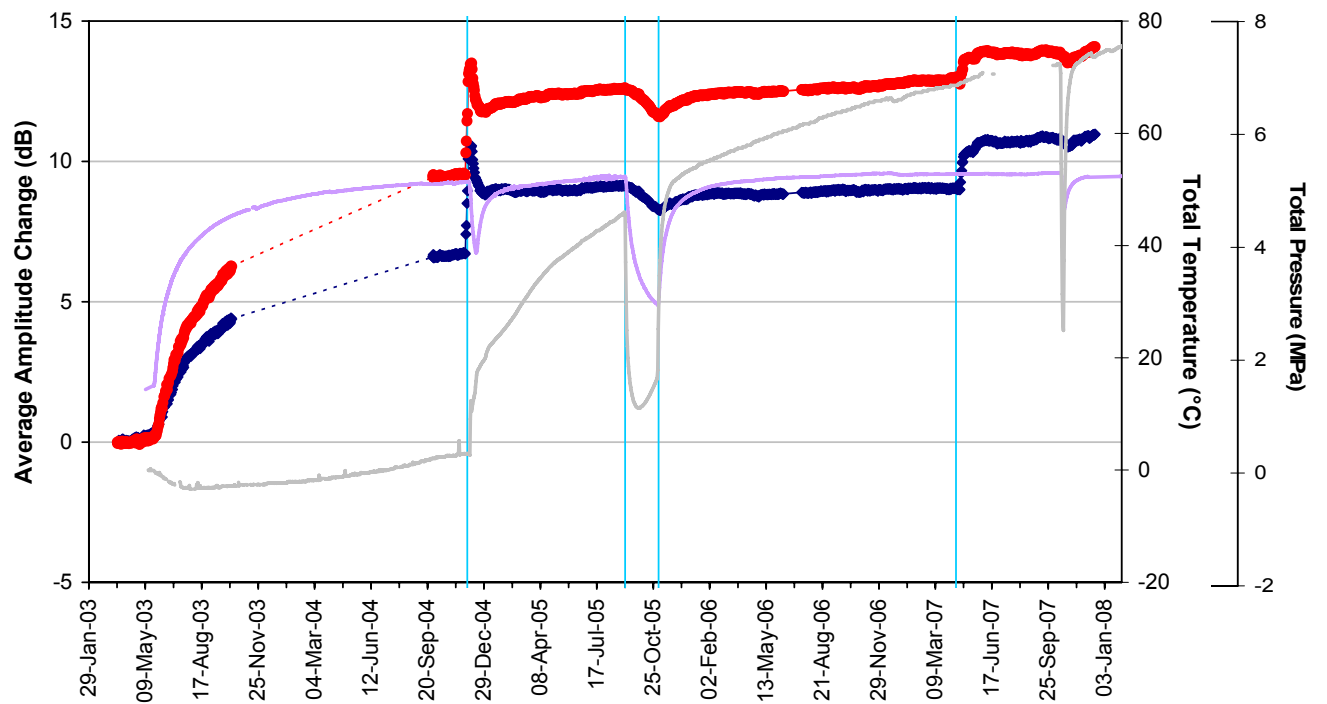
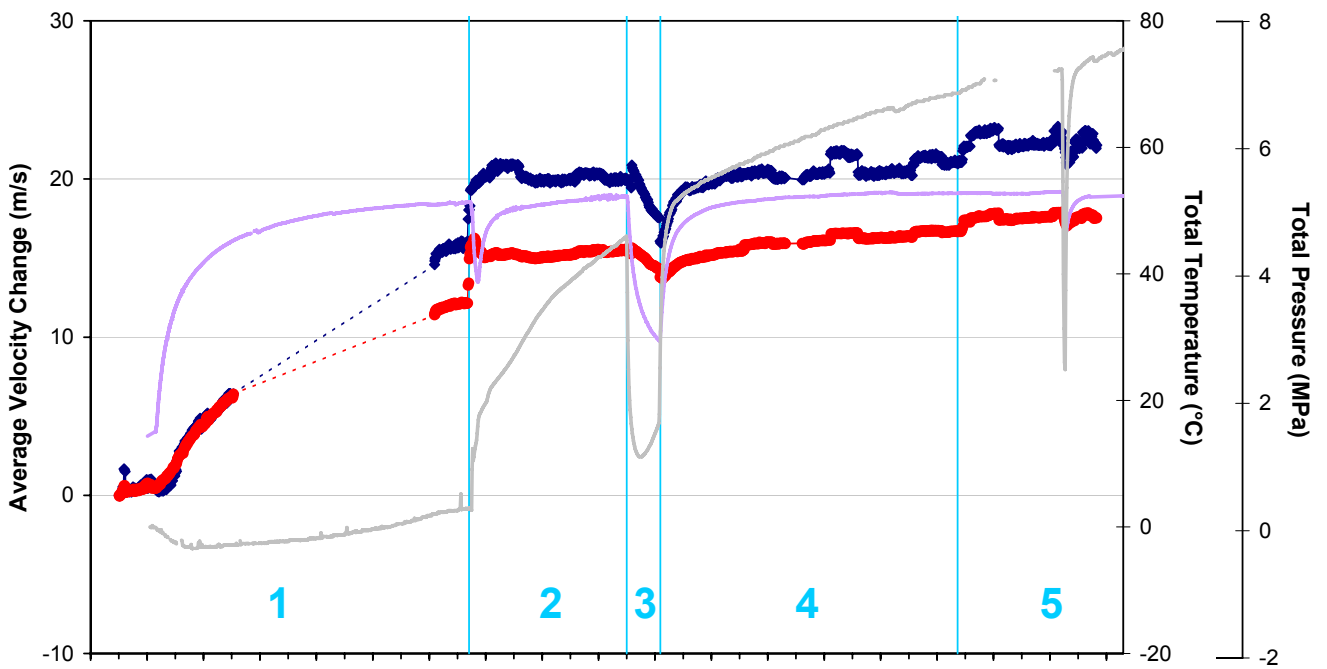
Table 4-1: Summary of velocity, amplitude and AE variation measured during five response periods of temperature and/or pressure change.

Name / Date	Temperature/Pressure	Velocity	Amplitude	AE
PERIOD 1 25 th May 2003 to 31 st October 2004	Heaters in canister switched on causing an initially rapid change in temperature which gradually levels out to a constant increase. An increase of 35°C is measured for an instrument in rock adjacent to the deposition hole. Pressure constant	Rapid increase in P- and S-wave velocity on 'S3' category. Other categories show increases but to a lesser extent. Initial decrease in P-wave velocity in comparison to S-wave velocity for all ray-paths except for 'S3'.	Amplitudes increase over this period by between 3dB and 9dB for P-wave amplitude, and 7dB and 12dB for S-wave amplitude.	AEs do not start immediately after heating. This could be a Kaiser-type effect in which AE rate remains close to background level until stress increases above the largest previous value. Peak of 13 events located on 26 th June 2003. Average Event Rate = 0.5 / day
PERIOD 2 1 st November 2004 to 4 th September 2005	Drainage to tunnel closed on 1 st November. Pressure in tunnel increases. Pressure increases measured in the deposition-hole buffer between 3 rd and 5 th December. Damage observed on canister on 6 th December so drainage reopened and heaters switched off. Power switched on 15 th December.	Velocity increases measured close to the tunnel from 26 th November. Larger increases measured on categories 'S1' and 'S3'.	Amplitude increases measured close to the tunnel from 26 th November.	Relatively large number of events recorded in this period. Peak rate of 32 AEs on 4 th and 5 th December. Events locate in clusters in previously observed damage zone. Average Event Rate = 0.4 / day
PERIOD 3 5 th September 2005 to 2 nd November 2005	Additional drainage is opened in August 2005 leading to a decrease in pressure and temperature. Heaters turned off on 5 th September	P- and S-wave velocities decrease on all ray-path categories except 'far'.	P-wave amplitude decrease on all category ray-paths.	Slight increase in event rate above background rate recorded in previous 5 months. Average Event Rate = 0.3 / day
PERIOD 4 3 rd November 2005 to 13 th April 2007	Pressure in tunnel increases. Constant increase in pressure in buffer above deposition hole. Heaters switched on again so temperature around the deposition hole increases.	P- and S-wave velocities increase on all category ray-paths. Larger increases measured on 'S3'.	P- and S-wave amplitude increase on the majority of ray-paths.	Cluster of 202 events located on SE side of deposition hole. Similar rate of AE locations. Average Event Rate = 0.46 / day
PERIOD 5 14 th April 2007 to 31 st March 2008	Short-term variations of pressure and temperature in the tunnel and deposition hole. Missing pressure data period (24/06/2007-09/09/2007).	P- and S-wave velocities generally increase on all category ray-paths. Larger increases measured on all ray-paths related to instrument 6. Largest decrease in October 2007 is observed on category 'C2'.	P- and S-wave amplitude increase on all ray-paths. Deviation observed during short-term pressure and temperature excursions.	286 events located in 4 distinct clusters on SE, SW and NE sides of deposition hole. Peak of 21 events on 22 nd January, 2008 locate in one anomalous cluster some distance from the deposition hole. Average Event Rate = 0.76 / day

Table 4-2: Summary of key interpretation of rock response from the ultrasonic measurements.

Period	Summary of Key Interpretations
1	<p>The heaters are switched on. The 'S3' category passes through a volume that is unloaded and hence experiences low compressive stresses. This volume responds more rapidly to thermal stresses because existing microfractures are initially unloaded and hence more open than microfractures in the compressive region. P- and S-wave velocities decrease a similar amount during excavation as they increase during heating. This suggests very strongly that the microfractures induced in the regions of tensile damage around the deposition hole close when thermal stresses are applied. The difference in the rate of response between ray-paths in the compressive categories was interpreted as a different magnitude of response of the microfractures in the rock mass to increasing thermal stresses.</p> <p>In the first few months of heating, another effect is superimposed onto the rock's response to thermal stresses. This is measured as a reduction in P-wave velocities compared to S-wave velocities in the first few months of heating. This is particularly noticeable on 'S1' category in Figure 4-2, in which P-wave velocity decreases by about 3.5ms^{-1} while S-wave velocity remains constant. A desaturation occurs on all ray-path categories, other than 'S3'. This must be caused by a drying of the rock mass, in the zones experiencing high compressive stresses, as heat is applied to the rock (i.e. both temperature and pressure are acting to expel moisture). In the low-compressed, or tensile, region saturation increases during this period. This is probably caused by hot fluids expanding into the open microfracture fabric.</p>
2	<p>Pressure rose rapidly after drainage from the tunnel was closed. This resulted in damage to the canister and the heaters being temporarily switched off. Temperature around the deposition hole dropped rapidly, but started increasing again after 13 days. Significant changes to the character of many recorded ultrasonic waveforms were observed as significant increases in signal quality. This suggests that as pressure increased in the rock surrounding the deposition hole, attenuation of the ultrasonic waves is significantly reduced meaning that they can pass more efficiently through the rock medium.</p> <p>The pressure increase can be interpreted as increasing the stiffness of the rock with a corresponding decrease in crack density. The magnitude of increase is greater for 'S1' and 'S3' categories because the volumes through which they pass are close to the deposition holes and contain a higher proportion of microfractures in an excavation damage zone. The pressure increase acts as a confining pressure on the rock mass leading to a closure of the pre-existing microcrack fabric and therefore a reduction in crack density. We observe that only a relatively small pressure increase is sufficient to close this microcrack fabric in the volumes already under high compressive stresses, leading to an initially high rate of change in measured velocities followed by a constant level, even though pressures may keep increasing afterwards. From Figure 4-2 the required pressure increase is approximately 1.5MPa.</p> <p>The rapid pressure increase led to 32 events locating in clusters over the course of two days. The events are interpreted as stress changes in the rock as it responds to the sudden pressure change. This induces small scale movement on pre-existing microcracks, or induces new microfractures in weaker volumes of the rock. Pore pressure increases may also have assisted in inducing slip on pre-existing microfractures, by reducing the normal stress on the fractures. Over the rest of this period, as pressure continued to increase, fewer events were located.</p> <p>Another effect at this time is a rapid cooling of the rock when the heater inside the canister is switched off (for 13 days between 2nd and 15th December 2004), followed by warming as the rock is reheated. The majority of categories do not show a significant change in P- or S-wave velocity during this period indicating they are relatively insensitive to temperature changes at this time (i.e. when pressures are high). The exception is category 'S3', which exhibits a decrease in P- and S-wave velocity followed by an increase that mirrors the rate at which temperature changes (Figure 4-3). This category was found to be the most sensitive to thermal stresses during the initial stages of heating. When the rock cools, thermal stresses acting in this volume of low compressive (or slightly tensile) stresses reduce causing unloading of the microcracks. Microcracks close again when the rock is reheated and thermal stresses increase.</p>

3	<p>In September 2005 additional drainage from a permeable mat placed on the inner surface of the outer plug was opened, and heaters were switched off. This resulted in a cooling and de-pressurisation of the deposition hole. Neither temperature nor pressure reduced to the background level.</p> <p>The decrease in velocity on most ray-paths is generally low compared to the increases observed previously. An exception to this is category 'S3'. This category is observed as the most sensitive. As temperature and pressure decreases, stresses again reduce in this volume causing microcracks to reopen and resulting in an increase in crack density and reduced stiffness of the rock.</p> <p>At the start of the period a sudden (over a few days), but relatively small change in velocity is observed, superimposed on the longer-term trends. We believe these are related to rapid changes in fluid pressure; a corresponding increase is observed at the end of the period (start of Period 4). For Period 3, an increase in Young's Modulus occurs which indicates a stiffening of the rock. This short term change is therefore likely to be a sudden reaction of the rock mass to the decrease in fluid pressure, perhaps caused by a general closing of microcracks caused by decreased pore pressures. The reverse is true for Period 4, when a pressure increase leads to a general opening of microcracks caused by increased pore pressures. This is believed to be a different response to long term trends from thermal stresses and general confining of the rock mass.</p>
4	<p>During the fourth period, heaters were turned back on once more causing temperature around the deposition hole to increase. Pressure increased rapidly again, probably caused by changes in the buffer temperature (changes in water volume caused by the temperature in combination with low hydraulic conductivity) [Goudarzi and Johannesson, 2006]. Velocity increases rapidly at first, then at a constant rate, following a similar pattern to the temperature and pressure.</p> <p>Ray-path category 'S3' exhibits the greatest increase in P and S-wave velocity. Similar patterns are observed on 'S1' and 'C1', and to a lesser extent on 'C2'. Velocity on the 'far' ray-path category remains constant throughout the period. When temperature and pressure start to increase the stiffness of the rock increases, particularly on 'S3'. This is accompanied by a reduction in crack density. The associated increase in stiffness and decrease in crack density can be interpreted as the closing of existing microfractures and pore spaces as observed previously. This effect has continued to the current day.</p> <p>Few events have been located during Periods 3 and 4. A rapid decrease, and then increase, in pressure and temperature appears to have no significant affect on the number, or distribution of AEs around the deposition hole. The AE rate marginally increased since February 2006 (Figure 4-8). The vast majority of events locate on a single cluster in the south-east of the deposition hole and at 455.1m depth. The low number of AEs suggests the rock mass has stabilised. The high pressures result in a confining pressure being placed on the rock around the deposition hole and inhibit the movement on microcracks or macrofractures.</p>
5	<p>During the fifth response period the excavation of a new tunnel near the prototype tunnel resulted in a gap in pressure data (from 24th June until 9th September 2007). Pressure in the tunnel backfill generally increased through the period (by ~0.5MPa) while the temperature has remained extremely stable (maximum change of only 1-2°C). Conditions in the buffer surrounding the canister remain stable with the exception of a sudden drop in both temperature and pressure that occurs on 21st October, this coincides with a decrease in P- and S-wave velocity and amplitude. As temperature and pressure decreases, stresses reduce in the volume causing microcracks to reopen and resulting in an increase in crack density and reduced stiffness of the rock. It is unclear whether the drop in pressure or temperature is responsible for the observed changes in velocity and amplitude, but both are likely to effect the stress field in some manner.</p> <p>In the first six months of this period the velocity and amplitude for both P- and S-waves increases between 20th and 24th April 2007. P-waves show higher variation than S-waves. The most sensitive ray-paths to the changes are those related with sensor 6. Analysis of the different ray-paths show that category 'Far' shows the maximum velocity changes for both P- and S- waves while category 'C1' shows minor changes. The minimum variation in signal amplitudes is observed for 'S3' category. In the following six months velocity and amplitude for both P- and S-waves decrease for a period between 21st and 26th October, 2007 then increase more gradually, with only minor variations observed, until the end of March 2008. P-wave velocity increases suddenly to a period high on 21st November, 2007.</p> <p>The most sensitive ray-path categories (with most observable variation) are 'C2', 'S3' and to a lesser extent 'C1'. Data for velocity and amplitude is not obtainable from ultrasonic surveys between 17th December 2007 and 31st March 2008 due to equipment failure.</p> <p>The AE rate has increased since the last response period (by ~50% in the second half of the period). Events generally locate in clusters around the deposition hole: three of these clusters are recurring in active volumes, one occurring in a volume around the canister deposition hole not previously seen, and one anomalous cluster representing a newly activated volume in the tunnel floor. The increase in AE activity would suggest that the rockmass has undergone some new fracturing or movement on existing fractures; the excavation of a nearby tunnel may be responsible for this increase. The relatively low number of AEs suggests the rock mass is generally stable.</p>



◆ Average P-wave Amplitude ● Average S-wave Amplitude — Temperature — Total Pressure

Figure 4-1: P- and S-wave velocity change (a) and amplitude change (b) from the start of monitoring, plotted alongside temperature (TR6045) and pressure (PB616) measurements in deposition hole DA3545G01. The vertical blue lines differentiate between periods of similar environmental conditions (see Table 4-1).

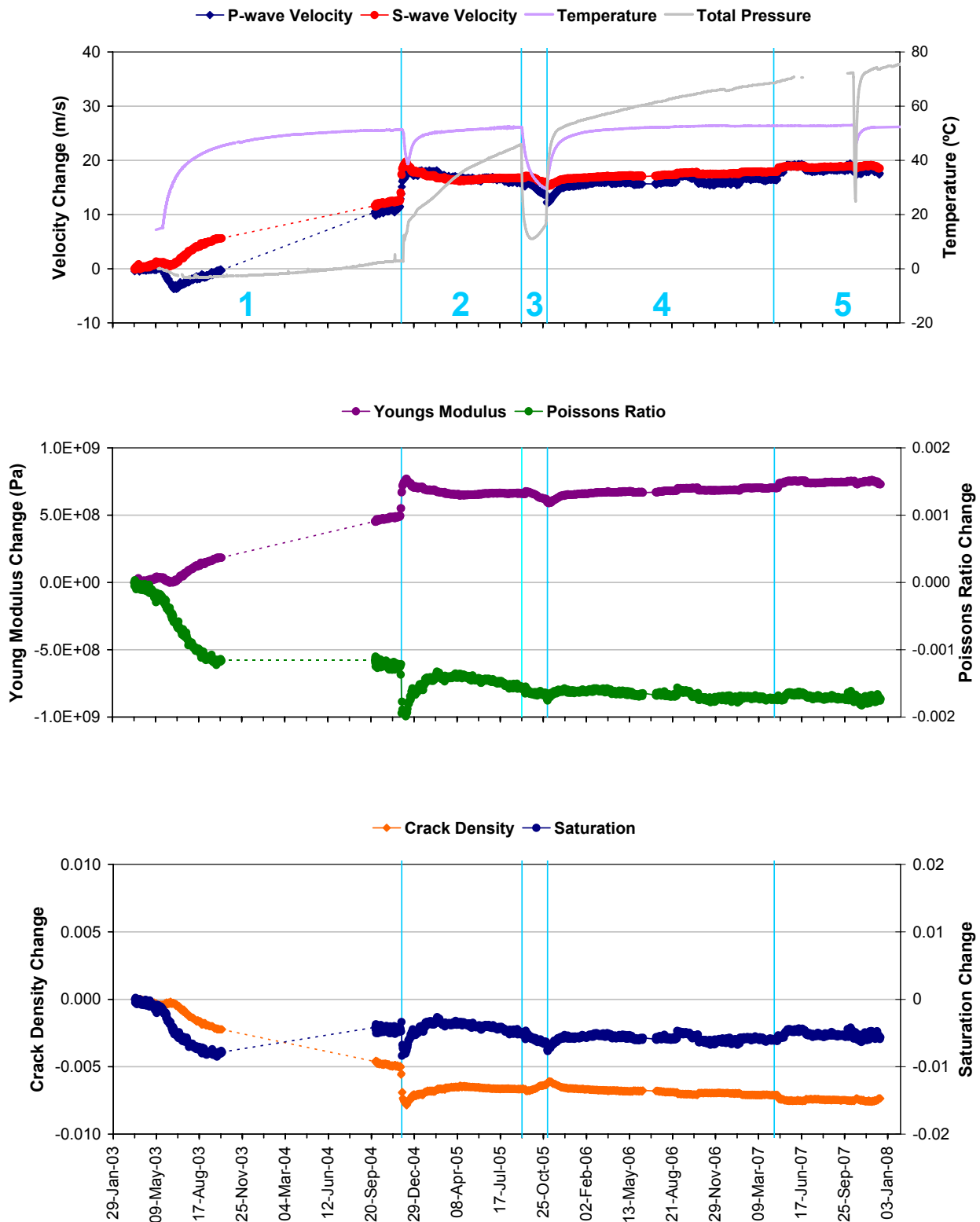


Figure 4-2: Average P- and S-wave velocity change for ray-paths on category 'S1' together with temperature (TR6045) and total pressure (PB616) (top), Young's Modulus and Poisson's Ratio change (middle), and Crack Density and Saturation change (bottom).

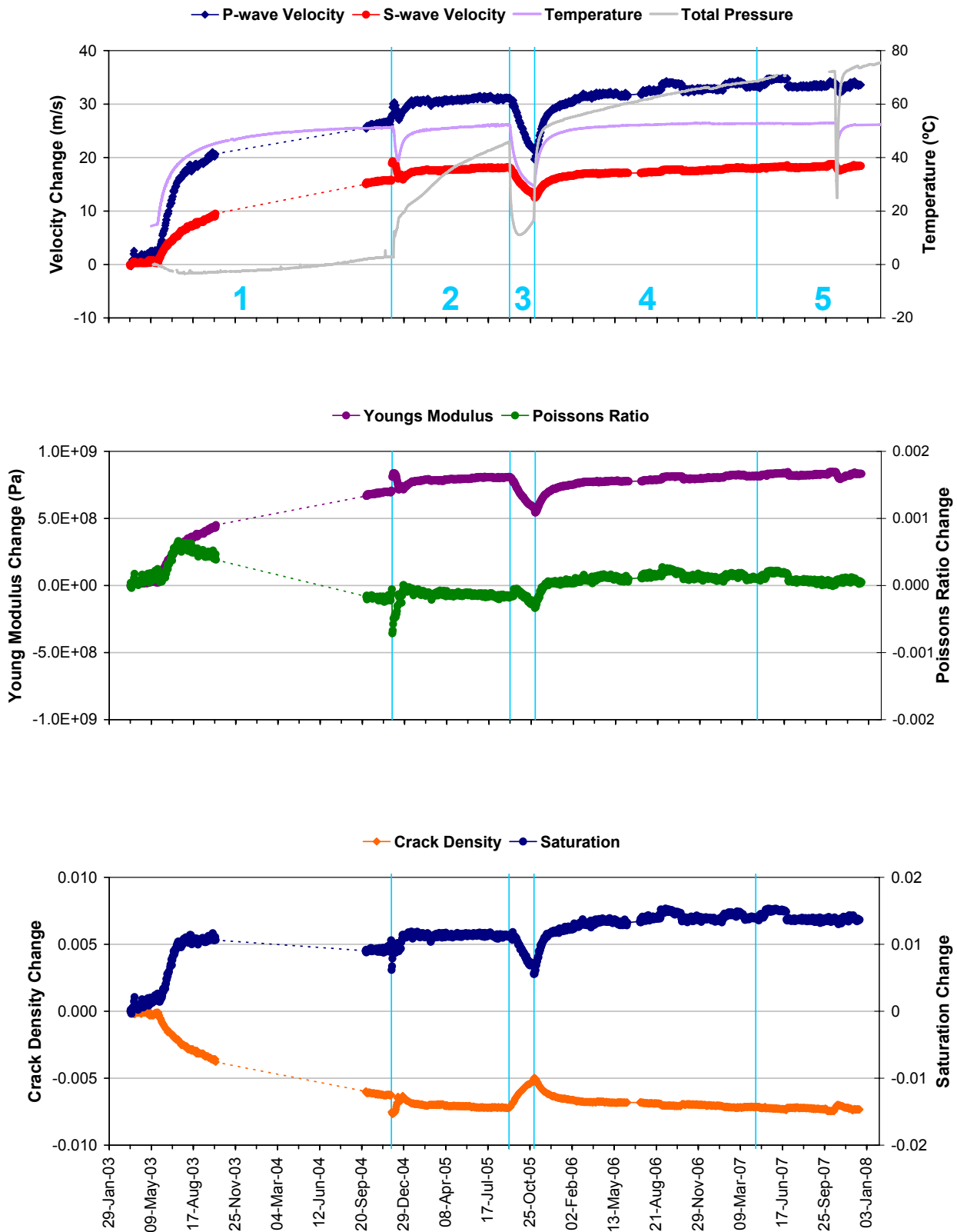


Figure 4-3: Average P- and S-wave velocity change for ray-paths on category 'S3' together with temperature (TR6045) and total pressure (PB616) (top), Young's Modulus and Poisson's Ratio change (middle), and Crack Density and Saturation change (bottom).

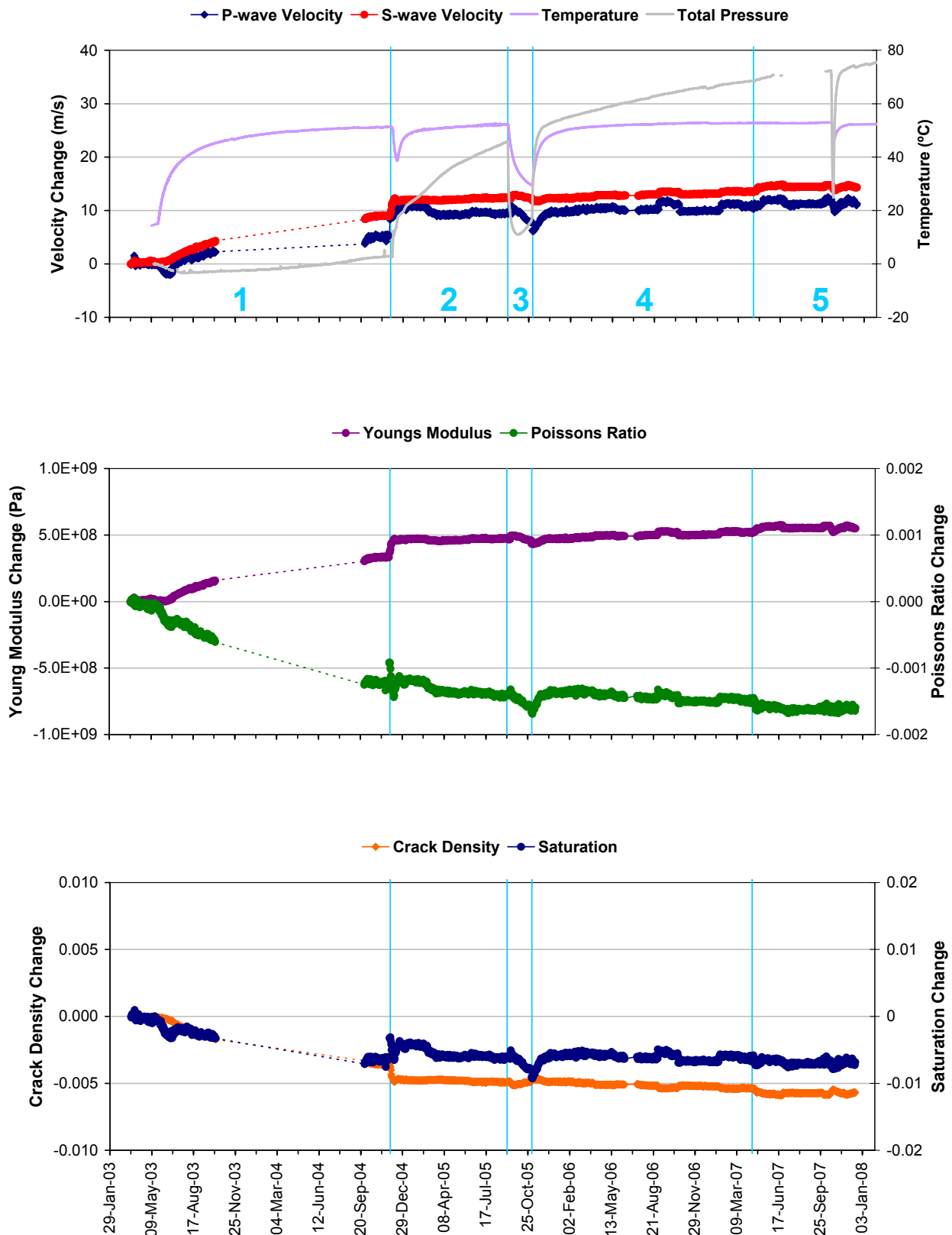


Figure 4-4: Average P- and S-wave velocity change for ray-paths on category 'C1' together with temperature (TR6045) and total pressure (PB616) (top), Young's Modulus and Poisson's Ratio change (middle), and Crack Density and Saturation change (bottom).

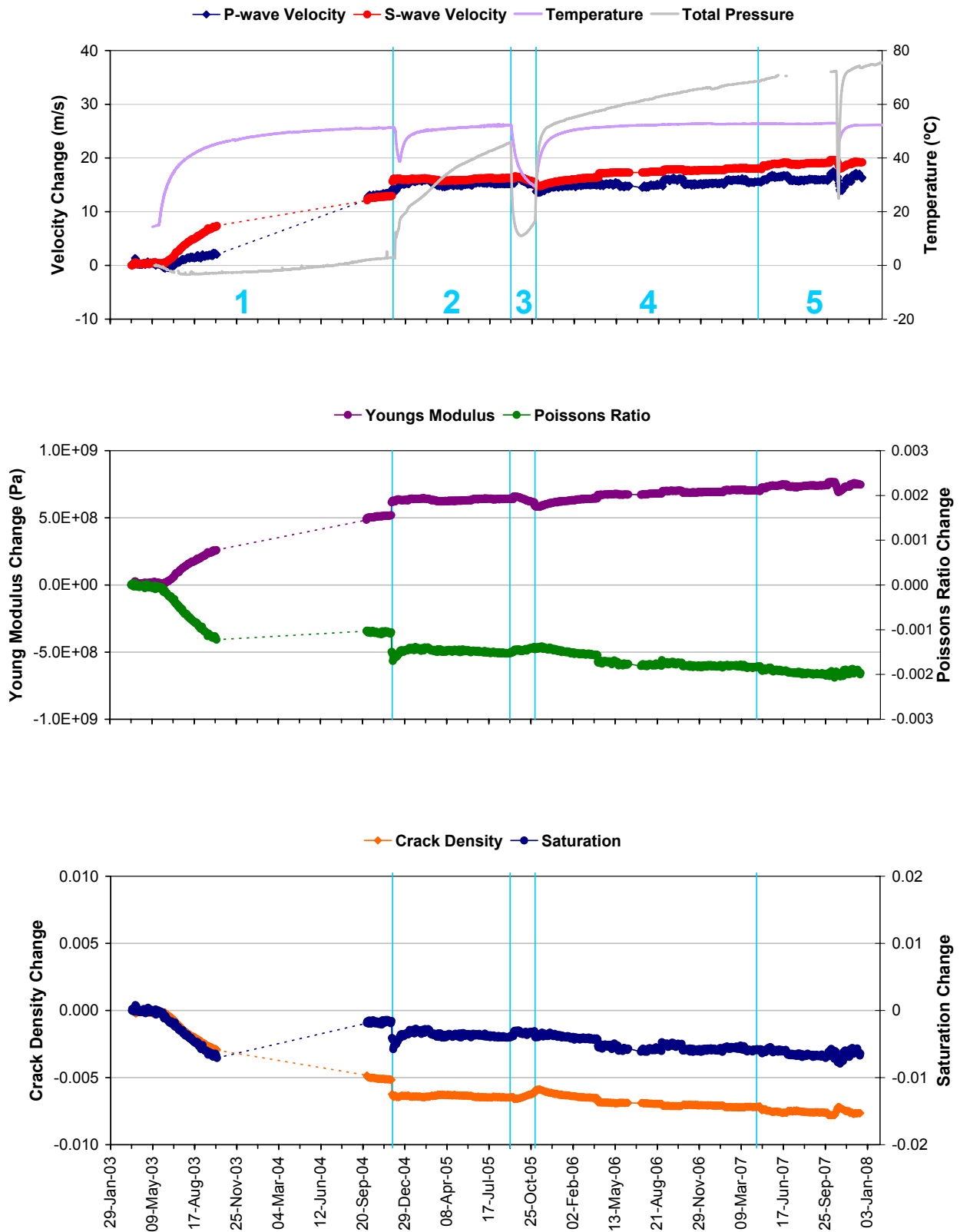


Figure 4-5: Average P- and S-wave velocity change for ray-paths on category 'C2' together with temperature (TR6045) and total pressure (PB616) (top), Young's Modulus and Poisson's Ratio change (middle), and Crack Density and Saturation change (bottom).

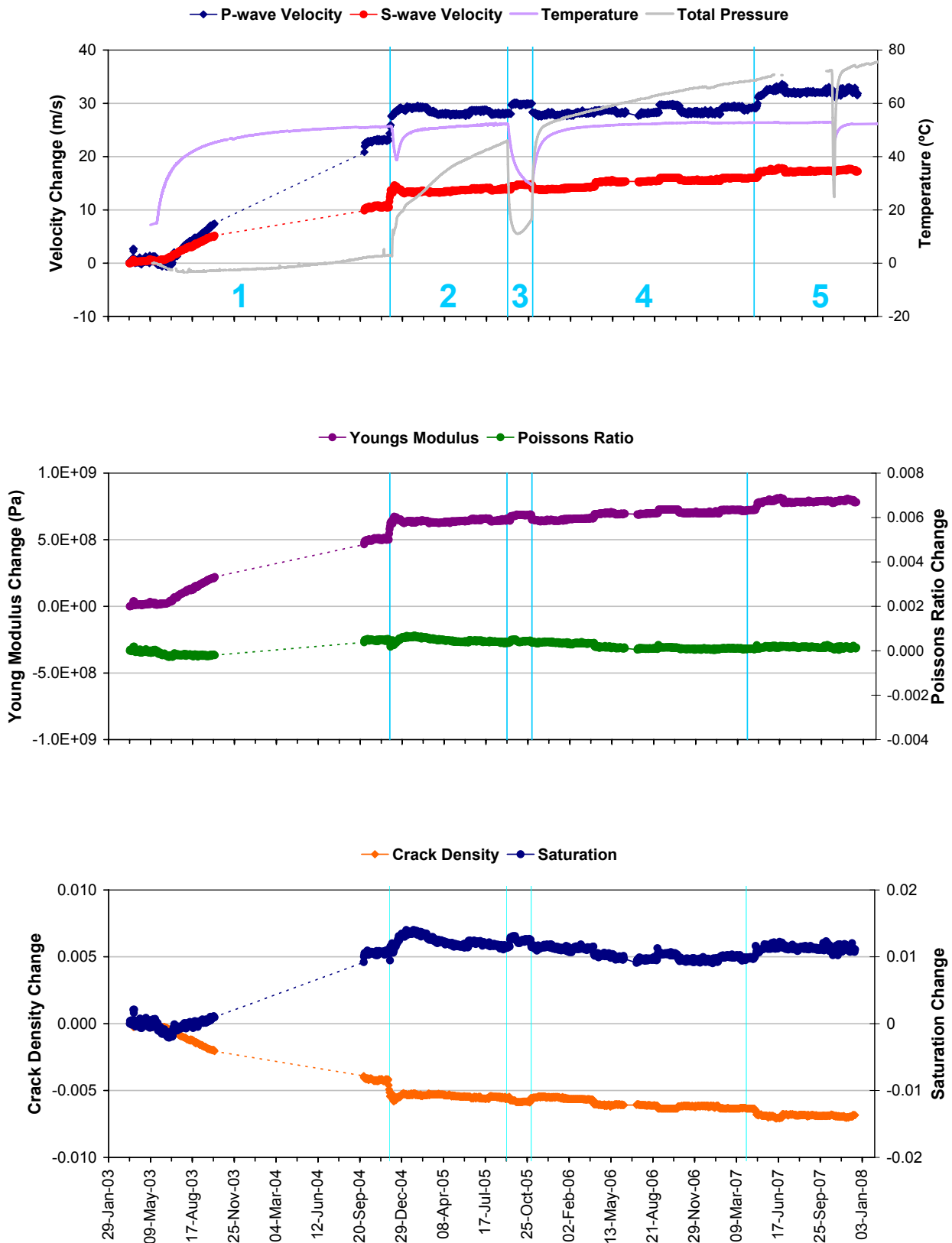


Figure 4-6: Average P- and S-wave velocity change for ray-paths on category 'Far' together with temperature (TR6045) and total pressure (PB616) (top), Young's Modulus and Poisson's Ratio change (middle), and Crack Density and Saturation change (bottom).

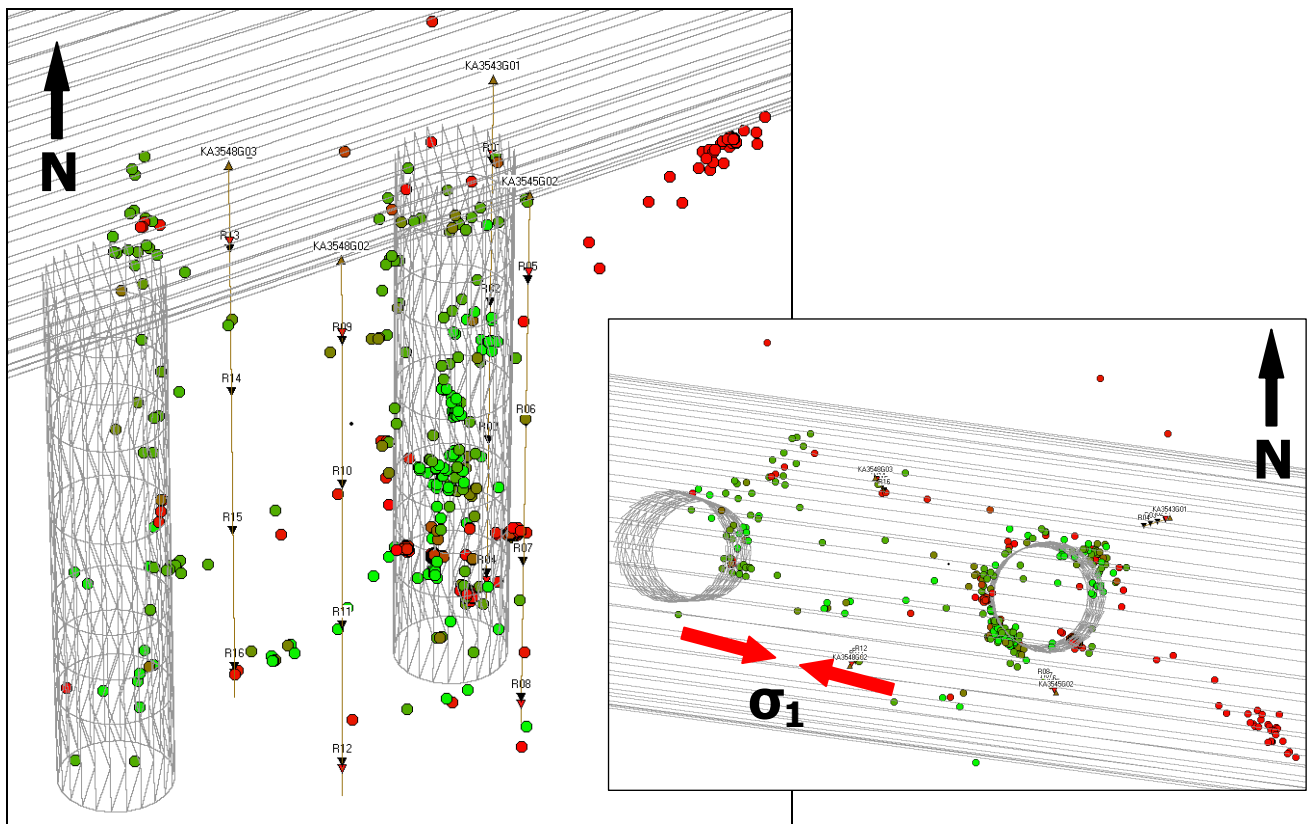
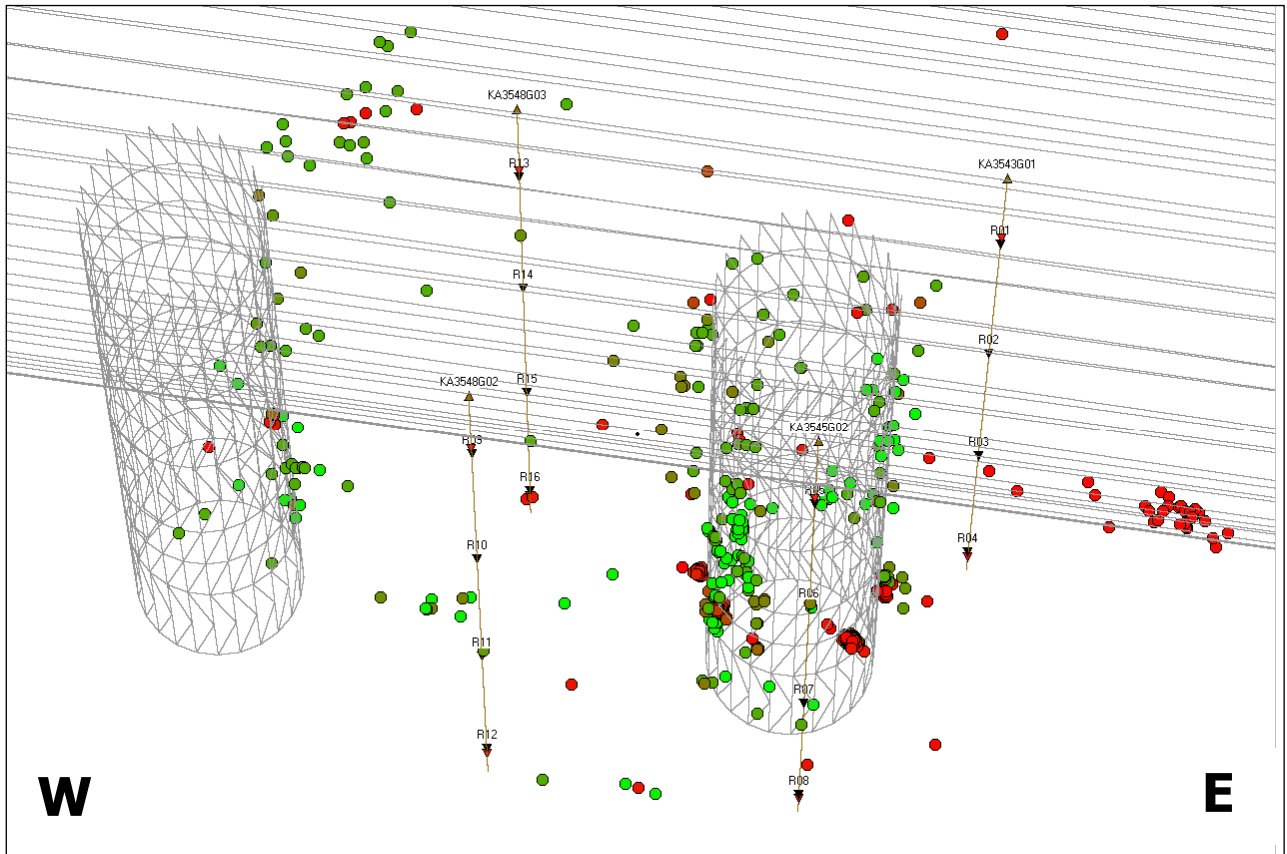


Figure 4-7: Projections of all AEs located during the heating phase (20th March 2003 to 31st March 2008). Events are scaled to time.

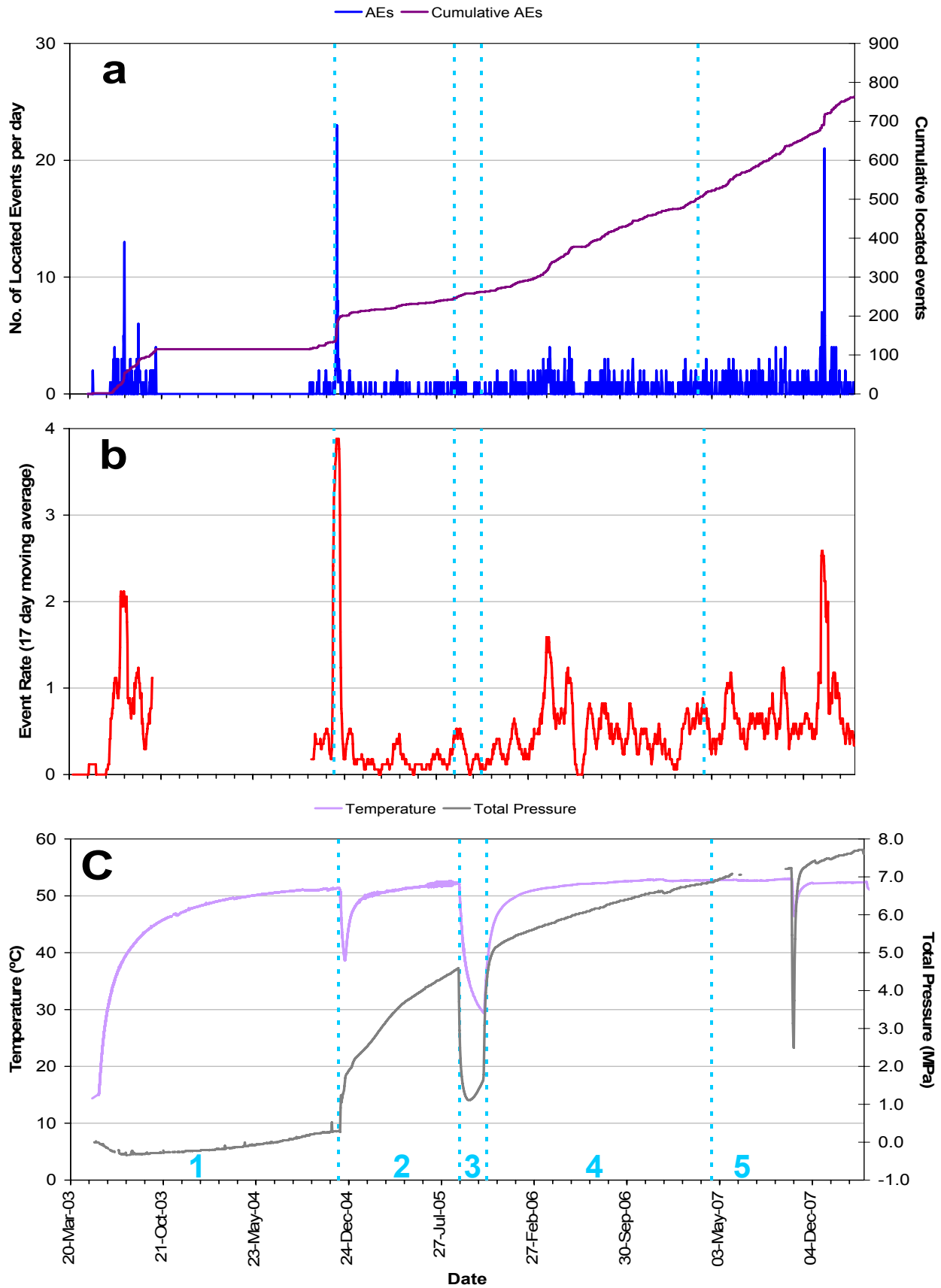
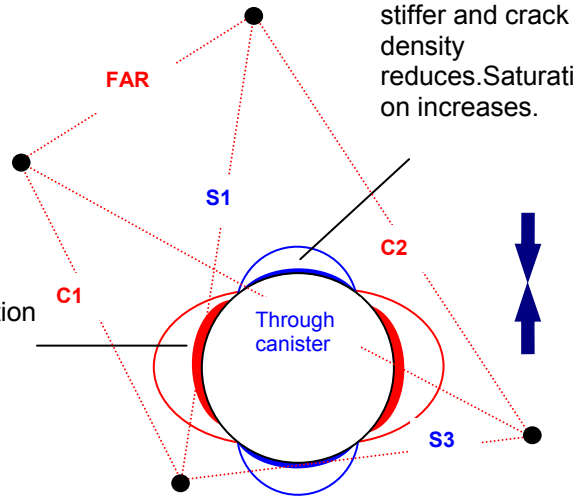


Figure 4-8: (a) Number and cumulative number of located events from the start of monitoring in March 2003, (b) 17 day moving average of located AE's, and (c) temperature (TR6045) and pressure (PB616) measurements in deposition hole DA3545G01.

PERIOD 125th May
2003 to 31st
October 2004

Region
desaturates and
has slight reduction
in crack density.



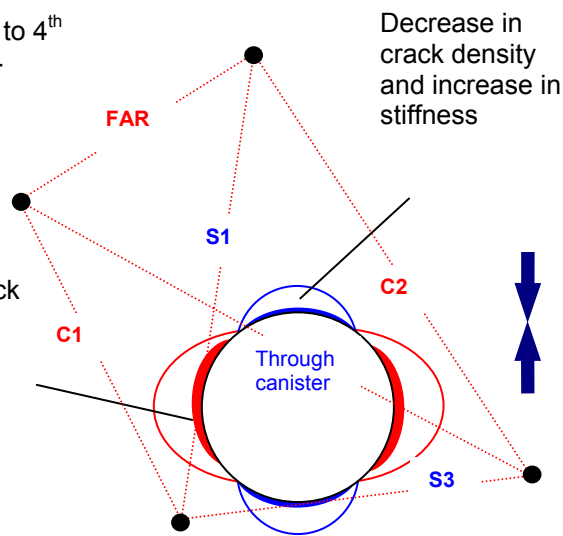
**Temperature
increase**

**Pressure
constant**

Figure 4-9: Schematic diagram of the deposition hole and explanation of changes experienced during Period 1.

PERIOD 21st
November 2004 to 4th
September 2004

Decrease in crack
density and
increase in
stiffness



**Temperature
decrease, then
increase**

**Pressure
increase**

Figure 4-10: Schematic diagram of the deposition hole and explanation of changes experienced during Period 2.

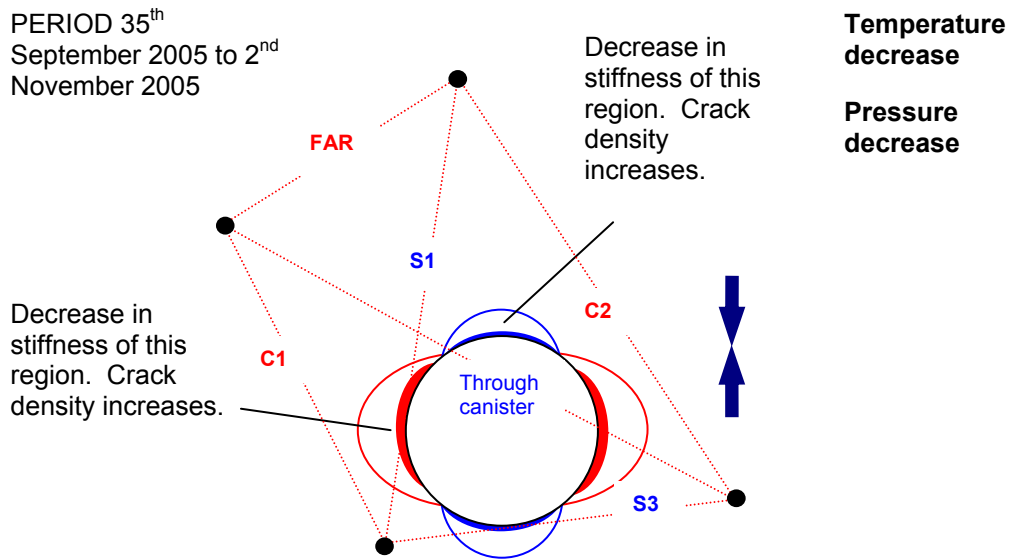


Figure 4-11: Schematic diagram of the deposition hole and explanation of changes experienced during Period 3.

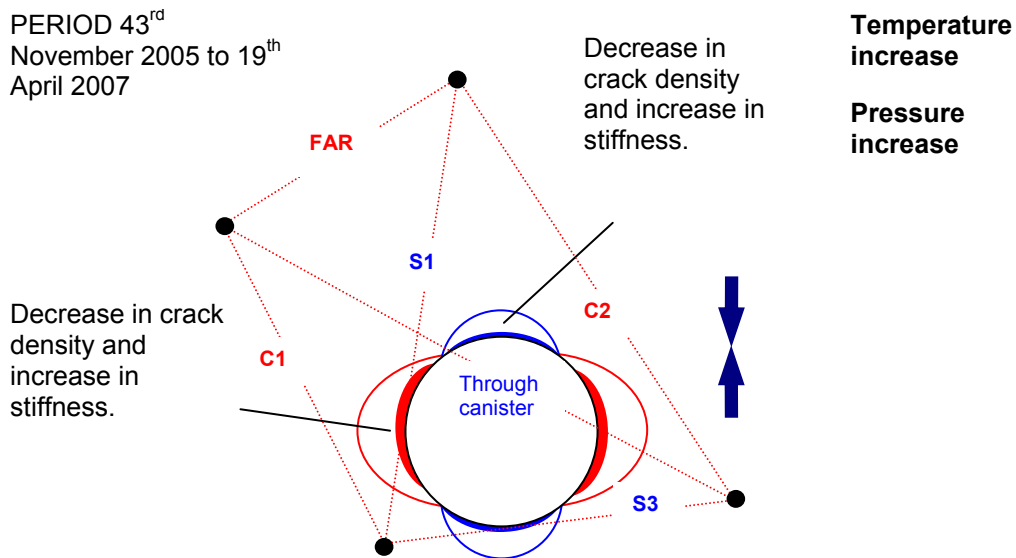


Figure 4-12: Schematic diagram of the deposition hole and explanation of changes experienced during Period 4.

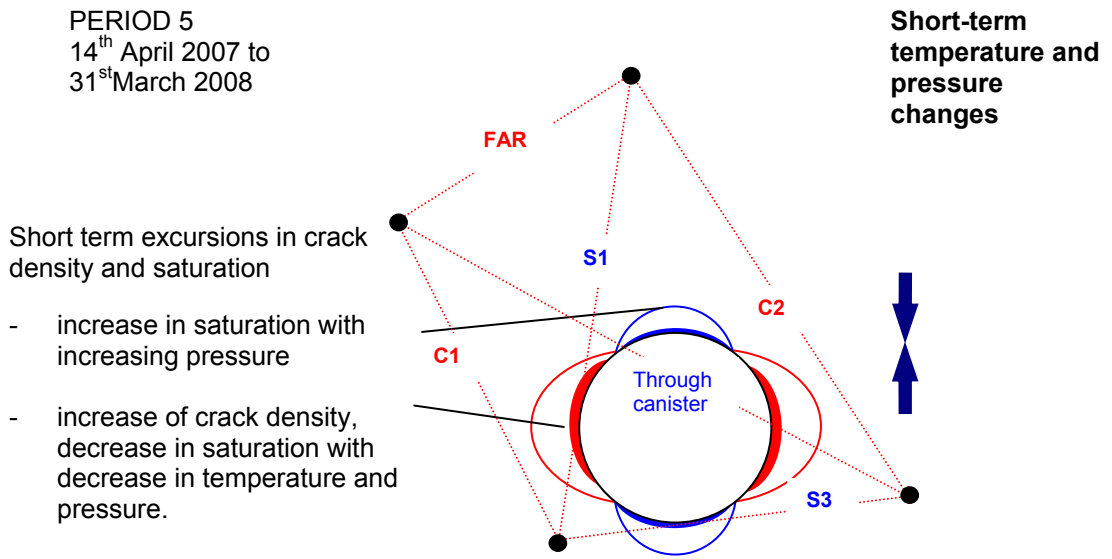


Figure 4-13: Schematic diagram of the deposition hole and explanation of changes experienced during Period 5.

References

Goudarzi, R., and Johannesson, L-E., 2006: Sensor Data Report (Period: 010917-061201). Prototype Repository, Report No: 16, International Progress Report IPR-07-05, Äspö Hard Rock Laboratory, Swedish Nuclear Fuel and Waste Management Company, Sweden.

Goudarzi, R., 2007 & 2008: Pers. Comm.

Haycox, J.R., Pettitt, W.S., and Young, R.P., 2005a: Acoustic Emission and Ultrasonic Monitoring During the Heating of Deposition hole DA3545G01 in the Prototype Repository to March 2005, International Progress Report IPR-05-30, Äspö Hard Rock Laboratory, Swedish Nuclear Fuel and Waste Management Co. Sweden.

Haycox, J.R., Pettitt, W.S., and Young, R.P., 2005b: Acoustic Emission and Ultrasonic Monitoring Results from Deposition Hole DA3545G01 in the Prototype Repository between April 2005 and September 2005, International Progress Report IPR-05-31, Äspö Hard Rock Laboratory, Swedish Nuclear Fuel and Waste Management Co. Sweden.

Haycox, J.R., Pettitt, W.S., and Young, R.P., 2006a: Acoustic Emission and Ultrasonic Monitoring Results from Deposition Hole DA3545G01 in the Prototype Repository between October 2005 and March 2006, International Progress Report IPR-06-23, Äspö Hard Rock Laboratory, Swedish Nuclear Fuel and Waste Management Co. Sweden.

Haycox, J.R., Pettitt, W.S., and Young, R.P., 2006b: Acoustic Emission and Ultrasonic Monitoring Results from Deposition Hole DA3545G01 in the Prototype Repository between April 2006 and September 2006, International Progress Report IPR-06-36, Äspö Hard Rock Laboratory, Swedish Nuclear Fuel and Waste Management Company, Sweden.

Maxwell, S.C., and Young, R.P., 1995: A controlled in-situ investigation of the relationship between stress, velocity and induced seismicity, *Geophys. Res. Lett.*, 22, pp. 1049-1052.

Patel, S., Dahlstrom, L.-O., and Stenberg, L., 1997: Characterisation of the Rock Mass in the Prototype Repository at Äspö HRL Stage 1, Äspö Hard Rock Laboratory Progress Report HRL-97-24, Swedish Nuclear Fuel and Waste Management Company, Sweden.

Pettitt, W.S., Baker, C., and Young, R.P., 1999: Acoustic emission and ultrasonic monitoring during the excavation of deposition holes in the Prototype Repository, International Progress Report IPR-01-01, Äspö Hard Rock Laboratory, Swedish Nuclear Fuel and Waste Management Company, Sweden.

Pettitt, W.S., Baker, C., and Young, R.P., 2000: Analysis of the in-situ principal stress field at the HRL using acoustic emission data, International Progress Report IPR-01-09, Äspö Hard Rock Laboratory, Swedish Nuclear Fuel and Waste Management Company, Sweden.

Pettitt, W.S., Baker, C., Young, R.P., Dahlstrom, L., and Ramqvist, G., 2002: The assessment of Damage around Critical Engineering Structures Using Induced Seismicity and Ultrasonic Techniques, *Pure and Applied Geophysics*, 159, 179-195.

Pettitt, W.S., and Young, R.P., 2007: InSite Seismic Processor – User Operations Manual Version 2.14, Applied Seismology Consultants Ltd. Shrewsbury, UK.

SKB, Äspö Hard Rock Laboratory: Current Research Projects 1999: Swedish Nuclear Fuel and Waste Management Company, Sweden.

Telford, W.M., Geldart, L.P., and Sheriff, R.E., Applied Geophysics: Second Edition, Cambridge University Press, 1990.

Young, R.P., and Pettitt, W.S., 2000: Investigating the stability of engineered structures using acoustic validation of numerical models, in *Geotechnical Special Publication No 102*, edited by J.F. Labuz, S.D. Glaser and Dawson. ASCE, USA, pp. 1-15.

Zimmerman, R.W., and King M.S., 1985: Propagation of acoustic waves through cracked rock, 20th Symposium on Rock Mechanics, Rapid City, SD.

Zolezzi F., Haycox J. R., And Pettitt W.P., 2007: Acoustic Emission and Ultrasonic Monitoring Results from Deposition Hole DA3545G01 in the Prototype Repository between October 2006 and March 2007, International Progress Report IPR-06-23, Äspö Hard Rock Laboratory, Swedish Nuclear Fuel and Waste Management Co. Sweden.

Zolezzi F., Haycox J.R., And Pettitt W.P., 2008: Acoustic Emission and Ultrasonic Monitoring Results from Deposition Hole DA3545G01 in the Prototype Repository between March 2007 and September 2007, Applied Seismology Consultants, Shrewsbury, UK.

Appendix I Previous Monitoring at the Prototype Repository

Ultrasonic monitoring has been conducted at the Prototype Repository since September 1999. During excavation, monitoring of both deposition holes in Tunnel Section 2 (DA3551G01 and DA3545G01) was undertaken to delineate zones of stress related fracturing and quantitatively measure fracturing in the damaged zone [Pettitt *et al.* 1999]. Monitoring has been undertaken on a single deposition hole (DA3545G01) since 2003, and the response of the surrounding rock to changes in temperature and pressure has been measured with reporting of results every six months (see Table 4-3). This report presents new results from the period 1st October 2007 to 31st March 2008.

Table 4-3: Summary of ultrasonic monitoring at the Prototype Repository to-date.

Report	Monitoring Period	Location	Response Period
<i>Pettitt et al.</i> [1999]	25/08/1999 to 18/09/1999	DA3551G01 and DA3545G01	Excavation
<i>Haycox et al.</i> [2005a]	20/03/2003 to 09/10/2003	DA3545G01	1
	29/04/2004 to 31/03/2005	DA3545G01	1, 2
<i>Haycox et al.</i> [2005b]	01/04/2005 to 30/09/2005	DA3545G01	2, 3
<i>Haycox et al.</i> [2006a]	01/10/2005 to 31/03/2006	DA3545G01	3, 4
<i>Haycox et al.</i> [2006b]	01/04/2006 to 30/09/2006	DA3545G01	4
<i>Zolezzi et al.</i> [2007]	01/10/2006 to 31/03/2007	DA3545G01	4
<i>Zolezzi et al.</i> [2008]	01/04/2007 to 31/09/2007	DA3545G01	4,5
<i>Duckworth et al.</i> [2008] (this report)	01/10/2007 to 31/03/2008	DA3545G01	5

A temporary ultrasonic array was installed around the rock volume when deposition holes DA3545G01 and its neighbour DA3551G01 were first excavated in September 1999 [Pettitt *et al.* 1999]. A total of 2467 AE triggers were obtained during monitoring of the two deposition holes. Of these 1153 were located. There was significantly more AE activity around the second deposition hole (labelled DA3545G01) than the first (DA3551G01). This difference is likely to depend upon intersection of the excavation with a greater number of pre-existing fractures. These fractures may be preferentially located in the side wall of the deposition hole or preferentially orientated to the *in situ* stress field. Fracturing associated with excavation-induced stresses was observed with AEs distributed mainly in regions orthogonal to the maximum principal stress, σ_1 . This was consistent with observations from the Canister Retrieval Tunnel and from dynamic numerical models. AEs, and hence microcrack damage, were shown to locate in

clusters down the deposition hole and not as a continuous 'thin skin'. *Pettitt et al.* [2000] showed that these clusters were associated with weaknesses in the rock mass generated by excavation through pre-existing fractures. Damage in the side wall of the deposition holes depended significantly on these pre-existing features. The *in situ* stress field was a contributing factor in that induced stresses were sufficiently high to create damage in these weakened regions although not sufficiently high to create significant damage in the rock mass as a whole.

A permanent ultrasonic array, with transducers grouted into instrumentation boreholes, was installed in the rock mass in June 2002. In this arrangement, ultrasonic monitoring has been conducted between 20th March and 9th October 2003, and then from 29th September 2004 to the present. A gap in monitoring occurred when the ultrasonic acquisition system was used for another experiment in the HRL (Pillar Stability Experiment). Processing and reporting of results has been undertaken, as shown in Table 4-3, and is further discussed in Section 4.2. A description of instruments measuring other environmental factors (such as temperature and pressure) and their locations can be found in *Goudarzi and Johannesson* [2006].

Appendix II Methodology

Data Acquisition

The ultrasonic array consists of twenty-four ultrasonic transducers configured as eight transmitters and sixteen receivers installed into four instrumentation boreholes. The transducers are fixed into the boreholes using specially designed frames (Figure 4-13) – two transmitters and four receivers per frame. The boreholes are vertical, 76mm in diameter and approximately 10 meters in length distributed around each deposition hole volume. The array has been designed to provide good coverage for AE locations and to provide ‘skimming’ ray-paths that pass within a few centimetres of the deposition-hole void so as to sample the rock immediately adjacent to the deposition-hole wall. The layout of the instrumentation boreholes is shown in Figure 4-14 and described further in Table 4-4. Each of the ultrasonic transducers has a hemispherical brass cap fixed over its active face and is then spring-loaded against the borehole surface so as to obtain good coupling to the rock mass. The boreholes have then been filled with a slightly expansive grout so as to permanently fix the transducers in place, reduce the likelihood of damage to the transducers and to remove the borehole voids.



Figure 4-13: Top: Schematic diagram of the locations of all transducers on a single frame. Left: Photo of a section of the transducer assembly. Right: The transducer assembly during installation.

The piezoelectric transducers operate by converting a transient elastic wave into an electric signal or visa versa. The monitoring system is then operated in one of two modes. The first is used to passively monitor AE activity preferentially within the array volume. AEs release elastic energy in the same way as 'earthquakes' but over a very small scale. At these frequencies AEs have a moment magnitude (M_w) of approximately -6. They occur either during the creation process of new fractures within the medium, or on pre-existing fractures due to small scale movements. Each receiver has a frequency response of approximately 35-350 kHz and contains a 40dB pre-amplifier. This minimises a reduction in signal-to-noise between the sensors and the acquisition system. The sensors have a vulcanised surround and a high pressure reinforced cable to protect them from water infiltration. In addition, polyamide tubes and *Swagelok* connectors have been fitted to the cables to reduce the likelihood of breakage.

Figure 4-15 shows a schematic diagram of the acquisition system used. Cables from each transducer pass through the pillar between the PRT and the G-tunnel. Data acquisition uses a Hyperion Ultrasonic System controlled by a PC, set up within a cabin provided by SKB. This has 16 receiving channels and 8 transmitting channels. An AE is recorded when the amplitude of the signal on a specified number of channels exceeds a trigger threshold within a time window of 5ms. The system then records the full-waveform signals from all 16 transducers. In this case a trigger threshold of 50mV on three channels was used. This allows the system to have sufficient sensitivity to record high quality data without recording an abundance of activity that cannot be processed due to very small signal to noise on only a few channels. The captured signals are digitised with a sampling interval of 1 μ s and a total length of 4096 data points. In general, low noise levels were observed (<2mV) giving high signal to noise and good quality data. AE monitoring is set to switch off during daytime working hours (6am-8pm) so as to minimise the amount of noise recorded from human activity.

A second operating mode actively acquires ultrasonic waveforms by scanning across the volume. This allows measurements of P- and S-wave velocities and signal amplitudes over a possible 128 different ray-paths. By repeating these ultrasonic surveys at increments in time, a temporal analysis is obtained for the variation in medium properties. Ultrasonic surveys are conducted daily at 1am in order to measure changes in P- and S-wave signals. At that time of night, no human activity will cause noise that can interfere with the signals received. A Panametrics signal generator is used to produce a high frequency electric spike. This is sent to each of the 8 transmitters in turn. The signal emitted from each transmitter is recorded over the 16 receivers in a similar fashion to that described above. An external trigger pulse from the signal generator is used to trigger the acquisition system and identifies the transmission start time to an accuracy of one sample point. In order to decrease random noise the signal from each transmitter is stacked 100 times.

Table 4-4: Boreholes used for AE monitoring of deposition hole DA3545G01.

SKB Borehole designation	ASC Borehole reference	Transducer Numbers
KA3543G01	1	T1, T2, R1-R4
KA3545G02	2	T3, T4, R5-R8
KA3548G03	3	T5, T6, R9-R12
KA3548G02	4	T7, T8, R13-R16

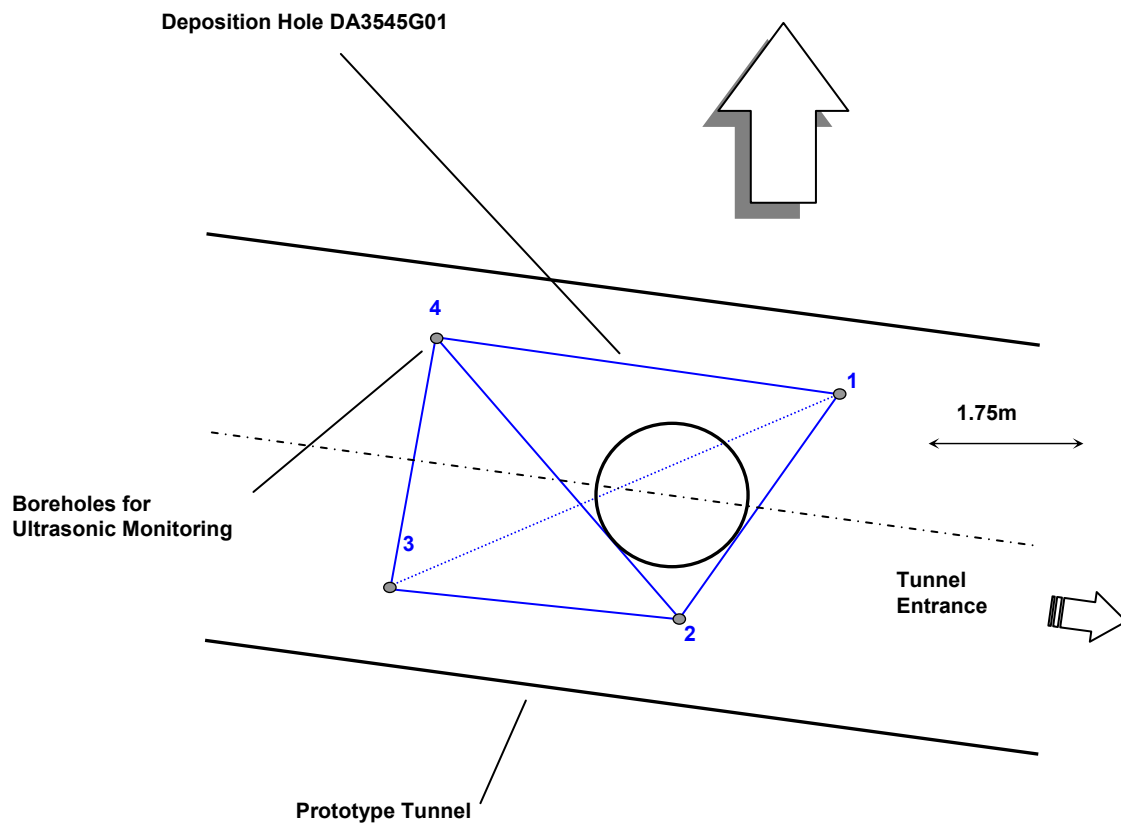


Figure 4-14: Plan view of the array geometry for Deposition Hole DA3545G01 during heating in the Prototype Tunnel. The blue solid lines represent direct ray-paths between sondes illustrating their ‘skimming’ nature. The blue dashed line represents a ray-path that travels through the deposition hole.

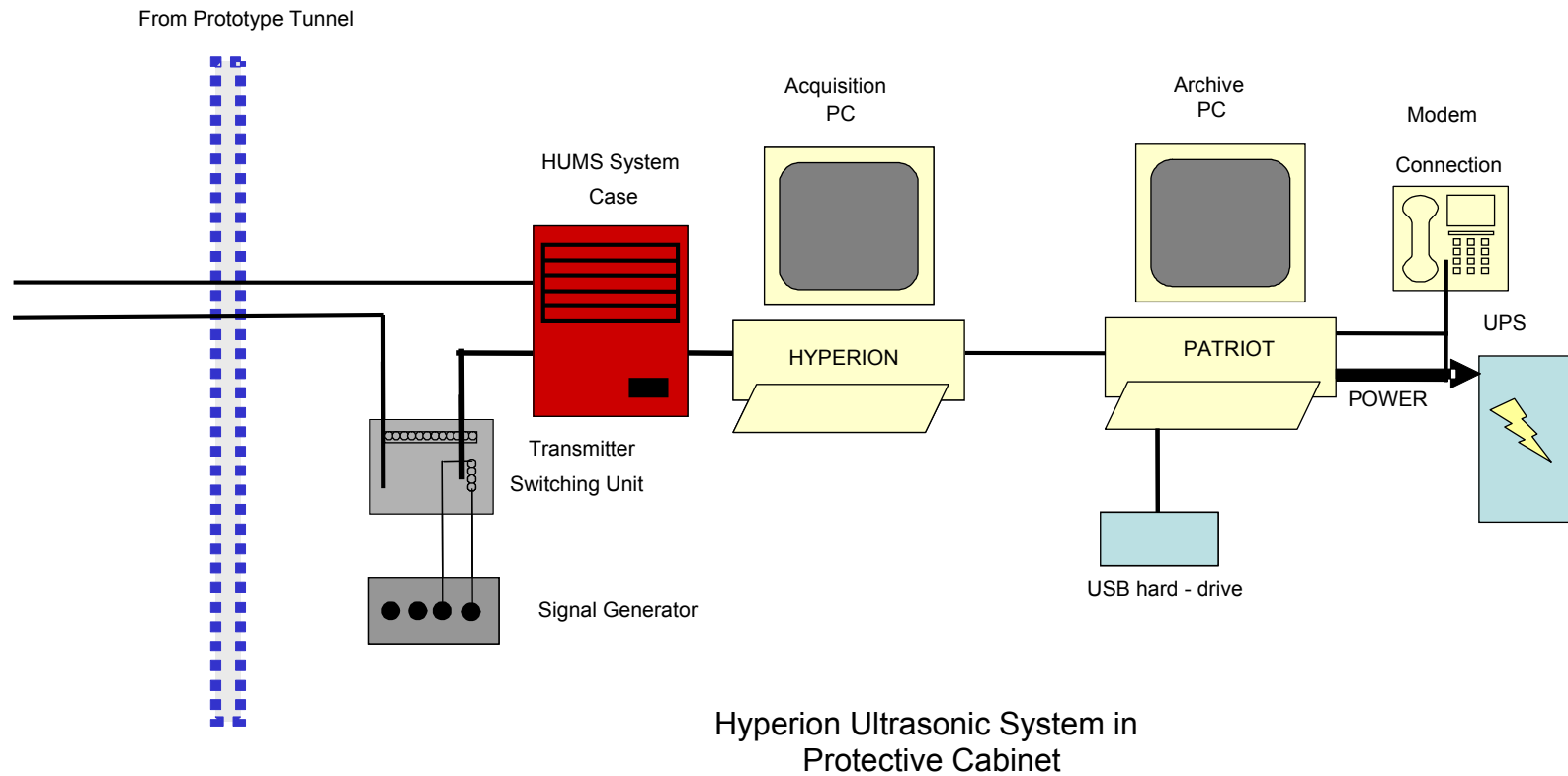


Figure 4-15: Schematic diagram of the hardware used for the heating stage in the Prototype Repository. The ultrasonic pulse generator sends a signal to each transmitter and the resulting signal is recorded on each receiver. The receivers are also used to listen for AE activity. The archive PC is required to make a copy of the data for backup purposes.

Processing Procedure

Overview

ASC's InSite Seismic Processor has been used to automatically process both the AE and ultrasonic survey data. Appendix IIIA and Appendix IIIB give the processing parameters used. *Pettitt et al.* [2005] provides a detailed description of this software.

Ultrasonic Data Procedure

The ultrasonic survey full-waveform data was initially stored with the AE data. This was automatically sorted and the survey data extracted to a separate processing project. A reference survey, taken from previous monitoring periods was imported into the project and used to process the ultrasonic results. The reference survey was recorded on 8th December 2004 and has had first P- and S-wave arrivals manually picked from the waveform [*Haycox et al.* 2006a]. Since transmitter and receiver locations are known, the ultrasonic velocity for each ray-path can be calculated with an estimated uncertainty of $\pm 30 \text{ ms}^{-1}$ (± 3 data points). Cross-correlation can then be used to automatically process subsequent surveys. This technique cross-correlates P- and S-wave arrivals from a transmitter-receiver pair with arrivals recorded on the same transmitter-receiver pair from the reference survey. Note that when the transmitter and receiver are on the same borehole, the ray-path is not used due to the introduction of transmission effects from the instrumentation borehole, grout and transducer frames.

Manual picking of arrivals by the examiner can often be erroneous due to random noise superimposed on the first few data points of the first break. By using the cross-correlation procedure it reduces this uncertainty and allows high-resolution analysis, with an estimated uncertainties of $\pm 2 \text{ ms}^{-1}$ between surveys on individual ray-paths, to be performed and hence small changes in velocity to be observed. This is extremely important when changes in rock properties occur over only a small section ($\sim 5\%$) of the ray-path.

Figure 4-16 gives example waveforms recorded from one of the transmitters during this reporting period. Each waveform is first automatically picked to obtain an estimate of the P-wave or S-wave arrival. A window is then automatically defined around the arrival and a bell function is applied, centred on the automatic pick. The data at the ends of the window then have a much smaller effect on the cross-correlation. The windowed data is then cross-correlated [*Telford et al.* 1990] with a similar window constructed around the arrival on the reference survey. The change in arrival time is then converted to a change in velocity knowing the manually-picked arrival time for the reference survey. Waveforms that do not provide automatic picks are not cross-correlated. This gives an automatic discrimination of signals that have very poor signal to noise ratios and could give spurious cross-correlation results from poor discrimination of the first arrival. During the automatic processing an arrival amplitude is also calculated from within a processing window defined by a minimum and maximum transmission velocity. This provides a robust measure of arrival amplitudes between surveys.

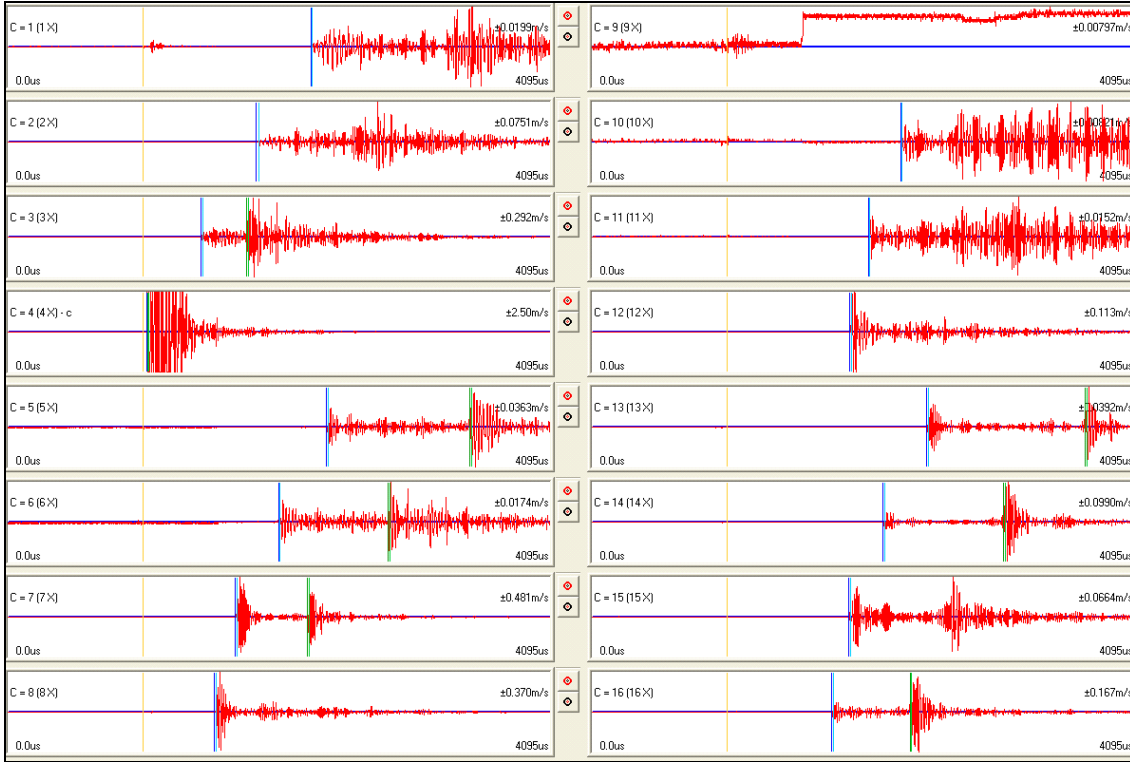


Figure 4-16: Waveforms recorded from one transmitter on the array of sixteen receivers. The gold markers indicate the transmission time. The blue and green markers indicate picked P- and S-wave arrivals respectively.

When calculating average velocities and amplitudes, ray-paths passing through the deposition hole are removed due to the uncertain transmission paths produced by the wave travelling in the rock around the deposition hole and through the bentonite, fluid and canister fill. Therefore the majority of ray-paths between boreholes 1 and 3 (transmitters 1, 2, 5, 6 and receivers 1, 2, 3, 4) are not used in the analysis. An exception is made for the deepest ray-paths that pass under the deposition hole entirely through rock.

The dynamic Young's modulus E , and dynamic Poisson's Ratio, ν , can be calculated from the velocity measurements using Equation 1 and Equation 2.

$$E = \rho V_S^2 \left(\frac{3V_P^2 - 4V_S^2}{V_P^2 - V_S^2} \right) \quad \text{Equation 1}$$

$$\nu = \frac{V_P^2 - 2V_S^2}{2(V_P^2 - V_S^2)} \quad \text{Equation 2}$$

V_P and V_S values are also used to model for crack density (c) and saturation (s) in the rock mass using the method of *Zimmerman and King* [1985]. The crack density parameter is defined by the number of cracks (penny-shaped) per unit volume multiplied by the mean value of the cube of the crack radius (Equation 3). This method assumes the elastic modulus E and ν in the damaged material normalized to the undisturbed material, decrease exponentially with crack density. Also assumed are the shear modulus (μ) is unaffected by s , and the bulk modulus (k) increases linearly with s , equalling that of uncracked rock when $s=1$. Equation 4 shows the calculation used to determine saturation.

$$c = \frac{9}{16} \ln \left(\frac{2\mu}{E_0 - 2\mu\nu_0} \right) \quad \text{Equation 3}$$

$$s = \frac{k(c,s) - k(c,0)}{k_0 - k(c,0)} \quad \text{Equation 4}$$

The calculations require an estimation of the completely undisturbed rock (i.e. an unsaturated, uncracked and intact rock mass). This study assumes values of $V_{OP} = 6660 \text{m.s}^{-1}$, and $V_{OS} = 3840 \text{m.s}^{-1}$ for the undisturbed material taken from laboratory tests on a similar granite, summarized in *Maxwell and Young* [1995]. A value of 2650kg m^{-3} is presented by *Pettitt et al.* [2002] for the density of the rock mass.

Young's Modulus and Poisson's ratio are calculated from measured velocities by making the assumption that the transmission medium is isotropic elastic. Under this assumption a rock can be completely characterised by two independent constants. One case of an isotropic elastic medium is a rock with a random distribution of cracks embedded in an isotropic mineral matrix. Under the application of a hydrostatic compressive stress, the rock will stay isotropic but become stiffer (characterised by increased velocity (V_P and V_S) and therefore increased Young's Modulus). In contrast, under the application of a uniaxial compressive stress, cracks with 'normals' parallel or nearly parallel to the applied stress will preferentially close and the rock will take on a transversely isotropic symmetry. Under this situation P- and S-wave velocities become variable with orientation. The crack density and saturation calculations also assume an isotropic elastic medium.

It should be noted that E and ν calculated in this report are dynamic measurements due to the small strains exerted on the rockmass at high frequencies from the passing ultrasonic waves. Static E and ν measurements, made from uniaxial laboratory tests on rock samples, may be different from dynamic values – even if sample disturbance is minimal – due to the larger strains exerted over relatively long periods of time.

Acoustic Emission Procedure

The procedure used to process the AEs in this reporting period has been undertaken as follows:

1. Calibration surveys from the installation phase (when the deposition hole was open) have been used to optimise an automatic picking and source location algorithm and check location uncertainties. ASC's InSite seismic processing software was used for location and visualisation.
2. Where possible, P- and S-wave arrival times were measured for each AE using the automatic picking procedure.
3. AEs with ≥ 6 P-wave arrival times were input into a downhill-simplex location algorithm [Pettitt *et al.* 2005]. This has the option of incorporating either a three-dimensional anisotropic velocity structure or an isotropic structure. Velocities calculated from the ultrasonic surveys were used.
4. The waveforms from all events were visually inspected to ensure they were 'real' acoustic emissions. Events were removed if they had the appearance of noise spikes (increase in amplitude is recorded on all channels at the same time) or they were the result of human noise (long period events that occur at close intervals during the day).
5. The acoustic emissions that remained had their arrivals manually picked to obtain the best possible location. Any events that located outside the expected region of activity were further checked to ensure accuracy. Experience from previous studies around deposition holes showed that large source location errors were produced if significant portions of a ray-path passed through the excavated deposition hole void. This only becomes a problem for the largest AEs. AEs were reprocessed with these ray-paths removed.
6. Finally, a filter was applied to remove all AEs with a location error greater than 1.0.

During the equipment installation phase, calibration shots were undertaken to assess the sensitivity of the system to AEs and to determine the accuracy with which real events could be located by the array of sensors. A series of tests, called 'shots', were performed on the wall of deposition hole DA3545G01 (Figure 4-17). The shots consisted of undertaking 10 'pencil lead breaks' and 10 hits with a screw-driver at 1 metre intervals down 4 lines along the wall of the deposition hole. The pencil-lead tests involved breaking the 0.5 mm lead from a mechanical pencil against the borehole wall. This is a 'standard' analogue for an AE as it generates a similar amount of high-frequency energy. An example of a pencil lead break test is shown in Figure 4-18. This was made at 6 metres below the tunnel surface on the wall of the deposition at a point adjacent to borehole KA3548G02. This corresponds to an AE source dimension on the millimetre scale (grain size).

The screw-driver hits provided a good amplitude signal for assessing the accuracy with which events can be located within the volume surrounded by the array. Figure 4-17 shows the results from one processed set of locations for a line of shots down the deposition hole. This shows that the array is able to locate events with good accuracy and consistency within an estimated uncertainty of approximately 10cm.

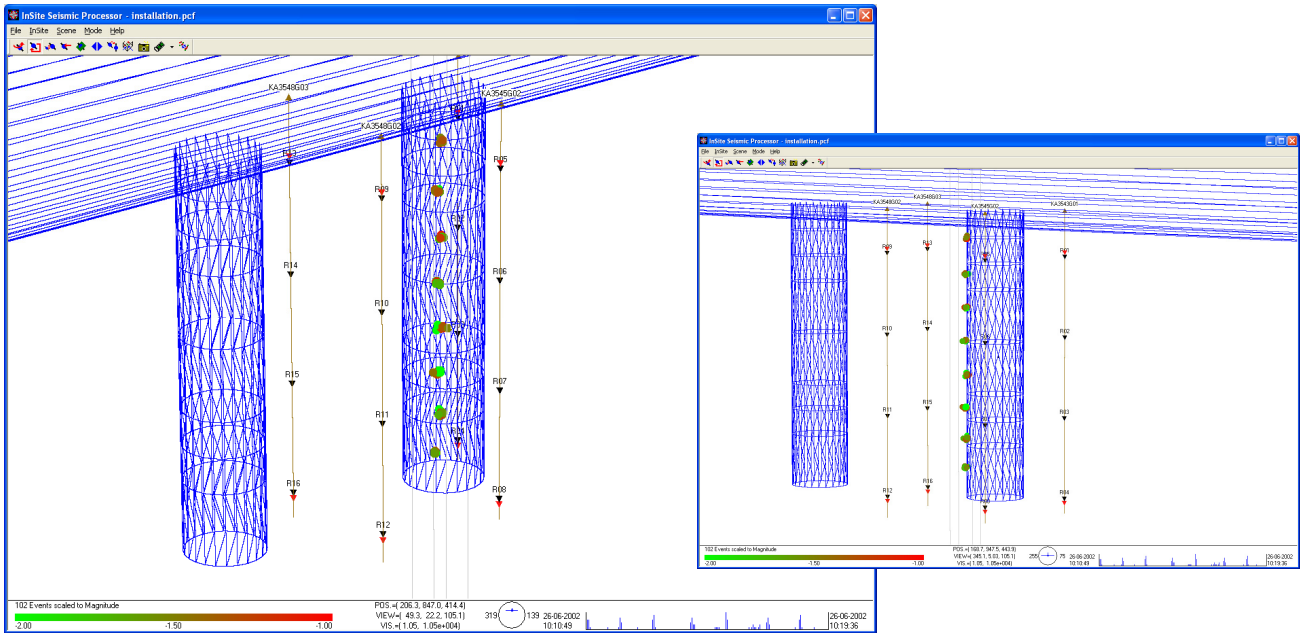


Figure 4-17: Locations of calibration shots obtained from a series of tests at 1 metre intervals down the wall of deposition hole DA3545G01. The two views show that these line up and are located close to the surface of the hole.

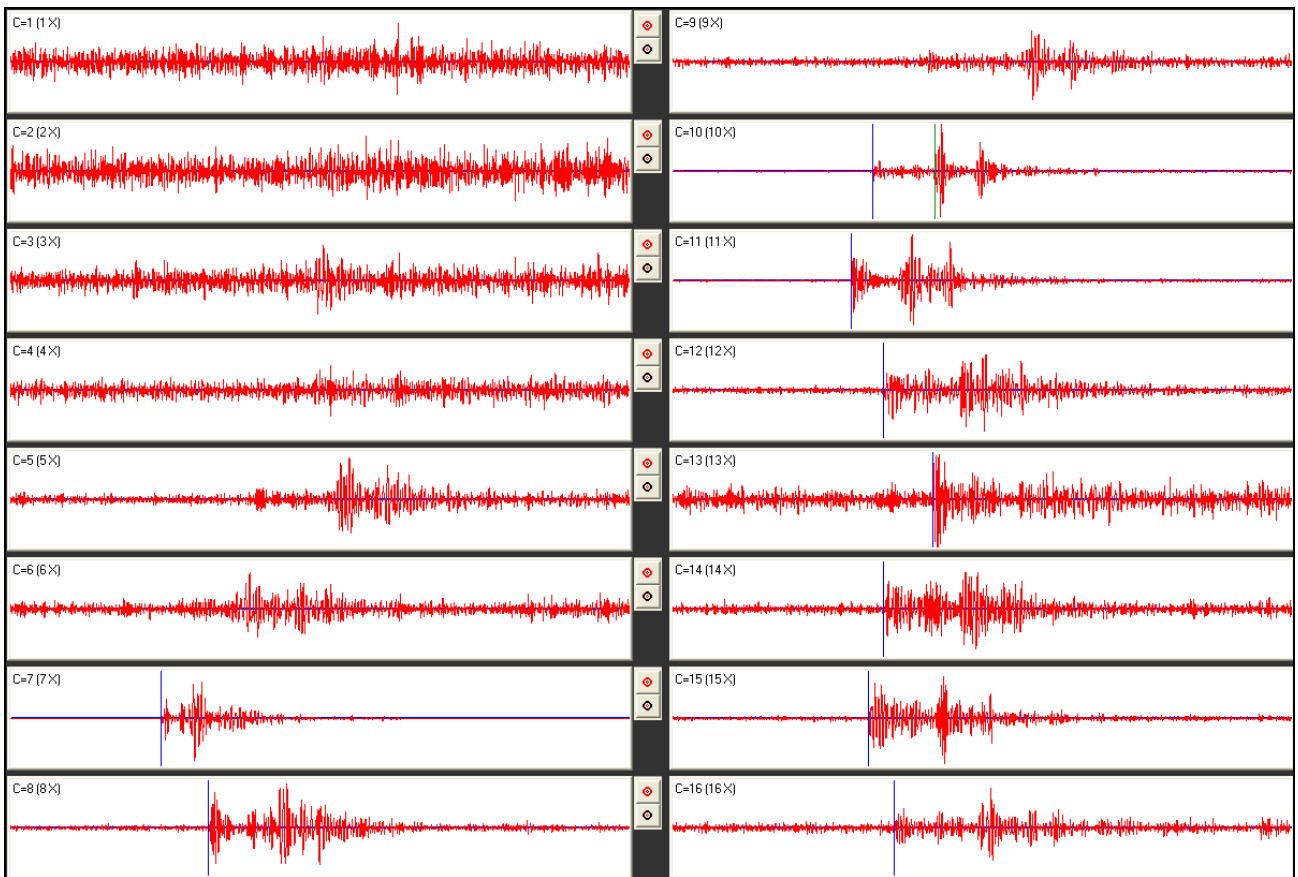


Figure 4-18: Example waveforms from each of the 16 receiving channels for a 'pencil-lead break' test undertaken against the Deposition Hole (DA3545G01) wall 6 metres below the tunnel floor.

Appendix III Processing Parameters

A: Ultrasonic survey processing parameters:

PROCESSING PARAMETERS	Velocity survey processing
EVENT INITIALISATION	
View/process waveforms by	Channel
Channel-view Width-to-height ratio	6
Waveform Response type	Set from sensor
Sampling time	1
Time units	Microseconds
Pre-signal points	200
Spline sampling time	0.2
Waveform To point	1023
P-Time correction	0
S-Time correction	0
Automatically update Channel Settings	NOT SET
Project Files	NULL

AUTO PICKING	
Allow P-wave-autopicking	YES, Use first peak in the auto-pick function
Back-window length	100
Front-window length	35
Picking Threshold	4
Min. Peak-to-Peak amplitude	0
Allow S-Wave Autopicking	YES, Use first peak in the auto-pick function
Back-window length	100
Front-window length	35
Picking Threshold	3
Min. Peak-to-Peak amplitude	0
Allow Automatic Amplitude Picking	YES
Use Velocity Window Picking	YES
P-wave Min. Velocity/Max. Velocity	4500, 6500
S-wave Min. Velocity/Max. Velocity	2500, 3500

CROSS-CORRELATION	
CCR Events	Referenced to a Survey
Reference Component	20041208005920
Reference Event	NULL
Window construction method	Front to Back
Window comparison method	Fixed to reference picks
Window Parameters	Back-window length = 20 Front-window length=30 Rise-time multiplier = NULL Power to raise waveform =1 Split to a Spline function = YES Obtain absolute waveform= NOT SET

LOCATER	<i>(not used in velocity surveys)</i>
Method	SIMPLEX INTO GEIGER
Method settings Simplex settings Geiger settings	Tolerance = 0.01 LPNorm = 1 P-wave weighting = 1 S-wave weighting = 1 Use Outlier Identification = NOT SET Arrival error factor = ×2 Tolerance (Loc. units) = 0.01 Step size (Loc.units) = 0.1 Max. Iterations = 100 Conditional No. Limit = 10000000000
Velocity Structure	Homogeneous Isotropic
Velocity Structure settings	P-wave velocity = 6000 m.s ⁻¹ S-wave velocity = 3350 m.s ⁻¹ Attenuation = 200 Q(S) value = 100
Data to use	P-wave Arrivals Only
Distance units	Metres
Working time units	Microseconds
Min P-wave arrivals	0
Min S-wave arrivals	0
Min Independent arrivals	5
Max. Residual	20
Start point	Start at the centroid of the array
Write report to RPT	NOT SET
Source parameters	Set to calculate automatically

B: AE processing parameters:

PROCESSING PARAMETERS

AE processing

EVENT INITIALISATION	
View/process waveforms by	Channel
Channel-view Width-to-height ratio	6
Waveform Response type	Set from sensor
Sampling time	1
Time units	Microseconds
Pre-signal points	200
Spline sampling time	0.2
Waveform To point	1023
P-Time correction	0
S-Time correction	0
Automatically update Channel Settings	SET
Project Files	NULL

AUTO PICKING	
Allow P-wave-autopicking	YES, Use max peak in the auto-pick function
Back-window length	100
Front-window length	35
Picking Threshold	5
Min. Peak-to-Peak amplitude	0
Allow S-Wave Autopicking	YES, Use max peak in the auto-pick function
Back-window length	100
Front-window length	35
Picking Threshold	5
Min. Peak-to-Peak amplitude	0
Allow Automatic Amplitude Picking	NOT SET
Use Velocity Window Picking	YES
P-wave Min. Velocity/Max. Velocity	4500, 6500
S-wave Min. Velocity/Max. Velocity	2500, 3500

CROSS-CORRELATION	<i>(not used in AE processing)</i>
CCR Events	NOT SET
Reference Component	NOT SET
Reference Event	NULL (not activated)
Window construction method	Individual
Window comparison method	Fixed to reference picks
Window Parameters	Back-window length = 20 Front-window length = 30 Rise-time multiplier = NULL Power to raise waveform = 1 Split to a Spline function = NOT SET Obtain absolute waveform = NOT SET

LOCATER	
Method	SIMPLEX INTO GEIGER
Method settings Simplex settings Geiger settings	Tolerance = 0.01 LPNorm = 1 P-wave weighting = 1 S-wave weighting = 1 Use Outlier Identification = NOT SET Arrival error factor = ×2 Tolerance (Loc. units) = 0.01 Step size (Loc.units) = 0.1 Max. Iterations = 100 Conditional No. Limit = 1000000000
Velocity Structure	Homogeneous Isotropic
Velocity Structure settings	P-wave velocity = 5986.106 m.s ⁻¹ S-wave velocity = 3349.171 m.s ⁻¹ Attenuation = 200 Q(S) value = 100
Data to use	P-wave Arrivals Only
Distance units	Metres
Working time units	Microseconds
Min P-wave arrivals	0
Min S-wave arrivals	0
Min Independent arrivals	5
Max. Residual	20
Start point	Start at the centroid of the array
Write report to RPT	NOT SET
Source parameters	Set to calculate automatically

EVENT FILTER	
Date and Time	NOT SET
Location volume	Minimum = (235, 880, 420)
	Maximum = (300, 964, 463)
L. Magnitude	NOT SET
Location Error	1
Independent Instruments	Minimum = 0

SOURCE PARAMETERS	
Automatic source-parameter windows	P-wave back window = 10
	P-wave front window = 50
	S-wave back window = 10
	S-wave front window = 50
Source parameter calculations	Min number to use = 3
Automatic source-parameter windows	Apply Q correction = SET
	Source density = 2640
	Source shear modulus = 39131400000
	Av. radiation coefficient: Fp = 0.52 ,Fs = 0.63
Source parameter calculations	Source coefficient: kp = 2.01 , ks = 1.32
Magnitude calculations	Instrument magnitude = 1 * log (ppV) +0
	Moment magnitude = 0.666667 * log(Mo) + -6

